Master Thesis

Spatiotemporal Analysis of Snow Regimes in the High Mountain Asian River Basins

Xinyu Liu

TU Delft

Spatiotemporal Analysis of Snow Regimes in the High Mountain Asian River Basins

by

Xinyu Liu

to obtain the degree of Master of Science in Environmental Engineering
at the Delft University of Technology
to be defended publicly on August 27, 2024 at 10:00

Thesis committee:

Main Supervisor:	Dr. Markus Hrachowitz
Co-supervisor:	Dr. Miren Vizcaino
Place:	Faculty of Civil Engineering and Geoscience, Delft
Project Duration:	February, 2024 - August, 2024
Student number:	5704456

An electronic version of this thesis is available at `http://repository.tudelft.nl/`.

Faculty of Civil Engineering and Geoscience · Delft University of Technology

TU Delft

Abstract

This study examines the spatiotemporal changes in snow regimes across High Mountain Asia (HMA), with a focus on snowfall, snowmelt and snow water equivalent (SWE) trends and their relationship with elevation, temperature, and precipitation. Utilizing ERA5-Land data, the analysis reveals a general decrease in snowfall and SWE, as well as snowmelt in low to mid-elevations. Notably, high-elevation zones, despite also experiencing declining snowfall, exhibit increased snowmelt due to the persistence of deep snowpacks. However, the overall reduction in snowmelt across all basins, and significant decline of total snowmelt in the Brahmaputra, Indus, and other major river basins, underscores the critical impact of climate change on water resources. Correlation analyses further highlight complex interactions between temperature, precipitation, and snow regimes, varying by season and elevation. The study acknowledges limitations in ERA5-Land's accuracy, particularly in high-elevation regions, and calls for future research to incorporate multiple data sources and uncertainty analysis to improve the reliability of findings. The implications of declining snowmelt for water availability in major river basins are significant, warranting continued investigation.

Contents

List of Figures

List of Tables

1 Introduction

1.1. Importance of cryosphere

Snowpack is an essential part of the nature systems. Both mountainous and low-elevation seasonal snow cover are playing a vital role in the Earth's hydroclimatic system due to its low thermal conductivity, large spatial extent, seasonal variations, as well as latitudinal distribution (Stewart 2009). Climatologically, the presence of snowpack could regulate the surface energy balance: in winter a large fraction of incoming solar radiation is reflected back as a result of high albedo of snow cover (Thackeray and Fletcher 2016), whereas in summer the snow-free surface absorbs more incoming energy (Callaghan et al. 2011). Specially, reductions in snow cover are expected to result in polar amplification of global warming (Serreze et al. 2000). Hydrologically, snowpack also accentuate its importance in the high latitudes and the mountainous regions (Li et al. 2022b). Many catchments receive the majority of their yearly water budget in the form of snow, particularly at high altitudes (Barnett et al. 2005). Moreover, in winter, a significant amount of fresh water is stored in snowpack, and when in spring and summer, snow melts gradually and water is released and redistributed (Kouki et al. 2023). In other words, streamflow in winter is reduced as water is retained in snowpack, and increased during and after the spring snowmelt. Soil moisture is also replenished (Qi et al. 2020).

Snowmelt is an crucial fresh water resource that sustains about one-sixth of the world's population directly and indirectly(Barnett et al. 2005, Kraaijenbrink et al. 2021). It is also critical for ecosystem productivity, groundwater recharge, food security, etc. (Musselman et al. 2021). Both the magnitude and timing of snowmelt could affect the efficacy of water provision for downstream applications profoundly, for instance, agriculture (Qin et al. 2020) and hydropower generation (Hale et al. 2023) requires consistent water availability . In addition, snowmelt could also act as water buffer late in the year when direct precipitation is unlikely. In this sense, changes in the onset, duration, or intensity of snowmelt season would influence the water security in high mountains and downstream (Smith et al. 2017).

Specifically, the High Mountain Asia (HMA) region comprises the major mountain ranges and headwaters of large rivers in Asia. It is characterized by exceedingly high elevation, complex terrain and pronounced glacier and snow cover (Liu et al. 2021). Over one billion people living downstream in its major river basins depend on fresh water from glacier and snowmelt (Barnhart et al. 2016). In this regard, this study is focused on the HMA and its 12 major river basins: Amu Darya, Brahmaputra, Eastern Asian, Ganges, Indus, Irrawaddy, Mekong, Tibetan, Salween, Tarim, Yangtze and Yellow river. Amu Darya and Indus receive about 50% of their yearly water budget as snow, whereas in Tarim and Tibetan, nearly two thirds of their yearly water budget is derived from snowmelt (Smith and Bookhagen 2018a).

1.2. Overview of changes in snow regimes

Climate is changing, with significant warming and many areas are suffering from extreme weathers (Kraaijenbrink et al. 2021). Air temperature at HMA was witnessed to increase remarkably with an above-average warming rate of the Northern Hemisphere specifically at Tien Shan, Qilian Mountain, Hengduan Shan and Tibetan Plataeu (Wang et al. 2024). In addition, strong warming trends have been identified in the central, norther, northeastern, and northwestern areas, with more noticeable warming in the north than south, and in cold seasons than summer (Li et al. 2022a). Significant wetting trend is also recognized in many regions in HMA, yet not uniformly distributed in neither spatial nor temporal scales: wetting trend dominates in

the central, northwestern, and northeastern HMA, whereas in the southern-east, eastern and western HMA, decreasing trend prevails (Yao et al. 2022).

These hydro-climatic factors act differently on the snow regimes. An increase in precipitation would lead to more snowfall and hence more snow water storage. However, combined with increasing temperature, its impact on snowpack is less straightforward. Increasing in temperature has been associated with precipitation phase shifting from snowfall to rainfall (Hale et al. 2023, Räisänen 2016) as it favours the occurrence of above-zero temperatures when close to the freezing point (Räisänen 2023). In addition, the snowpack is reduced by more frequent and intense melt events during the winter (Hale et al. 2023, Musselman et al. 2021). The net effect of temperature and precipitation change results in shorter snow season (Zhu et al. 2021 and decrease in SWE in most regions (Mudryk et al. 2020). Yet in the eastern Siberia and northern Canada, that are located in the coldest regions, the increase in total precipitation dominates and lead to increase in snow water storage in the snow season (Brown and Mote 2009).

Moreover, large-scale climate systems active in the HMA including the Indian summer monsoon (ISM), East Asian summer monsoon (EASM), and the winter westerly disturbances (WWD) also play vital role in regulating the snow patterns. For instance, the total annual precipitation in the ISM regions has not undergone significant changes, yet spatial variation in intensity of rainfall has led to disparity in snow distribution (Smith and Bookhagen 2018b). Similarly, the timing and magnitude of precipitation related to the WWD has shifted over the past 30 years (Cannon et al. 2014), and this has been substantiated to impact the snowfall in HMA (Lutz et al. 2014).

Snow water equivalent (SWE) is usually used to quantify snowpack as it represents the the amount of water that contained if the snowpack melted instantaneously, and it can be expressed in millimeters or in kilo grams per square meter, equivalently (Kouki et al. 2023). Overall, there is an decreasing trend in SWE in the HMA, but spatial variations also exist: increasing trend is also recognized in some high mountain regions(Smith and Bookhagen 2018a, Räisänen 2023). Moreover, the annual maximum SWE remained quite stable, yet in the mid-elevation regions SWE decreased significantly in spring and autumn (Yang et al. 2022). Specially, in mid-elevation mountain ranges, the decrease in snow storage is highly correlated with a warmer temperature as it favours rain over snow (Jenicek et al. 2016).

In terms of snowmelt, Warming in HMA has intensified the melting rate, and advanced the onset of melting season in recent years (Duan et al. 2022). The duration of melting season is also shortened (Tang et al. 2022). This changes in snowmelt regimes would compromise the natural water storage and supply process, posing hydrological risks to humanity and ecosystems downstreams where meltwater is used for irrigation, hydroelectric power and consumption (Gottlieb and Mankin 2024).

1.3. Measurements, observations, and reanalysis

SWE and snowmelt can be measured directly in situ through snow pillow and snow permitivity analysis (Seibert et al. 2021, but mapping SWE and snowmelt over large areas remains challenging for mountainous areas as a result of its terrain complexity(Dozier et al. 2016). Intallation and maintenance of in-situ measurements are usually expensive and difficult (Liu et al. 2021). Moreover, measurements are mostly located in the low valleys, hence resulting in a sparse and non-representative network (Kirkham et al. 2019).

In recent decades, since the launch of the Scanning Multichannel Microwave Radiometer, satellite observations also played a vital role in large-scale snow property estimates Smith et al. 2017. Specially, Passive Microwave sensors are frequently used to estimate SWE and snow depth directly. Moreover, as PM data are higher sensitive to liquid water present in the snowpack, snowmelt across large, complex, and unstationed regions could also be estimated as well (Takala et al. 2011). Passive Microwave data also excel in functioning in spite of cloud cover that is ubiquitous in high mountains in winter and during monsoon seasons (Smith et al. 2017). However, it accuracy was also challenged by the coarse spatial resolution (e.g. 25 km) and generally negatively biased in deep snowpack (Dozier et al. 2016). Other satellite techniques, for instance, C-band synthetic aperture radar show promise in snow depth retrieval yet are available over only recent years (Lievens et al. 2019).

Another approach that provide large-scale snow property estimates is global atmospheric reanalysis product. Reanalysis combines model data with observations from worldwide into a global dataset using the laws of physics, and the data goes back to several decades in time, therefore providing an accurate description of the climate of the past. Examples include, for instance, European Centre for Medium-Range Weather Forecasts reanalysis products (ERA5 Hersbach et al. 2020; ERA5-Land Muñoz Sabater et al. 2021a), Global Land Data Assimilation System (Rodell et al. 2004, Modern-Era Restrospective analysis for Research and Applications

(Merra-2, Gelaro et al. 2017), and others. Snow measurements in these dataset were found to be consistent with respect to its seasonal and inter-annual variabilities. However, uncertainties rise as different land surface models are used and its meteorological inputs, and this leads to significant difference in magnitude across regions (Wrzesien et al. 2019).

1.4. Research questions

In summary, this study focuses on analyzing the spatial distribution and temporal variations in snow regimes (i.e., snowfall, snowmelt, and SWE) in the major HMA river basins from 1980 to 2020. The heterogeneous topography and diverse climatic zones across those river basins are expected to largely influence spatial variability in snow accumulation and melt dynamics. Also, temporal changes of snow regimes are also encompassed. In addition, a preliminary analysis of the influence of hydroclimatic factors, i.e., temperature and total precipitation, on such variability are identified.

The overarching research question this thesis aims to address is: **How have snow regimes changed across the HMA river basins from 1980 to 2020?** This has been further divided into the following sub-questions:

1. How are snowfall, snowmelt, and SWE distributed spatially across the HMA basins?
2. How are snow distributed across elevation?
3. What is the temporal variability in snow regimes from 1980 to 2020?
4. How do temperature and total precipitation contribute to changes in snow regimes?

2

Methodology

2.1. Study area

This study area is bounded from 5 to 50 °N and from 50 to 130 °E, covering large-scale snowy and non-snowy area in 12 Himalayan river basins, namely: Amu Darya, Brahmaputra, Eastern Asian, Ganges, Indus, Irrawaddy, Mekong, Qinghai-Tibetan, Salween, Tarim, Yangtze and Yellow River (Figure 2.1). This area shows a diversity of climates and topography; elevations rise from near sea-level to over 8,000 m above sea level at the highest peak in the world, i.e., Mountain Everest in the Himalayas. Moreover, high mountain ranges including Tien Shan, Pamir Mountains, Hindu Kush, Karakoram, Kunlun Shan, Qilian Shan, the Himalayas, Tanggula Shan, Hengduan Shan, and eatern Tibetan Mountains, as well as the Tibetan Plateau, are also identified in Figure **??**. For convenience, hereafter the annotated mountainous areas are collectively termed as High Mountain Asia (HMA). HMA contains the headwaters for rivers that sustains over a billion population living downstream. In comparison, Indus, Ganges, and Yangtze basins are more densely populated than other high elevation areas, i.e., Tibetan, Eastern Asian, etc.

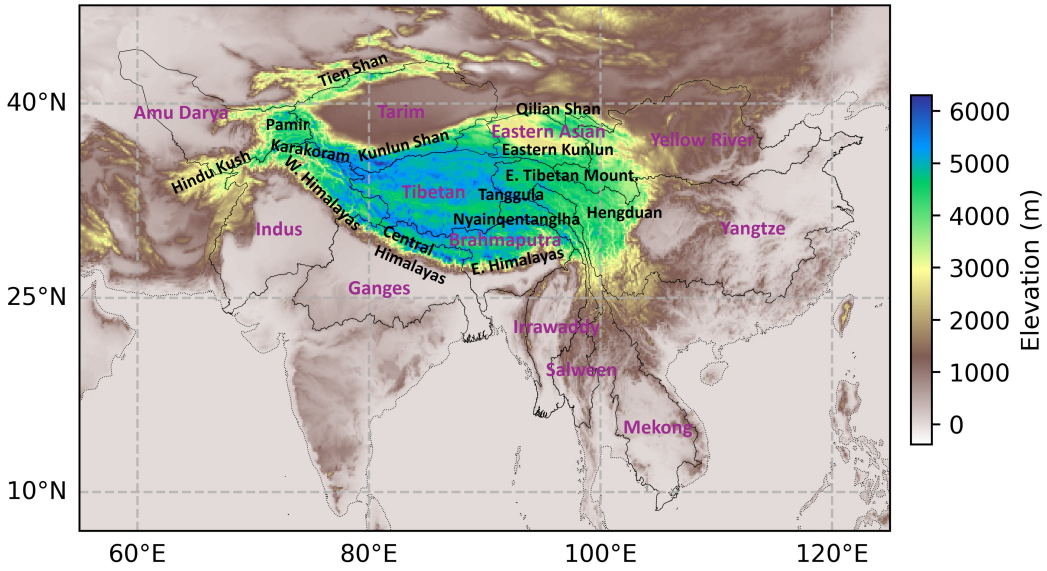

Figure 2.1: Map of the study area with 12 identified river basin

2.2. Data

This study aims to analyze the spatio-temporal patterns of snow regimes including seasonal snow as SWE and snowmelt, as well as the influence of temperature and monsoon rainfall on SWE and snowmelt. In this sense, SWE, snowmelt, temperature, and total precipitation, as well as elevation data across the study area

were required. Though networks of in-situ station data exists, e.g., for SWE measurements, their coverage is relatively limited to allow large-scale analysis of spatial patterns (Mortimer et al. 2020). Therefore, the current study employs reanalysis datasets that provides a comprehensive "observed" evolution spatially and temporally (Räisänen 2023.

ERA5-Land (https://cds.climate.copernicus.eu/cdsapp#!/dataset/reanalysis-era5-land-monthly-means?tab=overview) is a replay of the land component of the ERA5 climate reanalysis, with a down-scaled spatial resolution from 31km to 9km. Specifically, ERA5-Land dataset was used for several reasons. Firstly, it provides more coherent, and long-term record of past weather with a temporal coverage from January 1950 to 2-3 months before the present, which allows to conduct statistically meaningful analysis that requires at least four decades data (Räisänen 2023). Secondly, ERA5-Land datasets does not directly assimilate snow-related land surface variables as this would involve a disparity between SWE and the atmospheric forcing (temperature, precipitation, radiation, etc.) that regulates snowfall and snowmelt (Muñoz Sabater et al. 2021b). Thirdly, the climate variables that will be assessed in this study, i.e., snowfall, snowmelt, SWE, temperature, total precipitation are directly available in ERA5-Land in temporal resolution of both hourly and monthly. The information of the variables is detailed in Table 2.1.

Table 2.1: Information of variables from ERA5-Land

Variable name	Unit	Description
SWE	mm	The depth the water would have if the snow melted out and was spread evenly over the whole grid box.
Snowmelt	mm/month	Accumulated snowmelt averaged over the grid box from the beginning of the forecast time to the end of the forecast step.
Snowfall	mm/month	Accumulated snowfall averaged over the grid box from the beginning of the forecast time to the end of the forecast step.
Temperature	K	Temperature of air at 2m above the surface of land, sea, or in-land waters.
Total precipitation	mm/month	Accumulated liquid and frozen water, including rain and snow, that falls to the Earth's surface averaged over the grid box.

In addition, the elevation data is also entailed in this study. In this sense, the Global Multi-resolution Terrain Elevation Data 2010 (GMTED2010) (https://www.usgs.goov/coastal-changes-and-impacts/gmted2010#web-tools) is used as it provides several spatial resolutions and incorporates the current available global elevation data including Global Digital Terrain Elevation Data (DTED) from the Shuttle Radar Topography Mission (SRTM), Canadian elevation data, Spot 5 Reference3D data, and data from the Ice, Cloud, and land Elevation Satellite (ICESat).

The shape files of catchment boundaries is adopted from https://rds.icimod.org/home/datadetail?metadataid=2732, with which each basin could be clipped from the large dataset. In addition, the satellite-derived land cover data and shaded relief for making reference maps is retrived from https://www.naturalearthdata.com/downloads/10m-raster-data/10m-natural-earth-1/.

2.3. Statistical methods

The statistical methods involved in this study includes Mann-Kendall Trend Analysis, Correlation Analysis, and Linear Regression Analysis.

The Mann-Kendall Trend Analysis, which is a non-parametric test frequently used to test if linear, monotonically increasing or decreasing trend exists in time series, and to exhibit its statistical significance ($P < 0.05$)(Mann 1945), is applied to test the point-wise trend for each grid cell across the entire study area and also the trend for time-series data from 1980 to 2020. Furthermore, if missing values present in the raw data, the trend is calculated only when at least 15 values available during the study period (Kouki et al. 2023).

The mathematical expression of Mann-Kendall test is elaborated below (Yue et al. 2002):

$$S = \sum_{k=1}^{n-1} \sum_{j=k+1}^{n} sign(x_j - x_k) \tag{2.1}$$

$$sign(x_j - x_k) = \begin{cases} 1 & (x_i - x_k) > 0 \\ 0 & (x_i - x_k) = 0 \\ -1 & (x_i - x_k) < 0 \end{cases} \tag{2.2}$$

$$Var(S) = \left\{ [n(n-1)(2n+5)] - \sum_{i=1}^{m} t_i(t_i-1)(2t_i+5) \right\} /18 \tag{2.3}$$

$$Z = \begin{cases} S - 1/\sqrt{VarS} & S > 0 \\ 0 & S > 0 \\ S + 1/\sqrt{VarS} & S < 0 \end{cases} \tag{2.4}$$

where S represents the Mann-Kendall test statistics, n denotes data set length, x_i and x_k are the sequential data values, t_i is the number of ties of extent i, m is number of the tied groups and Z is the standardized statistics.

Meanwhile, the non-parametric Theil-Sen's slope is employed (Sen 1968) to calculate the exact trend of time series data. It is the median of all slopes between paired values, and is more robust to outliers than the least squares linear regression (Kouki et al. 2023).The mathematical representations are provided below:

$$Q_j = \frac{x_k - x_l}{k - l} \quad \text{for j = 1,..., R and K > 1} \tag{2.5}$$

$$R = n(n-1)/2 \tag{2.6}$$

$$Q = \begin{cases} Q_{(R+1)/2}, \text{ if } R \text{ is odd} \\ (1/2)[Q_{R/2} + Q_{(R+2)/2}], \text{ if } R \text{ is even} \end{cases} \tag{2.7}$$

where Q_j denotes the Sen's slope estimator which is the median of the R values, and x_k and x_l are the sequential values. In case of existing n values of $x + k$ at each period, R and Q can be calculated alternatively.

Then, correlation analysis and composite analysis are performed with the detrended data between snow variables (snowfall, snowmelt, and SWE) and climatic variables (temperature and total precipitation), respectively. Significance level was chosen to be 95%.

For correlation analysis, the Pearson correlation coefficient and its p values are calculated as:

$$r = \frac{\sum (x - m_x)(y - m_y)}{\sqrt{(x - m_x)^2 (y - m_y)^2}} \tag{2.8}$$

$$f(r) = \frac{(1 - r^2)^{n/2-2}}{\beta(1/2, n/2 - 1)} \tag{2.9}$$

$$p = 2 * F(-|r|) \tag{2.10}$$

where m_x and m_y are the mean of vector x and y, respectively. n is the number of samples, and β is the beta function, $f(r)$ is the probability density function of r and $F(r)$ is the cumulative density function of r.

In terms of composite analysis, the above-normal (below-normal) snow composite, is assembled from the detrended snow anomalies that correspond to the years that align with the above 90% quantile (below 10% quantile) climate variable anomalies. In this sense, the above 90% quantile refers to higher-most positive anomalies, whereas the below 10% quantile represents the lower-most negative anomalies. Moreover, the detrended anomalies are calculated by firstly subtracting the mean values and then removing the linear least square fit trend from the data (Prabhu et al. 2021).

2.4. Elevation analysis

For snow variables, its elevational distribution is analyzed. To examine the elevation dependence, snow variables at every 500 m elevation is aggregated and averaged. For SWE, the mean SWE at each elevation band is visualized directly. On the other hand, for snowfall and snowmelt, the averaged values are then normalized by the basin annual total by summing from all elevation bands. Thus the elevational contribution to basin total is quantified by examining the percentage of each elevation band to the basin total. Trend analysis is also performed to study the temporal changes in snowfall, snowmelt, and SWE at various elevations.

3

Results

In this chapter, results are showing in figures and tables. Figures are also available at `https://drive.google.com/drive/folders/1aa17xNDIr3zYL5xCu666Ib-Uurw5zsuW?usp=drive_link` to be freely reviewed.

3.1. Climatology of study area

The altitude, averaged at each grid point (0.1° resolution) in the study area, is plotted in Figure 2.1. Moreover, the elevation distribution is assessed for each catchment. As shown in Figure A.1, Qinghai-Tibetan is located at the plateau region where altitude is generally above 4km. In contrast, the Eastern Asian basin is constituted by mid-to-high elevation regions, from 2.5 km to 6 km. In addition, Irrawaddy lies at the low-to-mid altitude area where its elevation is mostly below 3 km. The rest catchments show a wide coverage of terrain characteristics, and their elevation ranges from 0 to 6 km. Their geographic difference would give rise to distinct climatic conditions, e.g., temperature and precipitation, in each catchment and hence its hydrological behaviors, e.g., snow regimes, which will be elaborated in the following sections.

Major moisture sources that affect the HMA catchments include Indian Summer Monsoon (ISM), Eastern Asian Summer Monsoon (EASM) and Winter Westerly Disturbance (WWD). The ISM is a tropic monsoon that extends from June to September, and responsible for the majority of precipitation in India and Nepal, which gradually migrates to the North-west along the Himalayan front (**?**,Menon et al. 2013). The EASM is a subtropic monsoon that triggers multiple precipitation peaks in April-May and September-October, and it brings moisture from the South China Sea onto the mainland and depositing precipitation on the far eastern edge of the Tibetan Plateau (Yihui and Chan 2005). On the other hand, the WWD is driven by a jet stream that originated at the Mediterranean sea, and generally lasts from December to March (Palazzi et al. 2013). As a result of topographic blocking and capture, heavy snowfall at high elevations and major valleys are always found (Cannon et al. 2014).

In terms of temperature (Figure 3.1), the monthly average from 1980 to 2020 is calculated and visualized. Spatial and seasonal variations are demonstrated. Generally, the HMA region (i.e., Tien Shan, Pamir, Karakoram, Hindu Kush, the Himalayas, Tibetan, eastern Tibetan, Kunlun Shan, Qilian Mountains, Tanggula Shan and Hengduan Shan, show lower temperature than other areas across year as a result of high altitudes. In the southern catchments, for instance, Indus, Ganges, Brahmaputra, Irrawaddy, Salween, Mekong, as well as in the east, for example, Yangtze and Yellow river, temperature is higher there.

In terms of total precipitation (Figure 3.2), the southern and eastern HMA basins are controlled by the interaction between the ISM and EASM, and receive substantial amount of summer precipitation. In contrast, the major moisture sources in the northern and western HMA is the WWD, which brings abundant precipitation as snowfall to the Pamir, Karakoram, and Eastern Himalayas in winter (Liu et al. 2021).

In addition, the snowfall over total precipitation ratio is computed (Figure 3.3). In the HMA and high latitude areas, precipitation falls completely as snow in winter seasons. However, in spring and summer seasons, only in Pamir, Karakoram, and Kunlun Shan, snowfall presents albeit to a lesser extent of about 0.5.

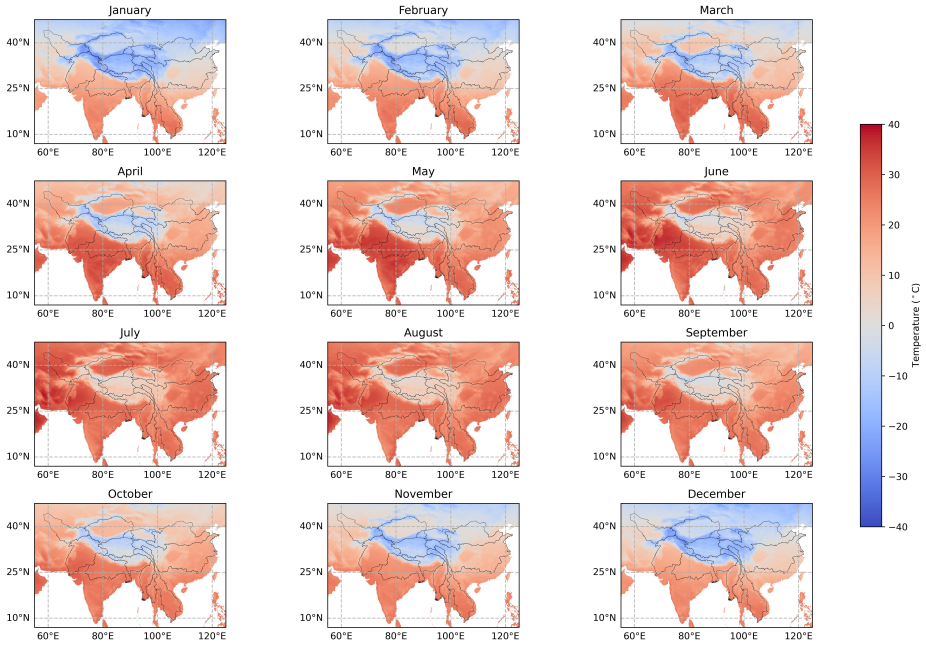

Figure 3.1: Average monthly temperature from 1980 to 2020

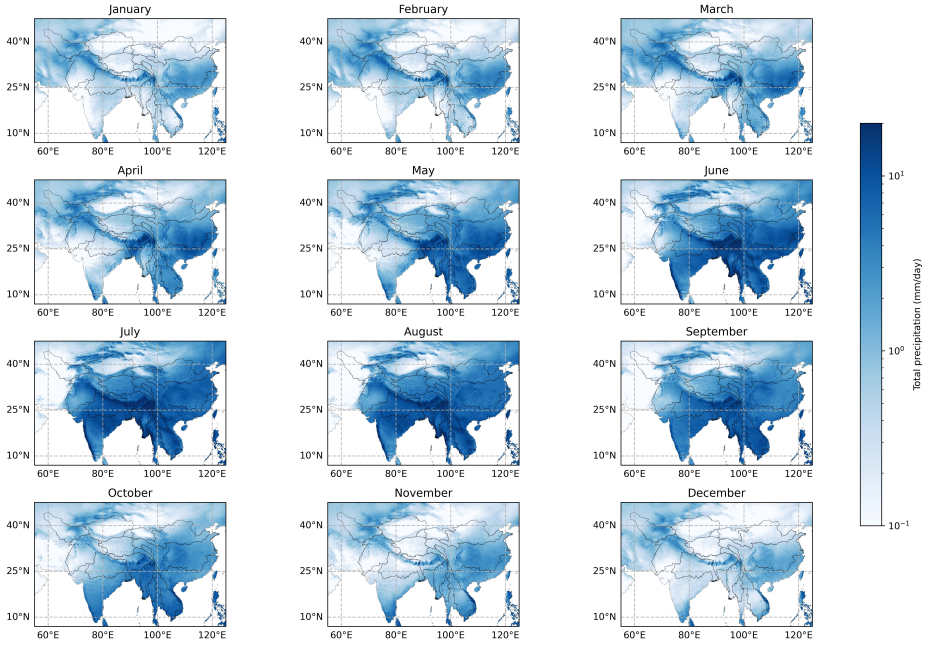

Figure 3.2: Average monthly total precipitation from 1980 to 2020

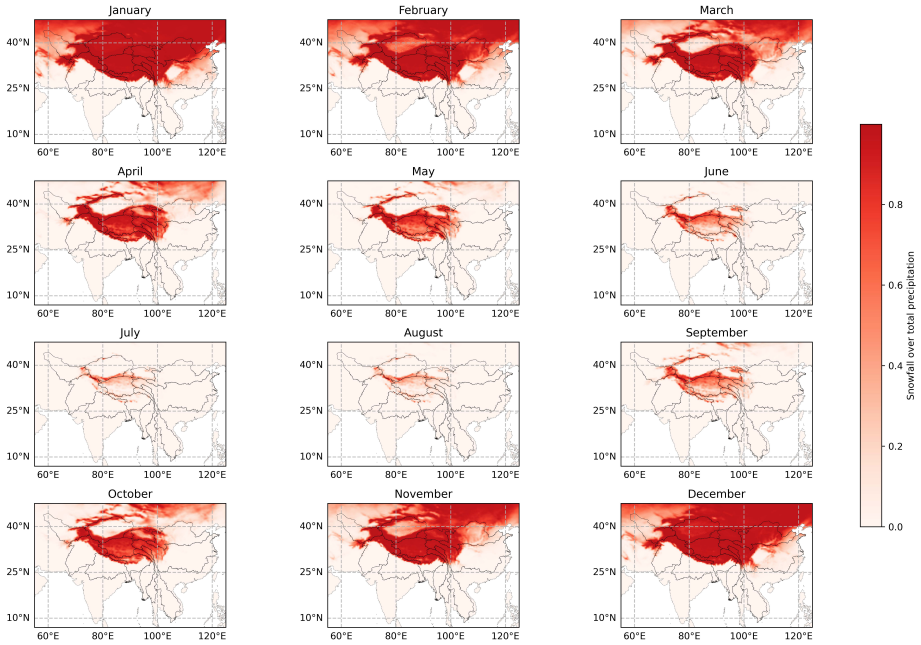

Figure 3.3: Average monthly snowfall to total precipitation from 1980 to 2020

3.2. Snowfall analysis

In this section, snowfall is analyzed spatially and temporally. Firstly, the distribution of snowfall is assessed, and how it has changed over the past 40 years. Inter-annual and inter-decadal variations in snowfall are also analyzed. Lastly, the elevational distribution and temporal changes at each 500 elevation bands are evaluated.

3.2.1. Spatiotemporal distribution of Snowfall

In general, the amount of snowfall is affected by seasons, latitude, and altitude: higher latitude and altitude tend to result in lower temperature and hence more snowfall is expected. As shown in Figure 3.4, significant snowfall deposits in the HMA where elevations are high, i.e., Tien Shan, Pamir, Hindu Kush, Karakoram, the Himalayas, Tibetan plateau, and the eastern Tibetan mountains in Hengduan and Tanggula Shan, but differs in timing as a result of monsoon influence. Tien Shan, Pamir, Karakoram and the Himalayas receives massive snowfall from the WWD from November to March, yet snowfall reduces gradually from April to August as season changes and temperature increase. In contrast, the eastern Tibetan mountains, Tanggula Shan and Hengduan Shan, which are under influence of the EASM, obtain substantial snowfall in April-May and September-October. This founding is in line with other study (Yihui and Chan 2005). Specially, from June to August, the eastern Himalayas, central Kunlun Shan, as well as part of the Tibetan plateau, also receive snowfall, due to its high elevation.

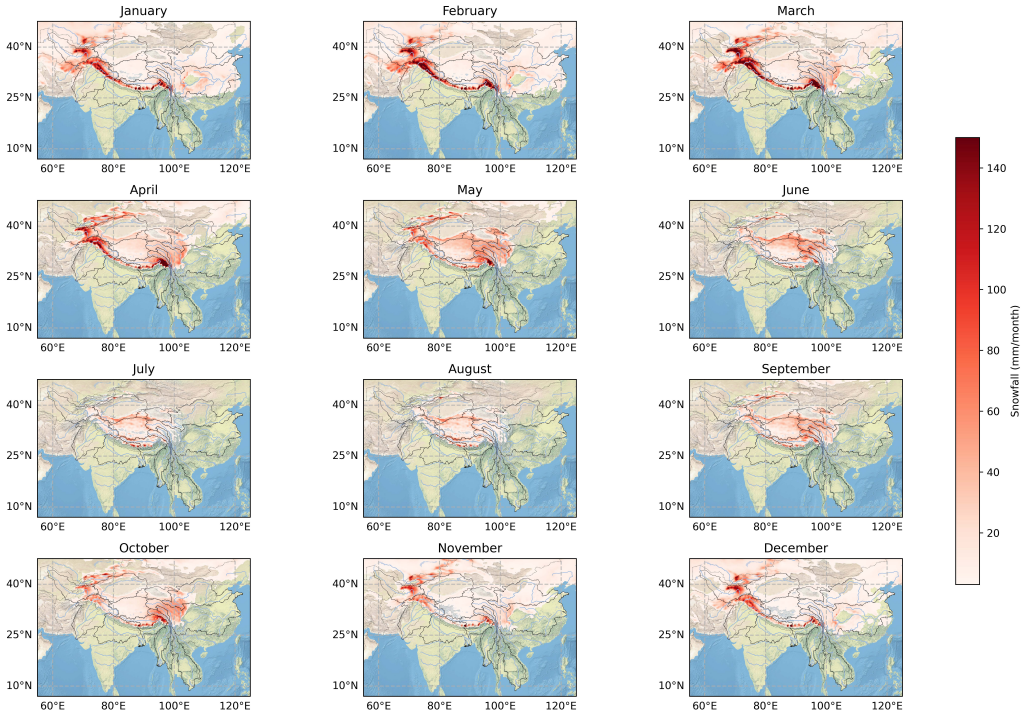

Figure 3.4: Average monthly snowfall (mm) from 1980 to 2020

Changes in snowfall are quantified from 1980 to 2020 through trend analysis. Results are shown in Figure 3.5 and Figure 3.6, which give information of absolute and relative, monthly snowfall trends. Collectively, temporal changes in annual average snowfall are also demonstrated in Figure 3.7.

Briefly, changes in snowfall are inhomogenous and varies spatially and seasonally. For example, Pamir, Hindu Kush, Karakoram, and the western-central Himalayas shows increasing trend with a magnitude of 1.2 mm/month/year in February, but a strong decreasing trend dominates in March, May and December. Similarly, the eastern Tibetan mountains undergo increasing snowfall of about 0.6 mm/month/year in May but decreasing trend from June to September. This jointly gives rise a slightly negative trend in these region in annual average snowfall. However, the central Kunlun Shan is witnessed with increasing snowfall from May-June, and August-September, but not counteracted by decreasing trend in other months. In this sense, slightly increasing snowfall is observed in the annual mean trend with a magnitude of about 0.3 mm/month/year.

In terms of relative changes, snowfall also presents considerable spatial differences. Tien Shan, Kunlun Shan, the Himalayas, and Tibetan plateau show intermittent strong increasing trend as high as 2%/year. However, other regions also exhibit intense negative trend, for example, Pamir, Karakoram, and the western Himalayas show decreasing snowfall (-2%/year) in December, March and May. This inhomogeneity also present in the annual mean snowfall trend in Figure 3.7, that positive snowfall trend exists in central Tarim, and central Kunlun Shan, and part of the Tibetan plateau. Other areas are dominated by decreasing trend in snowfall.

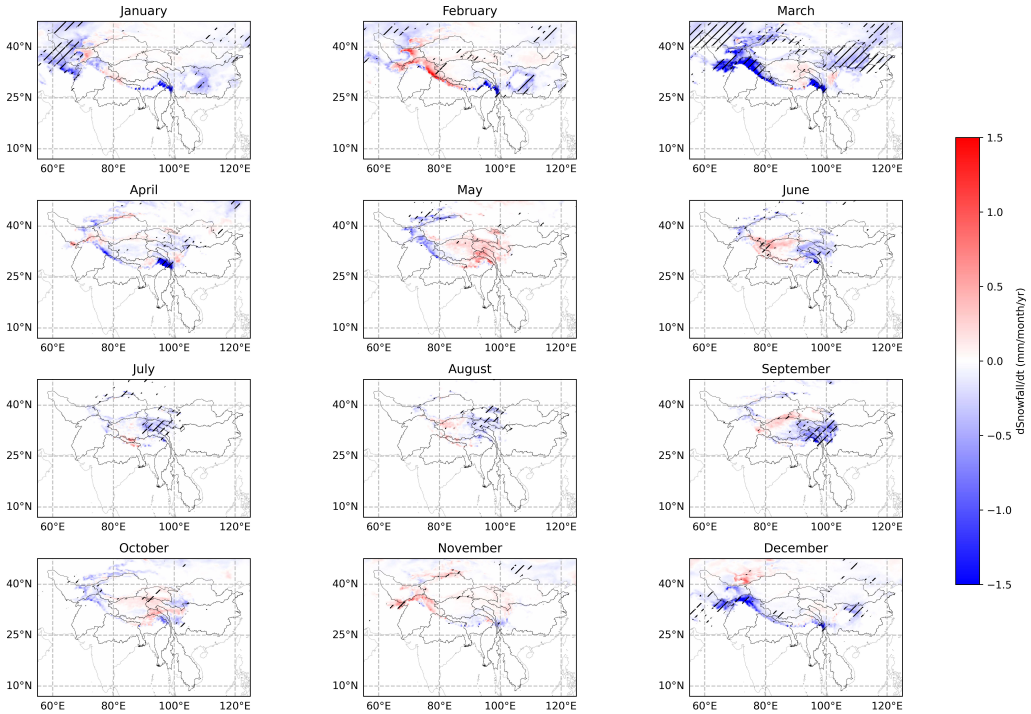

Figure 3.5: Temporal trend of monthly snowfall (mm/month/year) from 1980 to 2020, with hatched area implying the significant changes

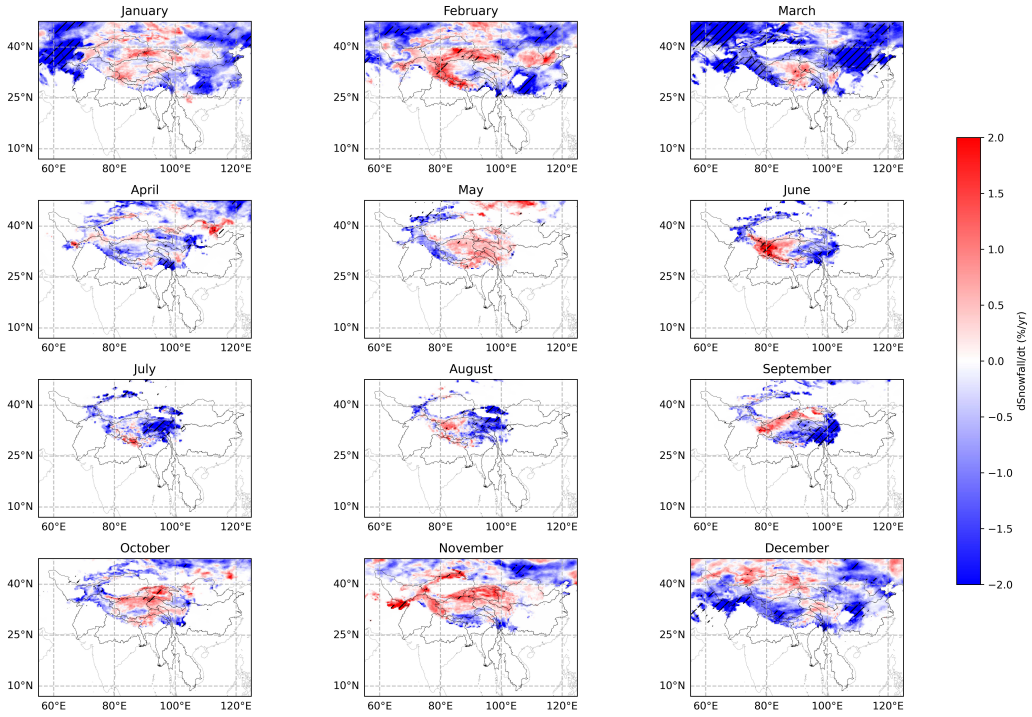

Figure 3.6: Temporal trend of monthly snowfall (%/year) from 1980 to 2020, relative to 40-year average Snowfall, with hatched area implying the significant changes

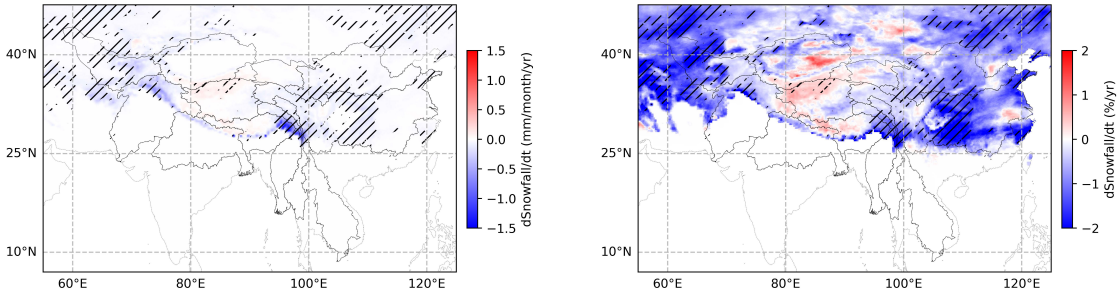

Figure 3.7: Absolute temporal trend (left) and relative temporal trend (right) of annual-average snowfall from 1980 to 2020, with hatched area implying the significant changes

Furthermore, Table 3.1 summarizes the basin-average, minimum and maximum trends, as well as the trends in mean snowfall volume (km^3/month/year) in Figure 3.7. Firstly, Brahmaputra demonstrates a largest annual-average monthly snowfall decreasing trend, with a magnitude of -0.1 mm/month/year, which accounts for -0.34%/year. However, in terms of average relative snowfall trend, Amu Darya shows an extremely most negative trend of -1.03%/year. However, when snow volume is taken into account, i.e., basin area is involved, Yangtze has the largest decreasing trend.

3.2.2. Interannual snowfall variability

In this part, the annual and inter-decadal variations, as well as the temporal trend are examined for each catchment. From Figure 3.8, Amu Darya, Brahmaputra, and Indus receive the most abundant snowfall in terms of basin average. Annual snowfall patterns also differ markedly due the the influence of monsoon.

Table 3.1: Statistics of annual-average monthly snowfall trend in each basin

	Trend (mm/month/year)			Trend (%/year)			Trend (km^3/month/year)
	Mean	Min	Max	Mean	Min	Max	Mean
Amu Darya	-0.07	-0.39	-0.004	-1.03	-2.44	-0.009	-0.108
Brahmaputra	-0.100	-1.61	0.211	-0.339	-3.34	0.729	-0.125
Eastern Asian	-0.001	-0.105	0.135	-0.069	-0.815	0.519	-0.001
Ganges	-0.010	-1.49	0.197	-0.270	-2.06	1.01	-0.019
Indus	-0.054	-0.659	0.112	-0.423	-3.78	0.611	-0.119
Irrawaddy	-0.024	-1.20	0	-0.931	-2.76	0	-0.019
Mekong	-0.015	-0.97	0	-0.331	-2.35	0.048	-0.065
Tibetan	0.017	-0.123	0.174	0.081	-0.939	0.787	0.018
Salween	-0.061	-1.14	0.021	-0.471	-2.37	0.097	-0.110
Tarim	-0.010	-0.204	0.178	-0.120	-1.65	1.58	-0.015
Yangtze	-0.045	-0.805	0.056	-0.932	-2.63	0.709	-0.201
Yellow River	-0.036	-0.169	0.030	-0.642	-1.81	0.335	-0.079

For instance, Amu Darya, Ganges, Indus, Irrawaddy and Brahmaputra present one-peak dominated seasonal snowfall pattern that snowfall maximizes in February-March and minimizes in July-August. In these area, the dominant moisture source is the WWD and hence snowfall is primarily precipitated in winter. In contrast, other basins, i.e., Eastern Asian, Mekong, Salween, Tarim, Tibetan, Yangtze and Yellow River demonstrate a two-peak pattern as a result of the EASM that brings considerable precipitation in April-May and September-October.

On the other hand, the inter-decadal changes primarily indicate the temporal trends. For all basins, the decadal average snowfall varied largely. The peak value has shifted in many catchments, for example, from March to February in Amu Darya and Indus, from September to October in Mekong and Salween. Peak and off-peak values in Brahmaputra, Irrawaddy and Yellow River also reduce. In order to better evaluate the temporal changes, trend analyses are performed hereby with significance test.

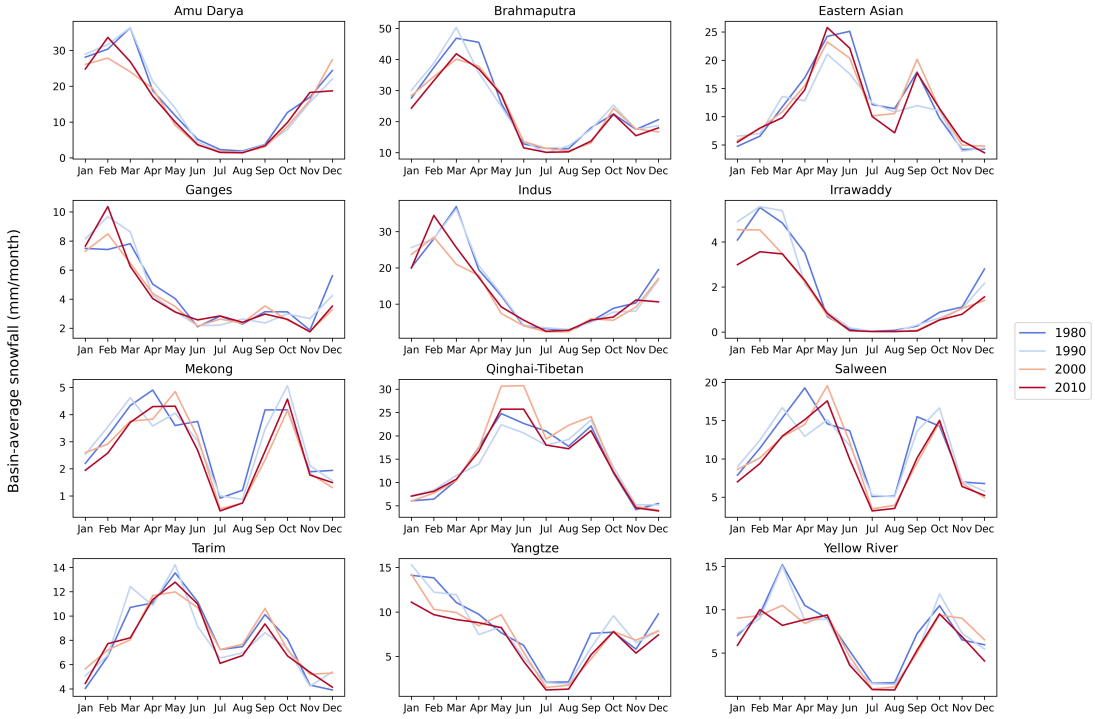

Figure 3.8: Seasonality and inter-annual variability of basin-averaged snowfall (mm/month), for every 10-year interval from 1980 to 2020

Results of absolute and relative trends are shown in Figure 3.9. Firstly, the monthly trends are largely diverse in all basins, no consistent trends are identified. Amu Darya and Indus has experienced the most pronounced reduction in snowfall in March, with a magnitude of about 0.0125 mm/day/year. Generally, in Amu Darya, Brahmaputra, Irrawaddy, Mekong, Salween, Yangtze, Yellow River, negative trends dominate there; intermittent increasing trends show in spring and winter. Specially, from June to September, strong negative trends prevails in Mekong, Salween, Yangtze, and Yellow river, with a value of about -1.5%/year.

To find out the temporal changes in annual-total snowfall amount, monthly basin-averaged snowfall is accumulated in each catchment. The 40-year time series of snowfall are plotted, trend and significance are also computed in Figure 3.9 and Table 3.10. Except for Eastern Asian and Tibetan, all other basins are recognized to receive less snowfall. Particularly, Amu Darya, Brahmaputra, Indus, Irrawaddy, Mekong, Salween, Yangtze and Yellow River undergo significant reduction.

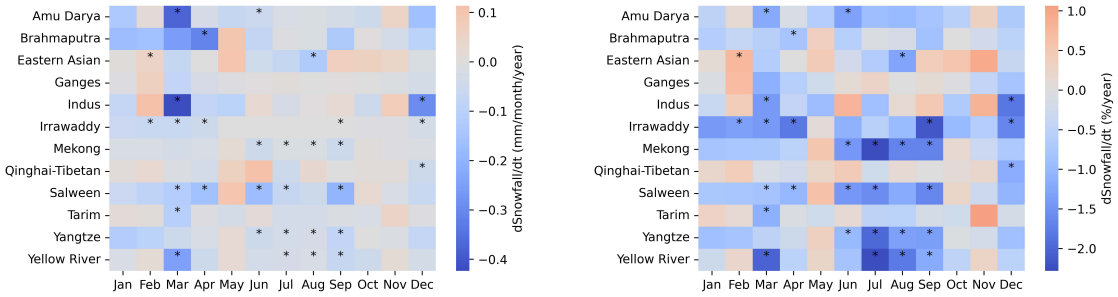

Figure 3.9: Absolute temporal trend (left) and relative temporal trend (right) of basin-average snowfall from 1980 to 2020, with the * sign indicating the significant values

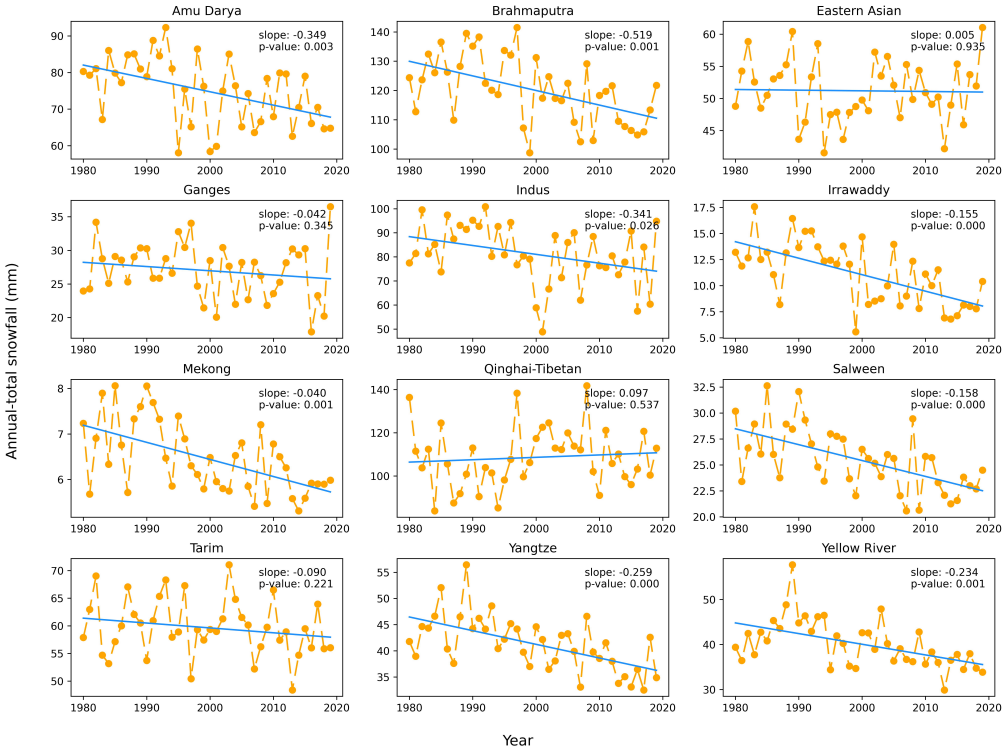

Figure 3.10: Temporal trend of accumulated annual, basin-mean snowfall from 1980 to 2020

Table 3.2: Statistics of trend analysis of annual-total basin snowfall from 1980 to 2020

Basin	Trend	Slope (mm/year)	p-value
Amu Darya	decreasing	-0.349	0.003
Brahmaputra	decreasing	-0.519	0.001
Eastern Asian	decreasing	0.005	0.935
Ganges	decreasing	-0.042	0.345
Indus	decreasing	-0.341	0.026
Irrawaddy	decreasing	-0.155	0.000
Mekong	decreasing	-0.040	0.001
Qinghai-Tibetan	decreasing	0.096	0.536
Salween	decreasing	-0.157	0.000
Tarim	decreasing	-0.090	0.221
Yangtze	decreasing	-0.259	0.000
Yellow River	decreasing	-0.233	0.001

3.2.3. Elevational distribution of snowfall

As snowfall is highly dependent on elevation, this part is then focus on its elevational distribution and temporal trends (Figure 3.11, 3.12, 3.13). Indus, Brahmaputra, Ganges, Indus, Irrawaddy, Mekong and Salween, as they cover a wide variation of terrains including high mountains ranges to low lands, and locate across the tropic and subtropic zone, snowfall only happens in mid-low elevations (above 2 km) in winter, spring, and autumn. Particularly in summer, snowfall is deposited mostly at altitudes higher than 4 km. Snowfall at elevation around 3.5-4 km in February-March contributes most to the annual total snowfall. In contrast, as Amu Darya lies in the temperate zone, lower temperature allows precipitation fall as snow even at low lands.

Still, snowfall at mid-high elevations in spring still accounts for the most important source in terms of annual total snow accumulation.

Eastern Asian, Tibetan, and Tarim, show slightly different snowfall patterns. Tibetan, as located in the high elevation region, snowfall happens all year. It is also characterized by delayed snowfall peaks in summer at elevation above 5 km. Eastern Asian and Tarim present similar pattern: snowfall is maximized in summer at high elevation. For Yangtze and Yellow River, snowfall occurs across all elevations due to the wide coverage of both basins. Moreover, the EASM influence on precipitation is prominent that snowfall peaks in both spring and autumn at high elevations.

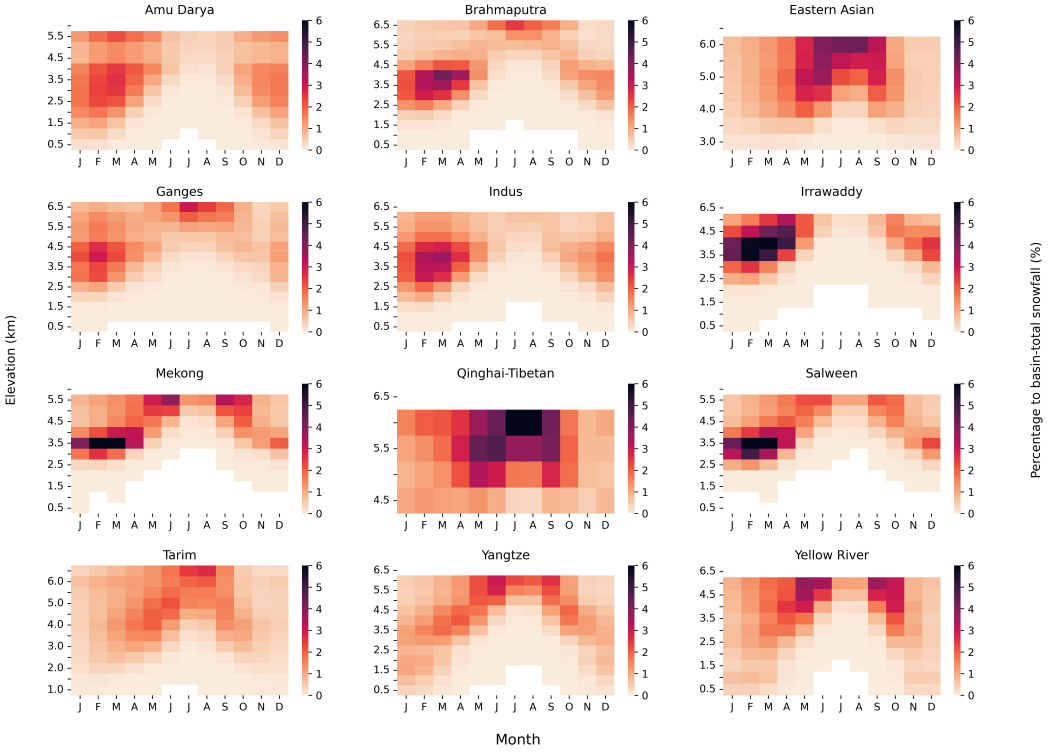

Figure 3.11: Elevational distribution of snowfall and its seasonal variations, the color representing the snowfall values in m at each 500 m elevation band

With an insight of how snowfall is distributed across elevation, its temporal trend is hereinafter analyzed. Figure 3.12 and Figure 3.13 give information about the absolute and relative trend, respectively. In general, snowfall at low-mid elevation has reduced over the 40 years in all catchments. For Amu Darya, Brahmaputra, Ganges, Indus, Irrawaddy, Mekong, Salween, a sharp decreasing trend of approximately 0.01 mm/month/year is identified. However, increasing trend is also found occasionally in mid-high elevations. Amu Darya, Ganges, and Indus showed strong increasing trend in February at elevations above 2 km. For Amu Darya and Indus, increasing trend also prevails in November. Specially, Eastern Asian, Tibetan, and Tarim, show pervasive increasing trend, albeit with a smaller magnitude of about 0.005 mm/month/year from September to November, January to February across all elevations, and in summer months at high elevations. With respect to relative changes, many basins experience decreasing snowfall of about 2%/year, for instance, Amu Darya, Brahmaputra, Eastern Asian, Irrawaddy, Mekong, Salween, Yangtze and Yellow River. In contrast, the increasing trends are comparatively less pronounced.

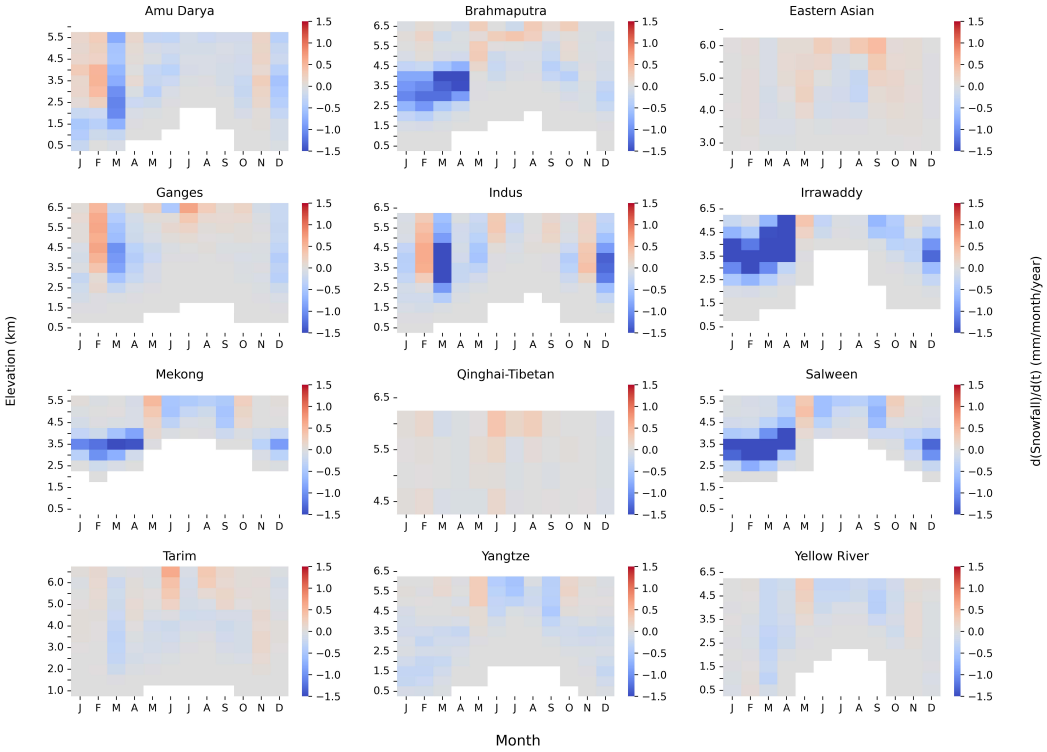

Figure 3.12: Absolute temporal trend of snowfall at each 500 m elevation band from 1980 to 2020, with the color representing the temporal trend in mm/month/year

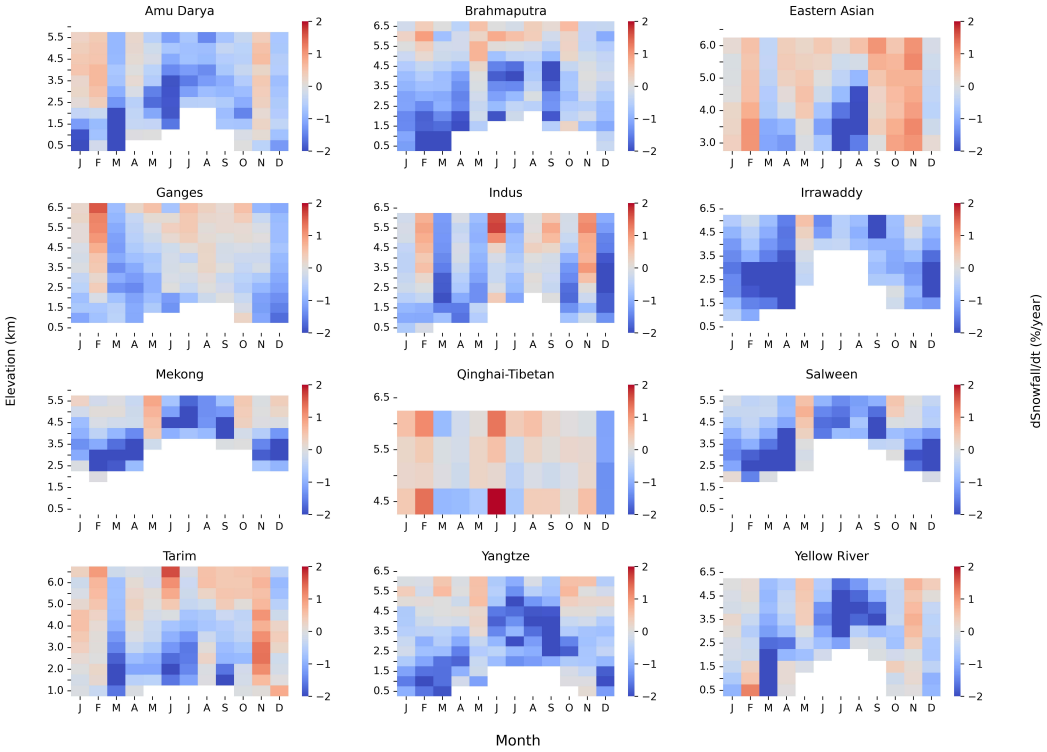

Figure 3.13: Temporal trend of snowfall at each 500 m elevation band from 1980 to 2020 relative to the mean over the period 1980-2020, with the color representing the changes in snowfall in %/year

3.3. Snowmelt analysis

In this section, spatiotemporal changes in snowmelt are also evaluated with respect to spatial distribution, basin-scale variability, and elevational distribution.

3.3.1. Spatio-temporal distribution of snowmelt

Figure 3.14 gives information about the spatial distribution and seasonal variations of snowmelt (>0.1 mm/day). In general, high mountain regions are identified as the hotspot area for snowmelt, especially in spring and summer seasons. In November and December, noticeable snowmelt only occurs in the eastern Himalayas (in Bramaputra). Gradually, in January, snowmelt along the Hiamalays is found. From February to June, snowmelt is highly dependent on elevation, and evolution of snowmelt from low-mid altitude toward high elevational area is recognized: massive snowmelt started from the outline of the northern-west Tien Shan, Pamir plateau, Karakoram, Hindu-Kush, along the southern front of Himalayas and around the mountain ranges in Sichuan basin in the western-central Yangtze catchment. In March and April, snowmelt at these regions intensifies and intrudes to higher elevations. Significant snowmelt is also identified in the Kunlun Shan, Qinling, Tanggula, Nyenchen-Tanglha, and Hengduan Mountains in May, and is maximized in June. In July and August, snowmelt in the high mountain regions is reduced, yet in September and October, increasing snowmelt in eastern Tibetan mountains, Nyainqentanglha, and Hengduan Shan is found.

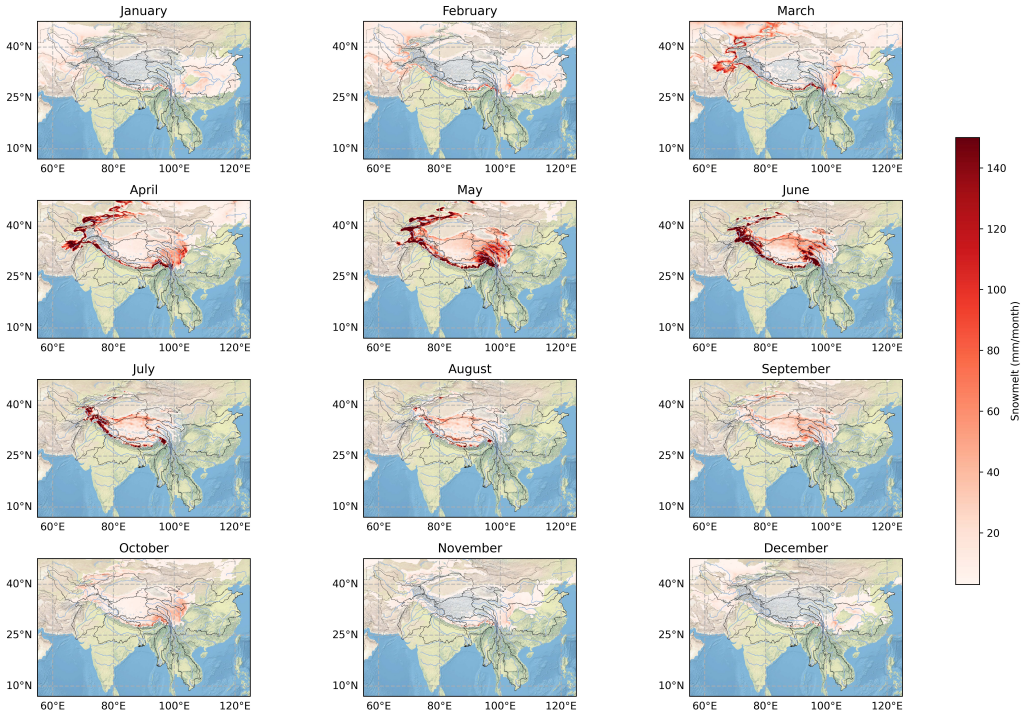

Figure 3.14: Monthly-averaged daily snowmelt (mm/month) from 1980 to 2020

To assess then temporal changes in snowmelt, the trend analysis is performed. Results show the absolute (Figure 3.15) and relative trend (Figure 3.16) distributions and seasonality of monthly-averaged daily snowmelt, as well as annual-averaged daily snowmelt (Figure 3.17).

Firstly, the absolute trend is analyzed. An decreasing trend presents in central Yangtze catchment from December to March. In the northern-west Yangtze, significant decreasing trend dominated from June to September. However, no increasing trend is found to compensate it and therefore it is expected to show an overall decreasing trend in the annual average. According to Figure 3.17 (left), significant decreasing trend prevails in the western and central Yangtze, albeit to a lesser extent. Similarly, in the low-land Amu Darya, significant decreasing trend is also found from January to March, which also presents in Figure 3.17). By contrast, Kunlun Shan shows an increasing trend in June, August and September, and results an overall increasing in annual average trend.

In addition, Figure 3.15 demonstrates a similar propagation of snowmelt trend as in Figure 3.14. Significant increasing trend is firstly identified in March along the outline (low elevation area) of the northern-west Tien Shan, Pamir, Karakoram, Hindu-Kush, the Himalayas, and Hengduan Shan. This increasing trend gradually migrates toward higher elevation in April, May, and June; the low-elevation area is left with decreasing trend. In July, increasing snowmelt trend only presents in the central Himalayas, and the high mountain regions are characterized by a strong decreasing snowmelt trend. However, this effect is averaged in Figure 3.17, and an overall significant decreasing trend dominate in the relatively low-elevation regions in Tien Shan, Karakoram, Hindu-Kush, and the Himalayas.

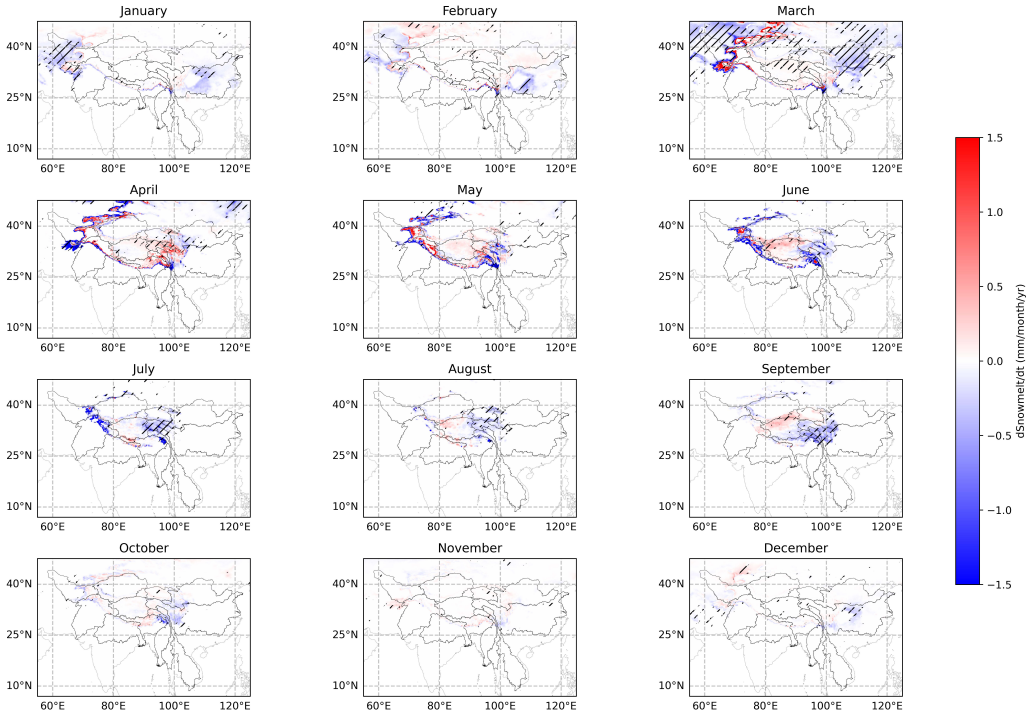

Figure 3.15: Temporal trend of monthly-averaged daily snowmelt (mm/month/year) from 1980 to 2020, with hatched area implying the significant changes

As the daily snowmelt amount is small in most areas, the relative trend would give better description of the spatial and seasonal variations. In Figure 3.16, the relative temporal trend is largely heterogeneous across the study area. In the central Yangtze, intensive, significant decreasing trend is found from December to March. Similarly in the Northern-west Yangtze, significant decreasing trend presents from June to September. This gives an overall decreasing trend about 2% per year in the central Yangtze, as shown in Figure 3.17. In Yellow river, robust and significant decreasing trend presents in January and March, yet increasing trend is also identified in part of the basin from October to February. Despite of this, an annual decreasing trend is recognized. Similarly, Amu Darya shows significant decreasing trend in Jan and March, which results the overall decreasing trend in annual pattern.

By contrast, the majority of Tarim and Eastern Asian is found with increasing trend from October to February, and this give rise to the overall increasing trend especially in the central of both basins. Specially, noticeable trend presents along the Kunlun Shan. For the central Kunlun Shan, significant increasing trend prevails from February to June, also November and October. However, pronounced decreasing trend also persists from July to September in the eastern Kunlun shan. These are further evidenced by the annual trend in Figure 3.17, that the central Kunlun Shan is characterized by significant increasing trend of about 1%/year and decreasing trend in the eastern Kunlun Shan. Likewise, the evolution of trend in Northern-west Kunlun, Pamir, Karakoram, Hindu-Kush, the Himalayas is again observed. This evolution of snowmelt along altitudes would be further evaluated in later section.

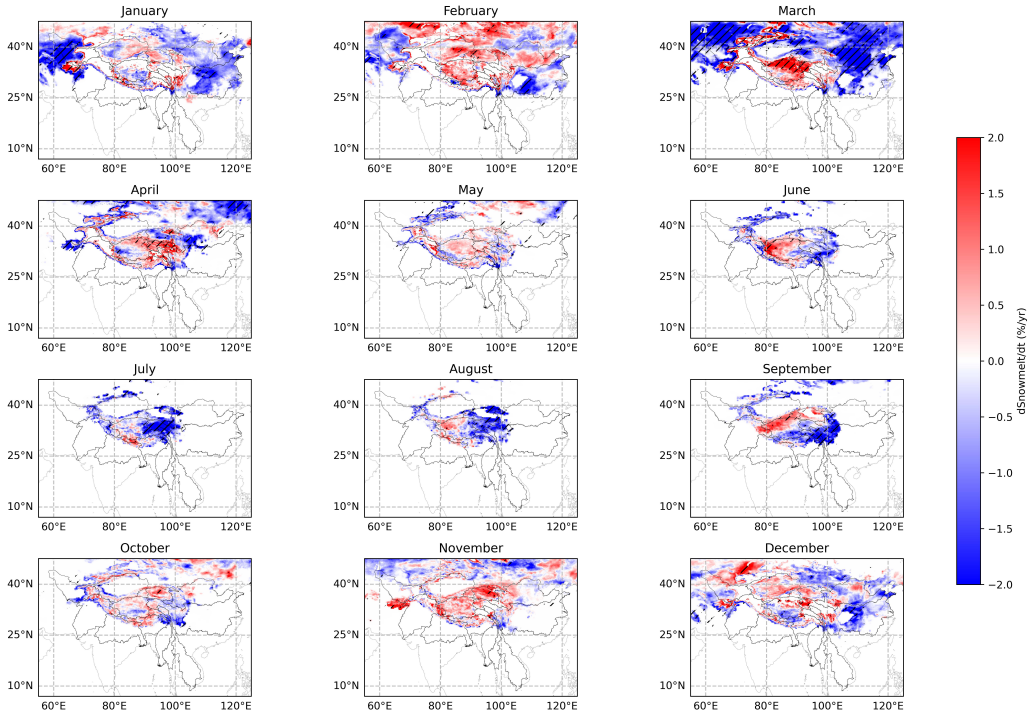

Figure 3.16: Temporal trend of monthly-averaged daily snowmelt (mm/month/year) from 1980 to 2020, relative to the mean of 1980-2020, with hatched area implying the significant changes

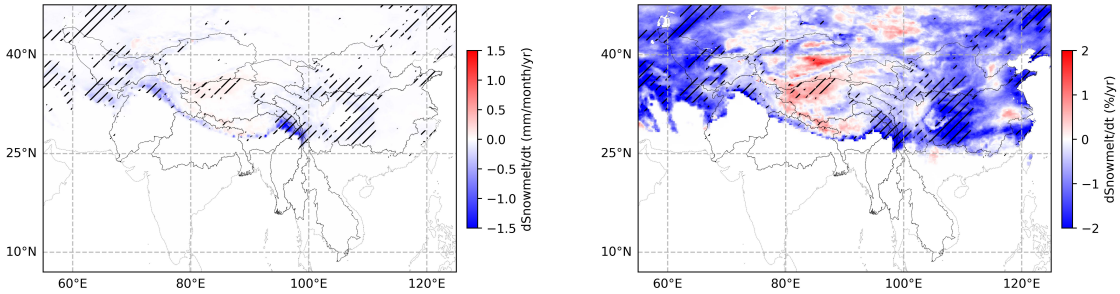

Figure 3.17: Absolute temporal trend (left) and relative temporal trend (right) of monthly-averaged daily snowmelt (mm/month/year) from 1980 to 2020

3.3.2. Inter-annual snowmelt variability

Building upon the spatial distribution of snowmelt, the analysis of inter-annual variability of basin-averaged snowmelt is conducted to facilitate comparing snowmelt patterns and showcasing temporal changes.

Figure 3.18 gives information about the seasonal and temporal changes in basin-average daily snowmelt, which differ greatly for catchments. Amu Darya, Brahmaputra, Ganges, Indus, and Irrawaddy show a single-peak melting pattern, with maximum snowmelt occurring in June, May, May, June, and May, respectively. Specially, for Irrawaddy, a sharp reduction in snowmelt from May to June is recognized. By contrast, Mekong and Salween present a two-peak melting pattern, with high peak snowmelt in May, and second snowmelt peak in September. The second peaks in snowmelt are as a result of EASM that brings abundant precipitation in September-October. Eastern Asian, Qinghai-Tibetan, and Tarim demonstrate a prolonged melting season, with maximum snowmelt arising in June. Similarly, in Yangtze and Yellow river, snowmelt also persists for

most of the year, excluding July and August. This could be caused by the wide-spread snow event in the central and eastern Yangtze and Yellow river in winter seasons. Temporal evolution of snowmelt could also be spotted from Figure 3.18. The maximum daily snowmelt is reduced in Amu Darya, Ganges, Indus, Irrawaddy, Salween, Yangtze and Yellow river. Moreover, many basins undergo snowmelt reduction in also off-peak months, for instance, Brahmaputra, Indus, Irrawaddy, Yellow river, suggesting decreasing in snowmelt water locally.

The temporal changes are further quantified by trend analysis and results are shown in Figure 3.19. Significant decreasing trend is found for many basins. From June to September, Brahmaputra, Irrawaddy, Mekong, Salween, Yangtze, and Yellow River, experience less snowmelt. The decreasing trend accounts for about 3%/year in Irrawaddy in June. Decreasing trend is also identified in Irrawaddy from December to May. In terms of increasing snowmelt, only Eastern Asian in November and Tibetan in March are recognized with significance.

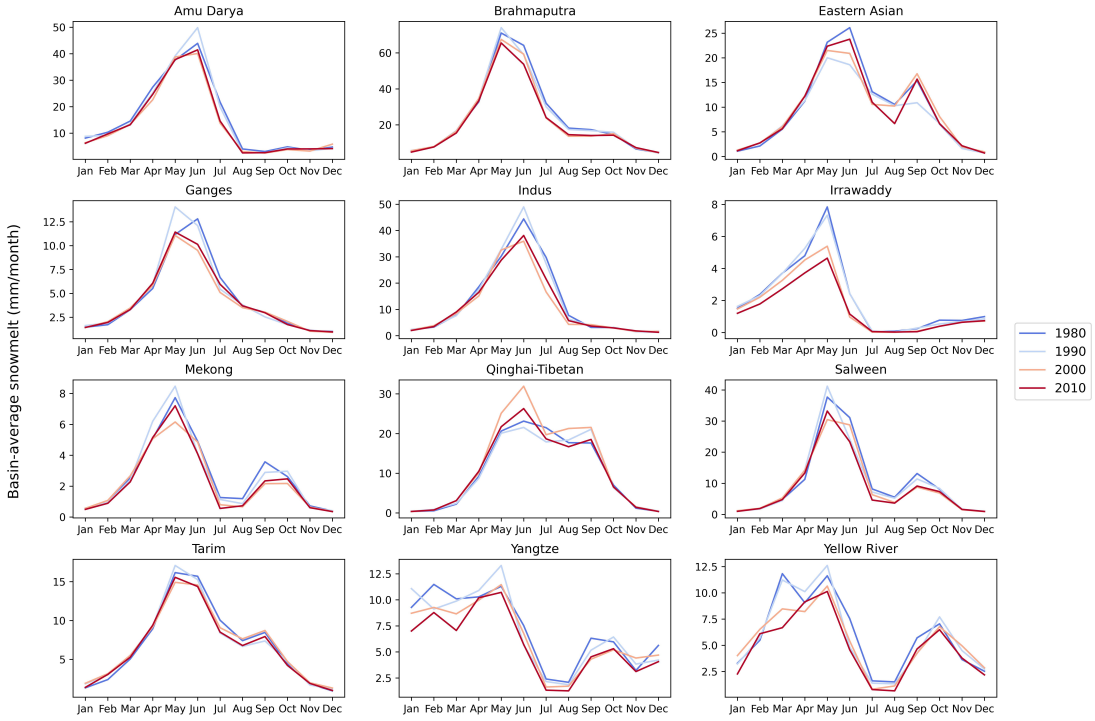

Figure 3.18: Seasonality and inter-annual variability of basin-average daily snowmelt (mm/month), for every 5 year interval from 1980 to 2020

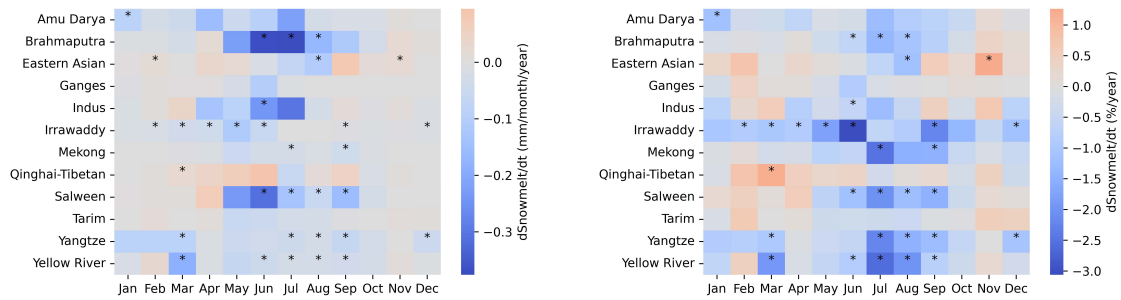

Figure 3.19: Absolute temporal trend (left) and relative temporal trend (right) of basin-average daily snowmelt (mm/month/year) from 1980 to 2020

Table 3.3: Statistics of annual average snowmelt trend in each basin

	Trend (mm/month/year)			Trend (%/year)			Trend (km^3/month/year)
	Mean	Min	Max	Mean	Min	Max	Mean
Amu Darya	-0.058	-0.319	0.626	-0.957	-2.26	2.56	-0.089
Brahmaputra	-0.111	-1.80	0.596	-0.328	-3.26	1.06	-0.139
Eastern Asian	-0.001	-0.133	0.340	0.0969	-0.987	2.79	-0.001
Ganges	-0.011	-1.05	0.220	-0.302	-2.02	1.31	-0.021
Indus	-0.056	-0.758	0.454	-0.462	-3.78	1.94	-0.124
Irrawaddy	-0.027	-1.34	0	-1.01	-2.69	0	-0.021
Mekong	-0.015	-1.08	0	-0.375	-2.46	0	-0.065
Tibetan	-0.024	-0.148	0.336	-0.195	-0.958	2.52	-0.025
Salween	-0.066	-1.217	0.056	-0.545	-2.49	0.150	-0.119
Tarim	-0.008	-0.209	0.439	-0.066	-1.73	3.08	-0.012
Yangtze	-0.042	-0.814	0.052	-0.915	-2.57	0.779	-0.188
Yellow River	-0.032	-0.212	0.027	-0.749	-1.81	0.342	-0.071

The annual total snowmelt for each basin is accumulated from daily snowmelt for each basin over the period 1980 to 2020, and trend analysis is also conducted to evaluate the temporal changes. Results are visualized in Figure 3.20 and test statistics are listed in Table 3.4. The significance level is chosen to be 0.05, which means that significant trends are only identified with p value smaller than 0.05. In this sense, Brahmaputra, Indus, Irrawaddy, Mekong, Salween, Yangtze and Yellow River are found to experience reduced annual snomwelt.

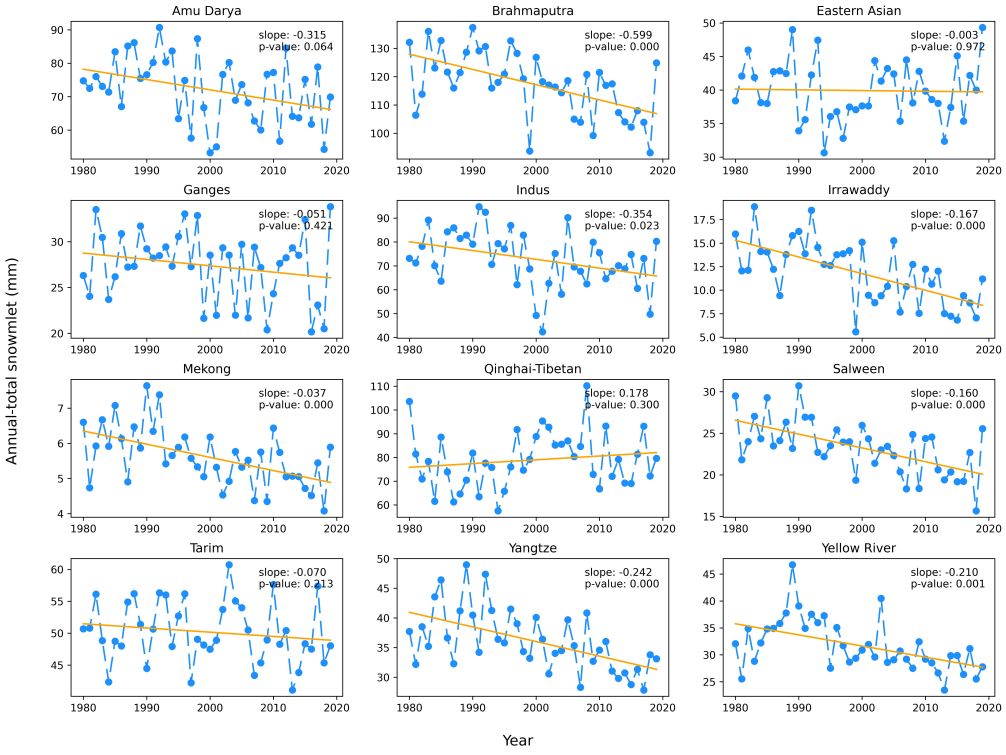

Figure 3.20: Time series and temporal trend for accumulated annual basin-average snowmelt (mm/year) from 1980 to 2020

Table 3.4: Statistics of trend analysis of accumulated annual basin-average snowmelt (mm/year) from 1980 to 2020

Basin	Trend	Slope (mm/year)	p-value
Amu Darya	decreasing	-0.315	0.064
Brahmaputra	decreasing	-0.599	0.000
Eastern Asian	decreasing	-0.002	0.972
Ganges	decreasing	-0.051	0.421
Indus	decreasing	-0.354	0.023
Irrawaddy	decreasing	-0.167	0.000
Mekong	decreasing	-0.036	0.000
Qinghai-Tibetan	increasing	0.178	0.300
Salween	decreasing	-0.160	0.000
Tarim	decreasing	-0.070	0.213
Yangtze	decreasing	-0.242	0.000
Yellow River	decreasing	-0.210	0.001

3.3.3. Elevational distribution of snowmelt

As found in Figure 3.14, there is an progression of snowmelt from low-elevation to high elevation in the HMA, i.e., Tien Shan, Pamir plateau, Karakoram, Hindu-Kush, and the Hiamalayas. This altitudinal evolution of snowmelt is further observed in Figure 3.21: pronounced snowmelt firstly occurs at low elevation in early spring, and it is gradually taken over by mid-high elevational snowmelt in later months.

Figure 3.21 shows distinct elevational distribution and evolution of snowmelt for each basin. In general, Amu Darya, Brahmaputra, Ganges, and Indus demonstrate similar patterns. The western basins, i.e., Amu Darya and Indus, show a relatively shorter snowmelt season from March to July, whereas for Ganges and Bramaputra, pronounced snowmelt persists from February to August. Moreover, Amu Darya and Indus are characterized with prominent snowmelt contribution from 2.5-5 km. By contrast, Brahmaputra and Ganges show considerable snomwelt from 3-6.5 km. However, from the perspective of maximum annual snowmelt contribution, all four basins depend primarily on the mid-elevation snowmelt either in May or June at about 4 km altitude.

Catchments in the south, i.e., Mekong, and Salween, also behave similarly in terms of snowmelt. From February to May, mid-elevational snowmelt prevails. However, from July to September, high-elevational snomwelt predominates. According to Figure 3.18, a minor peak presents as a result of snowmelt at high-elevation. Also it is noteworthy to address Irrawaddy here, as it experiences short season from March to June with snowmelt from 3.5-5 km contributing mostly.

For Eastern Asian and Tarim, both undergo melting period from March to October. Yet Tarim is characterized by pronounced snowmelt at mid-elevation in May and June, whereas Eastern Asian in July and August. However, for Qinghai-Tibetan, as it altitudinal distribution is more uniform and comprises of mostly high elevations, it shows a delayed, and more concentrated snowmelt period from April to October, with snowmelt from the high elevation in July and August contributing most to the annual total.

Lastly, in Yangtze and Yellow river basin, yearlong snowmelt is observed. In Yangtze, snowmelt at high mountains in June and July contributes most the annual total, yet for Yellow river snowmelt in May and June at high elevation regions is the most prominent contribution.

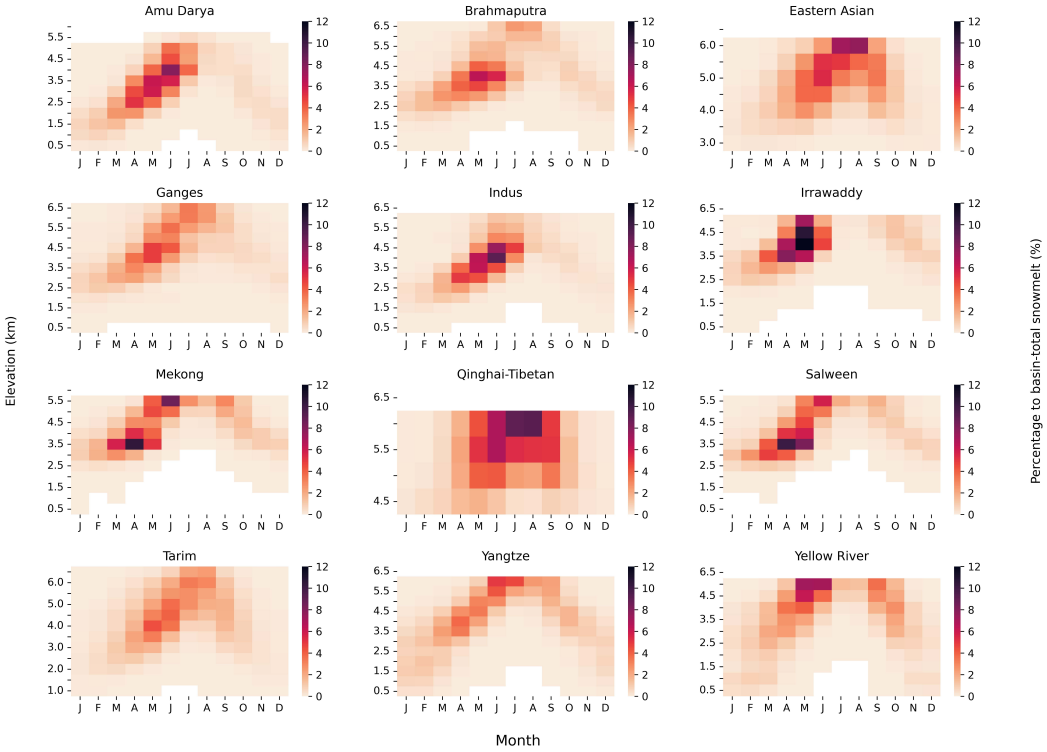

Figure 3.21: Elevational distribution of snowmelt and seasonal variations, the color representing the percentage of snowmelt at each 500 m elevation band to the annual total basin snowmelt

The elevational distribution differs for each basin. In general, mid-high altitude snowmelt is the most important contributor of the annual total snowmelt. How snowmelt at each elevation changes with time is then analyzed. Figure 3.22 and Figure 3.23 give information about the temporal trend from 1980 to 2020 for every 500 m elevation band. In general, most basins demonstrate decreasing trend of snowmelt in the lower elevation, yet increasingly more snowmelt in higher altitude at those elevational bands where considerable snowmelt occurs. However, Qinghai-Tibetan is distinguished from other basins as it shows mostly increasing trend across all elevation. This could result from its uniform, and high altitudinal distribution.

Hotspots identified that contributes most to the annual total snomwlet in Figure 3.21, experiences reduced snowmelt in most basins, except for Eastern Asian and Tibetan where increasing trend was recognized. Specially, in both basins, the hotspots are found in the highest elevation band. Similarly, high elevation bands in Brahmaputra, Ganges, Tarim, Yangtze, and Yellow River are also characterized by increasing snowmelt trend. This may suggest that more snowmelt widely arose across high elevations. This pattern is more notable in Figure 3.23: high mountain regions in winter and early spring that does not contribute markedly to annual total snowmelt are identified to experience increasing snowmelt, whereas spring and summer snowmelt that is pronounced undergo decreasing trend from 1980 to 2020. In this sense, it could be inferred that snowmelt from higher elevation is increasingly more important for spring and summer melt water.

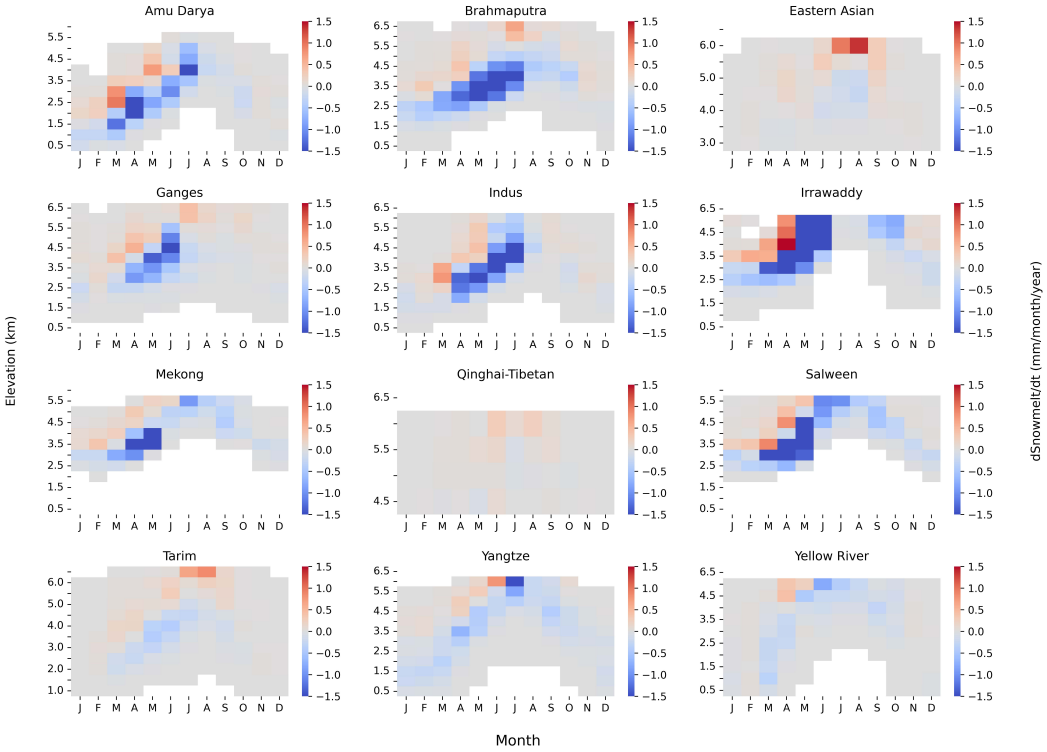

Figure 3.22: Temporal trend of snowmelt at each 500 m elevation band from 1980 to 2020, the color representing the changes in snowmelt in mm/year

In conclusion, this analysis provides insights into the elevational and seasonal distribution of snowmelt, with catchments displaying distinct patterns as a result of climatic and topographic differences. Specially, across all basins it is found that higher elevation snowmelt is intensified, whereas low-mid elevation snowmelt is reduced.

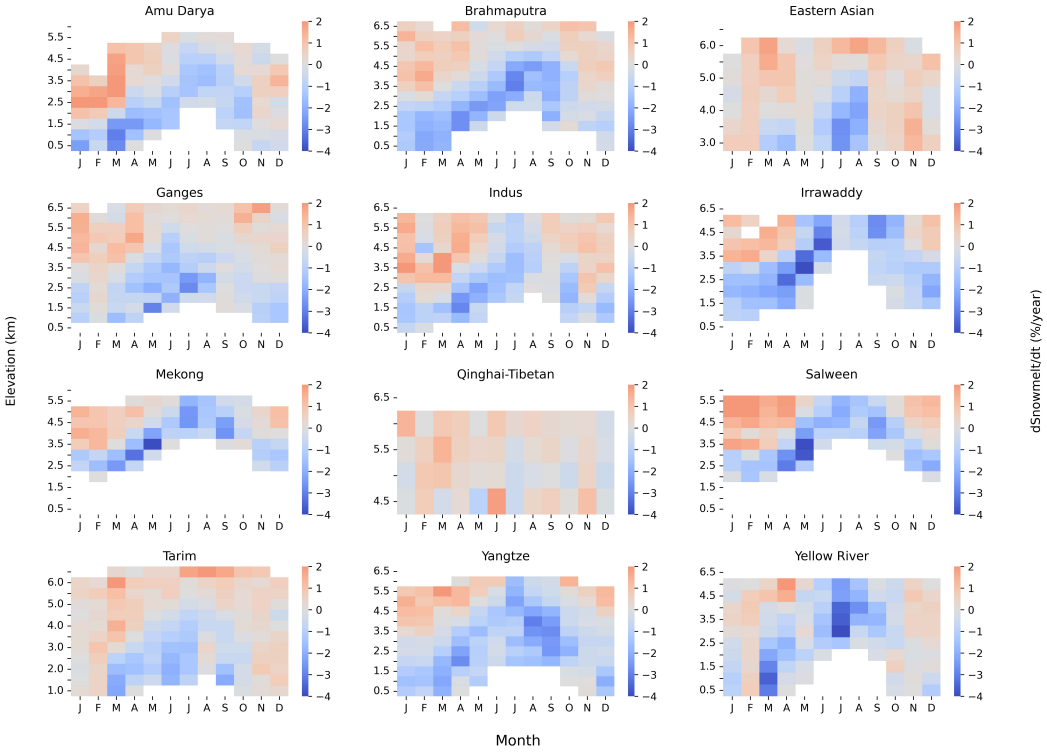

Figure 3.23: Temporal trend of snowmelt at each 500 m elevation band from 1980 to 2020 relative to the mean over the period 1980-2020, with the color representing the changes in snowmelt in %/year

3.4. SWE analysis

In this part, spatiotemporal changes in SWE are analyzed, and elaborated on spatial distribution of SWE, basin-scale inter-annual variability, and elevational distribution of SWE.

3.4.1. Spatial and seasonal distribution of snowpack

The spatial and temporal distribution of non-negligible SWE (> 5mm) varies greatly over the 12 HMA river basins, as shown in Figure 3.24. The 5mm threshold is derived from previous study, which has substantiated that the detection of shallow snow is unreliable (Smith and Bookhagen 2018a). Intense snowpack presents primarily in the Northern-west, i.e., in Tien Shan, Pamir, Kunlun Shan, Karakoram, the Hindu Kush Himalayas, where altitudes are high and directly exposed to the WWD. Specially, persistent snowpack identified in Pamir, Karakoram, and along the Himalayas, with SWE around 10 m. Snowpack in the southern-east of HMA, i.e, Tanggula Shan, Hengduan Shan, and Nyainqentanglha, are less abundant as they receive most precipitation in summer from ISM and EASM. The Northern-east of HMA, where the eastern Kunlun Shan, Qilian Shan, and the eastern Tibetan show the least abundant snowmpack as a result of being distant from major moisture sources.

Accumulation of snow is observed from September, in Tien Shan, Pamir, Kunlun Shan, Karakoram, the Hindu Kush Himalayas, Tanggula Shan, Hengduan Shan, and Nyainqentanglha, and peaks in April. From May onwards, snowpack depletes gradually, and in August, minimal SWE magnitude exhibits across the entire HMA and most regions are snow-free. In the accumulation phase, SWE in Tanggula Shan, Nyaingentanglha, and Hengduan Shan grow considerably in September due the summer monsoon precipitation. By contrast, snowpack in the northern-west HMA arises significantly in December, January, and February as a result of the WWD.

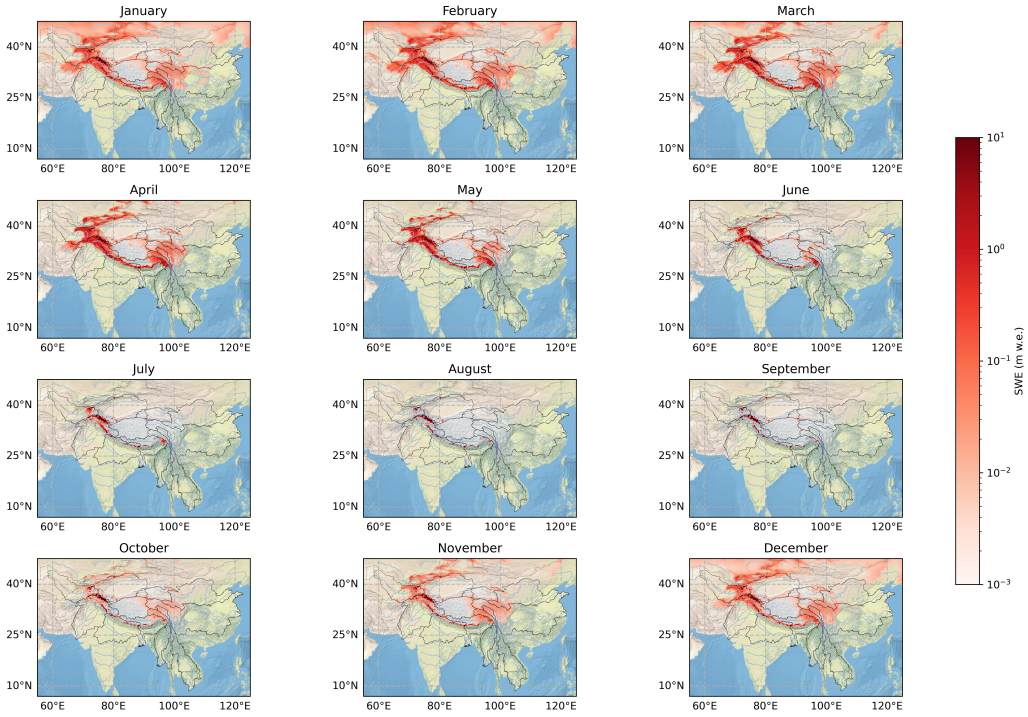

Figure 3.24: Average monthly SWE (mm) from 1980 to 2020

This seasonal cycle of snow accumulation and reduction would provide a considerable amount of water for over a billion people living across Asia (Kouki et al. 2023). Therefore, the temporal changes in SWE is assessed from the study period 1980 to 2020. In Figure 3.25, the absolute monthly SWE changes are quantified. Strong increasing trends, albeit insignificant are observed in the Tien Shan, Pamir, Eastern Tibetan Mountains, and Tanggula areas from November to March, but are compensated by intense decreasing trend from April to June. Similarly, the central Himalayas ranges in Ganges, show increasing trend in February and March, yet is counteracted by strong decreasing trend in other months. By contrast, the Kunlun Shan ranges presents an increasing trend for most of the seasons and is expected to have an overall increasing SWE. However, in the Hindu-Kush, western and eastern Himalayas, as well as Nyainqentanglha regions, yearlong decreasing trends are recognized.

Relative trends in annual-average SWE are also computed and visualized, as shown in Figure 3.27 (left). Overall increasing trends are identified in Pamir, Kunlun Shan, Qilian, and Tanggula-Qinling regions, though not considered as significant. In contrast, significant decreasing trends are detected in the mid-elevation regions in Pamir, Hindu-Kush Himalayas, Nyainqentanglha, Hengduan Shan, and the central Yangtze basins.

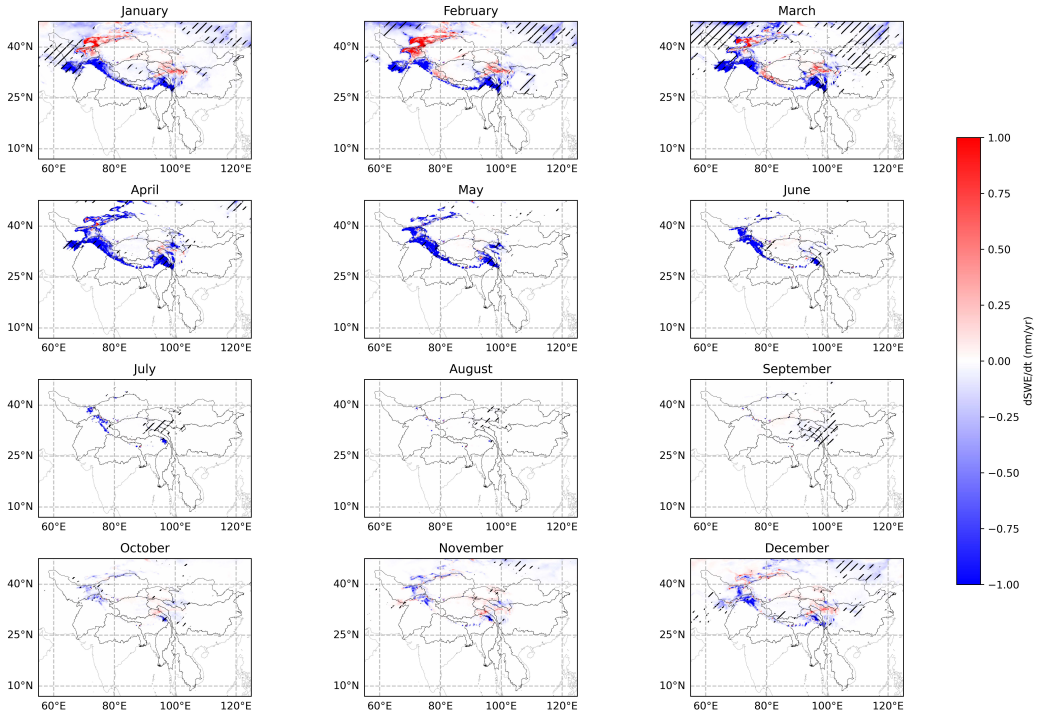

Figure 3.25: Temporal trend of monthly SWE (mm) from 1980 to 2020, with hatched area implying the significant changes

However, as SWE varies spatially and seasonally, the relative temporal SWE trend is calculated to have a better estimation of local SWE changes in terms of percentage. Figure 3.26 gives information about the temporal trend of monthly SWE relative to the average SWE from 1980-2020, which shows heterogeneous changes in SWE across the study area. Significant decreasing trends are found in the western Amu Darya in January, but not compensated by increasing trend in other months. Significant decreasing trends in the central Yangzte were also identified in winter from January to March. By contrast, considerable long-term increasing trends are found in Tien Shan, Kunlun Shan, and Qilian Shan mostly in winter and spring.

Temporal changes in annual-mean SWE are shown in the Figure 3.27 (right). The low-land of Amu Darya, Hindu-Kush, the western Himalayas, Hengduan Shan and the central Yangtze basin, as well as the Shandong peninsula, show significant decreasing trend of SWE, which approximately account for 2% of 40-year annual mean SWE. However, in the eastern Tarim, western Qaidam, and the Kunlun-Qinling mountain ranges, positive trends of increasing SWE are presented.

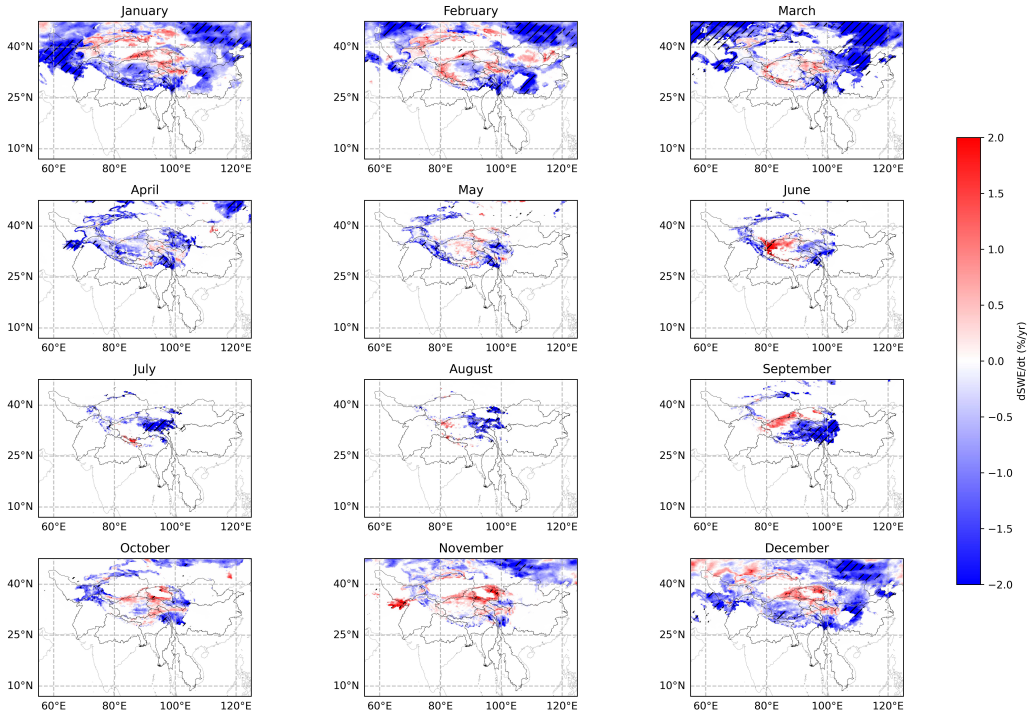

Figure 3.26: Temporal trend of monthly SWE (%) from 1980 to 2020, relative to 40-year average SWE, with hatched area implying the significant changes

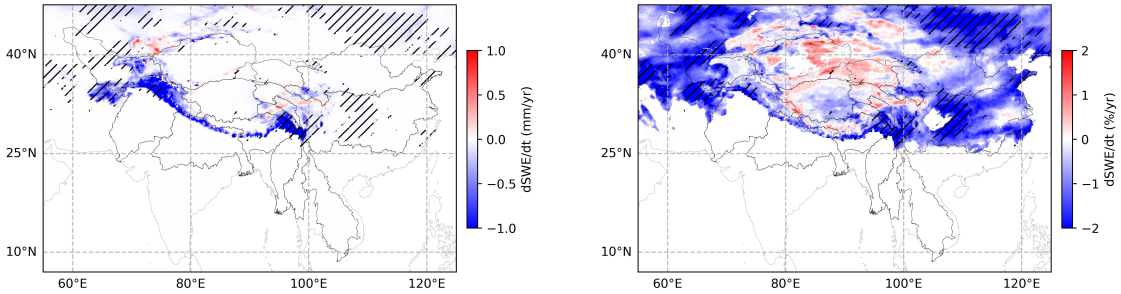

Figure 3.27: Absolute temporal trend (left) and relative temporal trend (right) of annual-average SWE from 1980 to 2020, with hatched area implying the significant changes

3.4.2. Inter-annual SWE variability

With understanding of spatial distribution of SWE, it is then focused on basin-average climatology to evaluate intra-annual and inter-annual changes, as well as comparing magnitude of SWE for all basins. The basin-average SWE is firstly computed and every 10-year mean values are then calculated to evaluate the seasonal patterns and temporal changes in seasonality, and the results are shown in Figure 3.28.

In general, Indus, Amu Darya, and Bramaputra possess the most snow water, and show seasonal accumulation (reduction) of about 100 mm. Salween, Ganges, and Tarim demonstrate mediocre snow water storage, and approximately 40 mm, 20 mm, and 10 mm changes in seasonal SWE are found. Other basins, for instance, Eastern Asian, Irrawaddy, Mekong, Tibetan, Yangtze and Yellow River, are characterized by less basin-average SWE, and exhibit changes in SWE of less than 10 mm in seasonal cycles.

Table 3.5: Statistics of annual average SWE trend in each basin

	Trend (mm/month/year)			Trend (%/year)			Trend (km^3/month/year)
	Mean	Min	Max	Mean	Min	Max	Mean
Amu Darya	-0.119	-17.6	8.66	-1.10	-3.22	0.308	-0.183
Brahmaputra	-0.417	-13.5	9.37	-0.706	-3.81	1.02	-0.521
Eastern Asian	-0.005	-14.3	0.142	0.234	-1.53	1.12	-0.004
Ganges	-0.006	-14.0	0.468	-0.586	-3.29	0.628	-0.011
Indus	-0.257	-28.2	9.85	-0.652	-3.42	1.39	-0.568
Irrawaddy	-0.057	-5.08	0	-1.38	-3.94	0	-0.045
Mekong	-0.016	-3.16	0.499	-0.443	-3.61	1.29	-0.071
Tibetan	-0.013	-13.1	0.272	-0.220	-2.31	1.44	-0.014
Salween	-0.141	-4.82	0.518	-0.799	-3.46	0.670	-0.254
Tarim	-0.038	-23.2	10.4	0.027	-2.38	1.65	-0.057
Yangtze	-0.023	-2.28	0.507	-0.962	-3.53	1.60	-0.103
Yellow River	-0.022	-0.954	0.490	-0.569	-2.72	1.16	-0.049

SWE varies considerably in basins in different seasons. Firstly, Irrawaddy experiences a prolonged snow-free period, i.e., from June to November. Yet Mekong, Yangtze and Yellow river endure a shorter snow-free period only in July and August. In contrast, other basins show yearlong snow cover. Secondly, in terms of seasonality, all basins exhibit a peak basin-average SWE in between March and April, and minimal SWE in August. Eastern Asian, Qinghai-Tibetan, and Tarim present snow accumulation phase from August to April, and snow reduction phase from April to July. However, other catchments show shorter snow accumulation phase. In September, Mekong, Salween, Yangzte and Yellow river start to gain snow water storage. Then, in October, Amu Darya, Brahmaputra, Ganges, and Indus, SWE increases gradually. However, only for Irrawaddy, it exhibits a delayed timing in snow accumulation in November.

Figure 3.28 also gives information about the temporal evolution of monthly basin-average SWE. In terms of the peak values, Amu Darya, Brahmaputra, Irrawaddy, and Salween, experience a pronounced reduction over 1980-2020. For Amu Darya, the peak SWE reduces approximately from 225 to 200 mm, for Brahmaputra from 210 to 175 mm, Irrawaddy from 12.5 to 5 mm, and Salween from 55 to 40 mm. Other basins, i.e., Ganges, Indus, and Tarim, show less consistent inter-annual reduction in peak SWE, yet overall decreasing trend could be recognized. However, Eastern Asian, Mekong, Tibetan, Yangtze and Yellow River present considerable intra-annual and inter-annual variability, but no conclusion could be generally drawn here. In this sense, trend analysis for basin-average SWE is entailed to provide quantitative insights into the temporal changes.

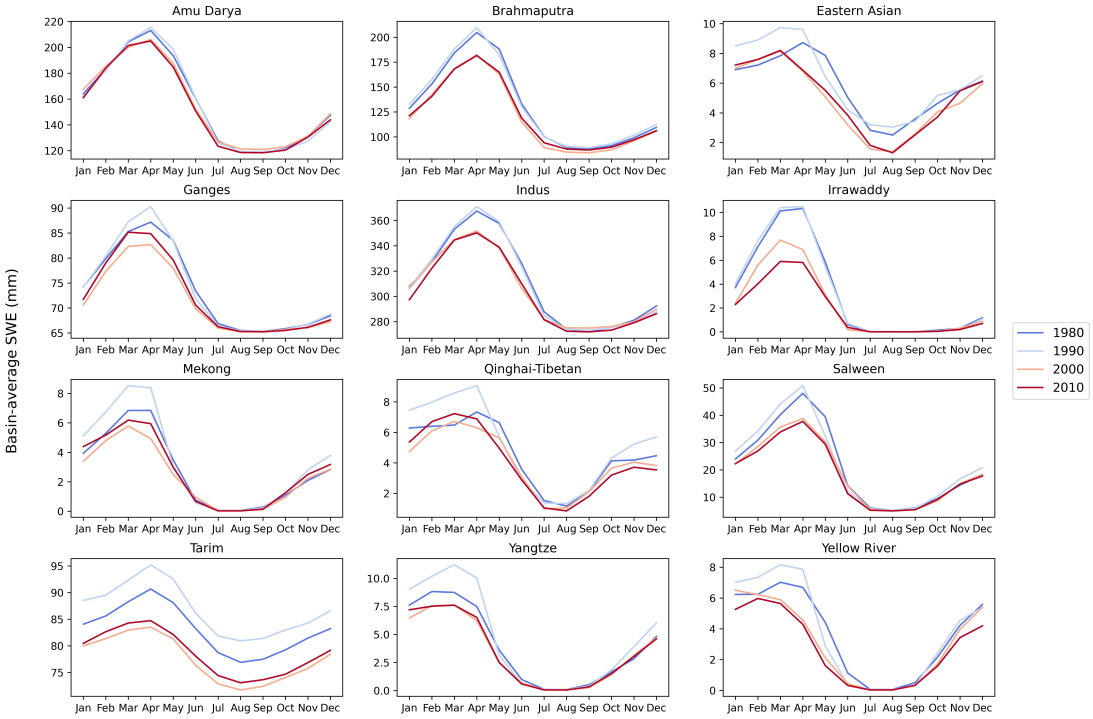

Figure 3.28: Seasonality and inter-annual variability of basin-averaged SWE (mm), for every 10-year interval from 1980 to 2020

Figure 3.29 gives information about the interannual variation of monthly total snowfall and snowmelt, as well as monthly average SWE, collectively. Snowfall and snowmelt differ in their peaking time, hence result in distinct SWE patterns. Generally, SWE increases when snowfall amount exceeds snowmelt, and decreases when snowfall is less than snowmelt. HMA basins show spatiotemporal differences in seasonal SWE patterns as a result of the interplay between geographical and climatic conditions that affect timing and magnitude of snowfall and snowmelt.

Figure 3.29: Interannual variability of 40-year-averaged monthly SWE (mm), snowmelt, and snowfall (mm/month)

Figure 3.30 showd the absolute temporal trend of monthly basin-average SWE from 1980 to 2020, as well as the temporal trend relative the the mean basin-average SWE over the period 1980-2020. Here only the significant trend values are plotted. Many basins are identified to have prominent negative trend in monthly basin-average SWE. Brahmaputra shows significant decreasing trend in basin average SWE from January to August, with a sharp reduction in peak SWE values of about 1 mm/year. Similarly, in Irrawaddy and Salween, albeit to a less extent (0-0.5 mm/year), significant decreasing trends are also recognized from January to June and September, respectively. Apart from Amu Darya, Mekong and Qinghai-Tibetan, all other basins experience reduction in peak SWE values in the spring season (March, April and May): Brahmaputra, Indus, Salween and Tarim show large negative trend, indicating significant decrease in peak SWE over 1980-2020.

As SWE distribution varies spatially for each basin, the relative trend is calculated as well to provide an in-depth understanding of local SWE changes. From Figure 3.30 (right), though Bramaputra is considered to have sharp SWE reduction, relative to its abundant snow water storage, the reduction is less prominent. In contrast, Irrawaddy shows significant decreasing trend from December to June, which accounted for about 2%/year of the basin-mean SWE in that month. In addition, Yangtze and Yellow river are also identified to experience from May to September. Salween also shows a prolonged reduction in SWE from January to September, albeit in a less prominent trend of about 1%/year.

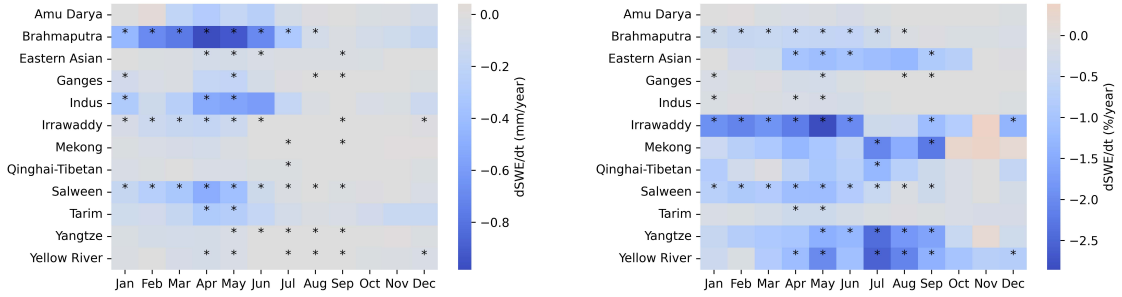

Figure 3.30: Absolute temporal trend (left) and relative temporal trend (right) of basin-average SWE from 1980 to 2020

In addition, time series and temporal trend of the annual-averaged, basin-mean SWE are also quantified to assess yearly SWE changes. As shown in Figure 3.31 and Table 3.6, all basins exhibit decreasing trend. Yet only Brahmaputra, Indus, Irrawaddy, Salween and Yellow River are considered to have significant reduction in SWE with a p-value less than 0.05.

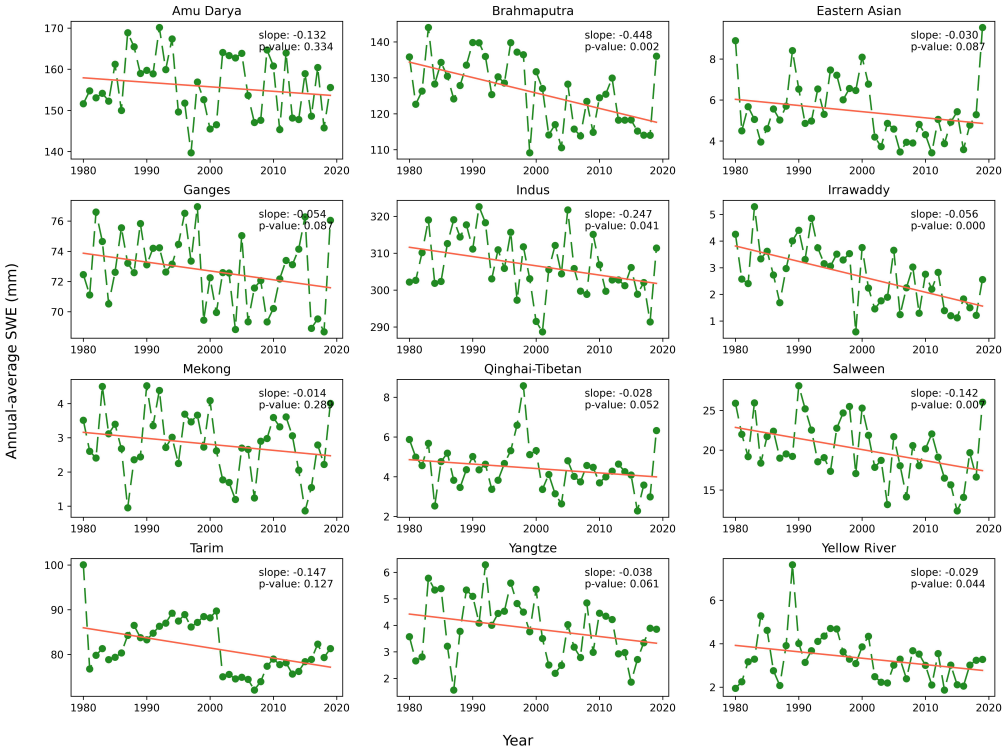

Figure 3.31: Temporal trend of Annual-average, basin-mean SWE from 1980 to 2020

3.4.3. Elevational distribution of snowpacks

As seen in Figure 3.24, the magnitude of SWE at the study area ranges from millimeters to meters. In Tien Shan, Kunlun Shan, Pamir, Karakoram, and along the Himalayas, giant snowpack persists. Yet at relatively lower altitude it is in diminutive quantity, accumulating and melting seasonally. Though spatial and temporal analyses provide insights into changes in snow water storage, where these changes occur in low- or high-SWE accumulated areas and the elevational distribution of these changes are not taken into account. In this sense, the elevational distribution of snowpack for each catchment is calculated and shown in Figure 3.32.

Table 3.6: Statistics of trend analysis of annual-average basin SWE from 1980 to 2020

Basin	Trend	Slope (mm/year)	p-value
Amu Darya	decreasing	-0.132	0.334
Brahmaputra	decreasing	-0.448	0.002
Eastern Asian	decreasing	-0.030	0.086
Ganges	decreasing	-0.054	0.086
Indus	decreasing	-0.247	0.041
Irrawaddy	decreasing	-0.056	0.000
Mekong	decreasing	-0.014	0.289
Qinghai-Tibetan	decreasing	-0.028	0.051
Salween	decreasing	-0.142	0.007
Tarim	decreasing	-0.147	0.127
Yangtze	decreasing	-0.038	0.061
Yellow River	decreasing	-0.029	0.044

Firstly, in Amu Darya, Brahmaputra, Ganges, Indus, Tarim and Eastern Asian, high elevation snowpack, i.e., above 5 km, shows no noticeable changes in SWE as yearlong snowpack persists at this elevation. For mid-high altitudinal areas (2-5 km), seasonal cycles of snow could be observed. Generally, snow accumulates in these catchments from September to April, and SWE reaches the maximum. From April to August, snowpack reduces gradually. At lower elevation (0-2 km), seasonal effect also plays a role. However, later snow accumulation and earlier SWE depletion is identified compared with mid-high areas. Moreover, at this elevation, snow-free days also occurs. As for Irrawaddy, Mekong, Qinghai-Tibetan, Salween, Yangtze, and Yellow river, SWE across all elevations shows seasonal accumulation and reduction. Lower elevations are characterized by delayed timing in accumulation and earlier onset of SWE reduction, contrary to higher elevations. In addition, Irrawaddy, Mekong and Salween show long snow-free periods across large regions. By contrast, as located in high plateau, Qinghai-Tibetan demonstrates yearlong persistent snowpack albeit in small values.

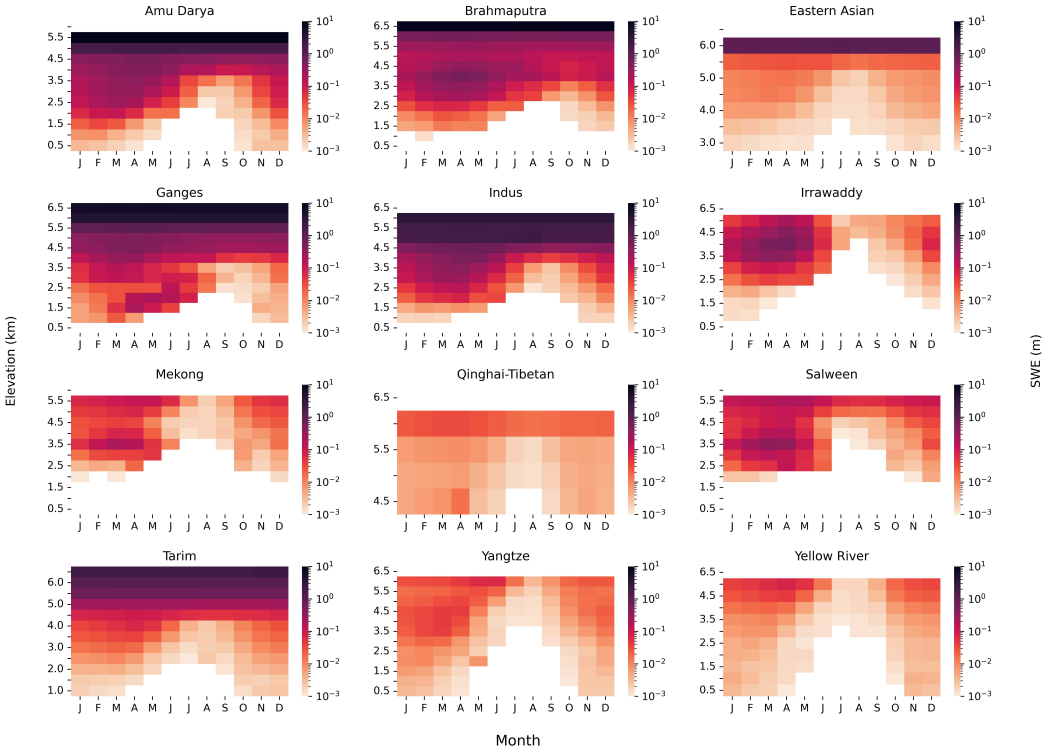

Figure 3.32: Elevational distribution of SWE and its seasonal variations, the color representing the SWE values in m at each 500 m elevation band

Aware of how SWE distributes across altitudes and changes with seasons, the temporal trend of SWE at each elevation band is therefore evaluated. Results are visualized in Figure 3.33. Relative trends were also available in Figure 3.34.Eastern Asian, Tibetan and Tarim is identified to experience consistent temporal SWE reduction over 1980-2020 at elevation greater than 6 km. Moreover, for all basins, decreasing trend is recognized in spring seasons, yet in different magnitude. Irrawaddy experiences the overall most negative SWE reduction of 10 mm/year at elevation around 4km in April and May. On the other hand, Amu Darya undergoes increasing SWE in winter seasons at mid-high elevation, and accounts for at most 0.5mm/year change. Other catchment, for instance, Indus, Tibetan and Yangtze, are also found with increasing trend, though in very small values.

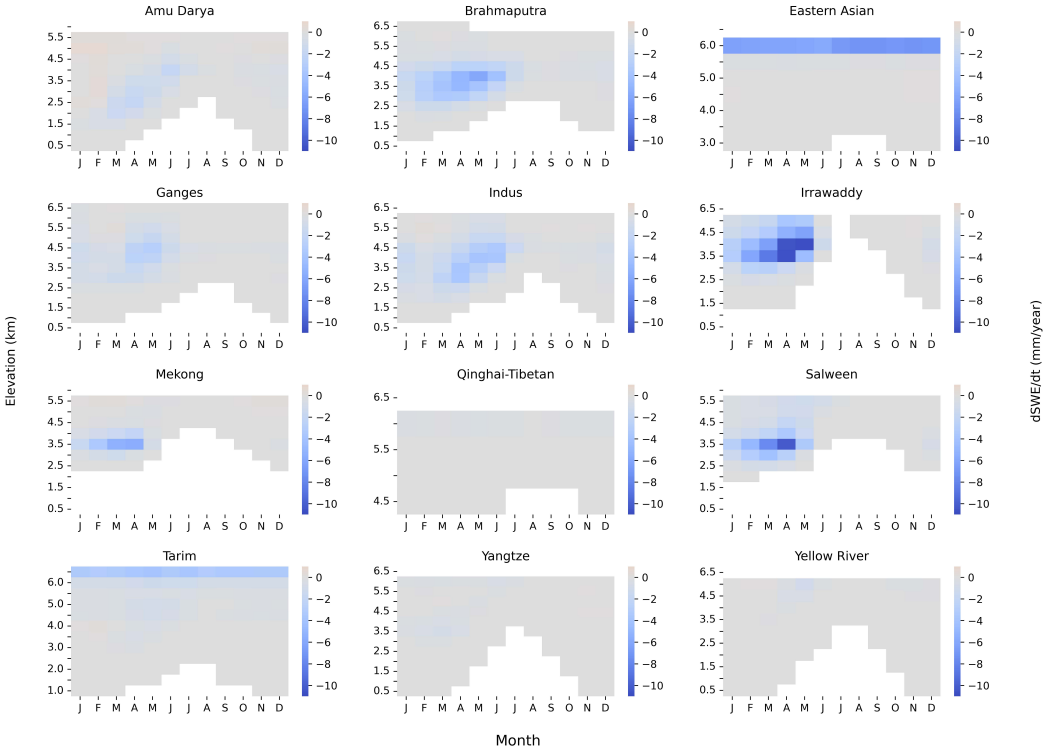

Figure 3.33: Absolute temporal trend of SWE at each 500 m elevation band from 1980 to 2020, with the color representing the temporal trend in mm/year

The relative trend gives more information about the temporal changes in SWE at local scale. The yearlong decreasing trend at high elevations in Eastern Asian, Tibetan and Tarim again is identified, yet in small percentages of about 1%/year. Tibetan also shows intermittent increasing trend. Similarly, Irrawaddy, Salween, Yangtze, and Yellow River show SWE reduction for most seasons at high elevations. By contrast, at high elevations Mekong is only recognized with decreasing SWE trend in summer. Then for low-mid elevations, many catchments, i.e., Amu Darya, Brahmaputra, Ganges, Indus, Irrawaddy, Mekong, Salween, Yangtze and Yellow river, are dominated by negative trend across year with magnitude ranging from 0 to -4%/year. However, for Eastern Asian and Tarim, in winter from October to February, increasing trend about 0-1%/year prevails in low-mid elevations, but in spring and summer decreasing SWE appears again. In summary, SWE distribution and temporal changes also display elevational and seasonal variations. Overall, snowpack at low-mid elevations is mostly decreasing, whereas at high elevations it is either unchanged or experiencing minor reduction.

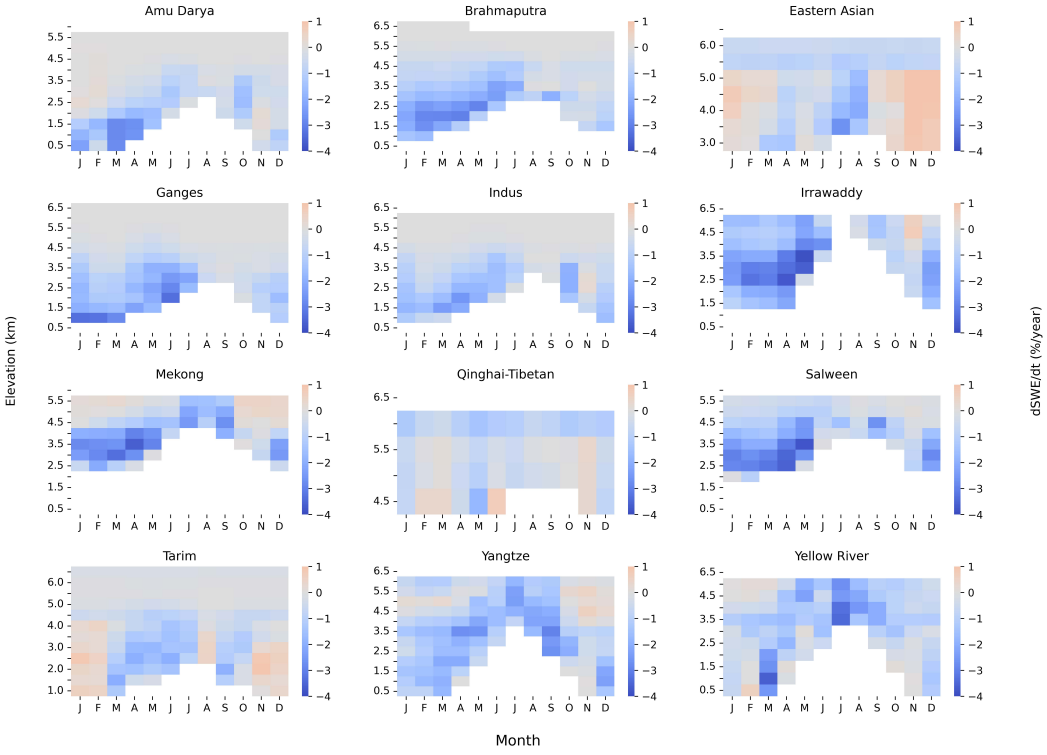

Figure 3.34: Temporal trend of SWE at each 500 m elevation band from 1980 to 2020 relative to the mean over the period 1980-2020, with the color representing the changes in SWE in %/year

3.5. Sensitivity to hydroclimatic factors

The variations in snow are influenced by multiple factors, including temperature, total precipitation, rainfall ration, and snow-related variables (Yang et al. 2022). In addition, topography, vegetation types and regional climate systems (i.e., monsoon), etc., are also important (Jenicek et al. 2016). Therefore, in this part, correlation analysis and composite was conducted to explore the climate sensitivity of snowfall, snowmelt, and SWE to temperature and precipitation. The influence of (extreme) temperature and total precipitation on SWE and snowmelt was again spatially and seasonally heterogeneous.

3.5.1. Correlation analysis

Snowfall is generally negatively correlated with temperature: the lower the temperature, the more snowfall is deposited (Figure 3.35). However, from November to March, snowfall in part of Tien Shan, Pamir, Karakoram and the eastern Himalayas are positively correlated with temperature. Moreover, from June to September, snowfall is more strongly connected with temperature than other months. In addition, spatial difference also present: snowfall in Tibetan and the central Yangtze is overall more negatively correlated with temperature than for instance, Tarim and Eastern Asian.

The relationship between precipitation and snowfall is more straightforward (3.36). For all basins, precipitation is directly correlated with precipitation if the temperature is below the freezing point in winter: moisture is deposited completely as snow. However, as temperature varies considerably with seasonal and elevations, some basins also demonstrate temporal difference in precipitation-snowfall correlation. For example, snowfall is Tibetan, Tien Shan, Pamir, and Kunlun Shan is directly associated with precipitation from October to May, but its intensity decreases in summer.

In conclusion, snowfall is largely influenced by the total precipitation, but its relationship shows significantly spatial and temporal differences. In general, temperature and snowfall are negatively correlated, while total precipitation exerted an difference effect on the snowfall behavior in the HMA catchments.

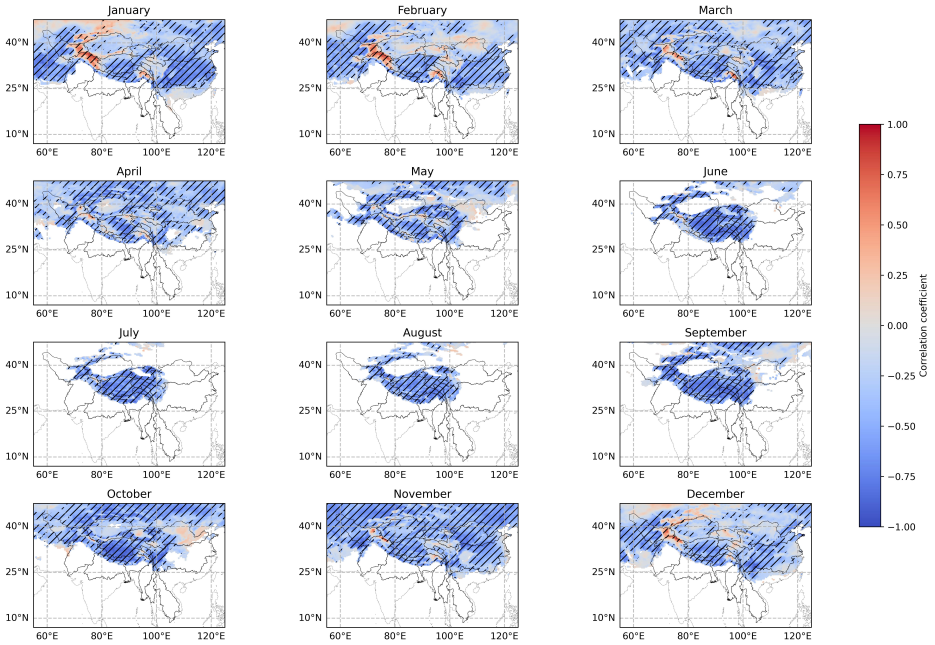

Figure 3.35: Correlation between temperature and snowfall, with hatched area implying the 0.95 significance

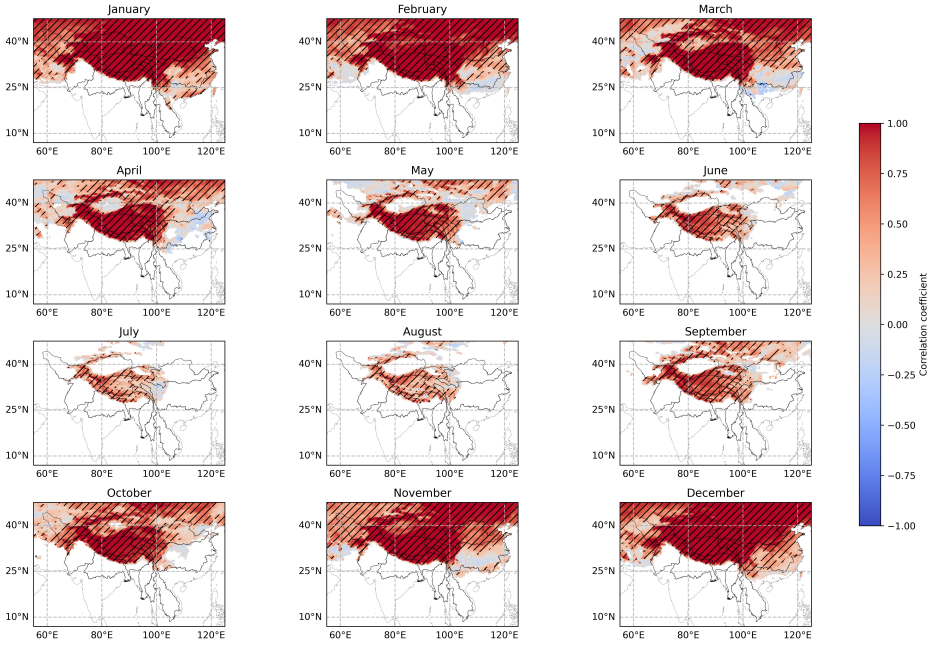

Figure 3.36: Correlation between total precipitation and snowfall, with hatched area implying the 0.95 significance

With respect to snowmelt, temperature and total precipitation play different roles. Figure 3.37 demonstrates the the spatial distribution of correlation coefficient and its seasonal evolution. In part of Tien Shan, Kunlun Shan, Pamir, Hindun-Kush, Himalayas, Tanggula Shan, Hengduan Shan, Qilian mountains, and nothern-east Yellow River, significant positive correlation dominates from October to June, suggesting that higher temperature would lead to more snowmelt in this regions considering its abundant snow water storage. Yet from July to September, this positive correlation is replaced by strong negativity. On the other hand, pronounced negative correlation prevails in other low-mid elevations areas, which could be argued as reduced SWE presence would lead to less snowmelt.

On the contrary, correlation between total precipitation and snowmelt show a distinct pattern. Opposite to temperature, snowmelt at high altitudinal regions, for instance, Tien Shan, Kunlun Shan, Pamir, Hindun-Kush, Himalayas, Tanggula Shan, and Hengduan Shan, is negatively correlated with precipitation from October to June when temperatures are relatively low. Yet this correlation is also replaced from July to September by positivity, when temperautre exceeds the freezing point and starts to play a role in shifing snowfall to rainfall that directly contribute the snowmelt (3.1, 3.3). Other regions, for instance, central Tibetan, central Tarim, Eastern Asian (Chaidam), Yangtze and Yellow river, positive correlation dictates all year long.

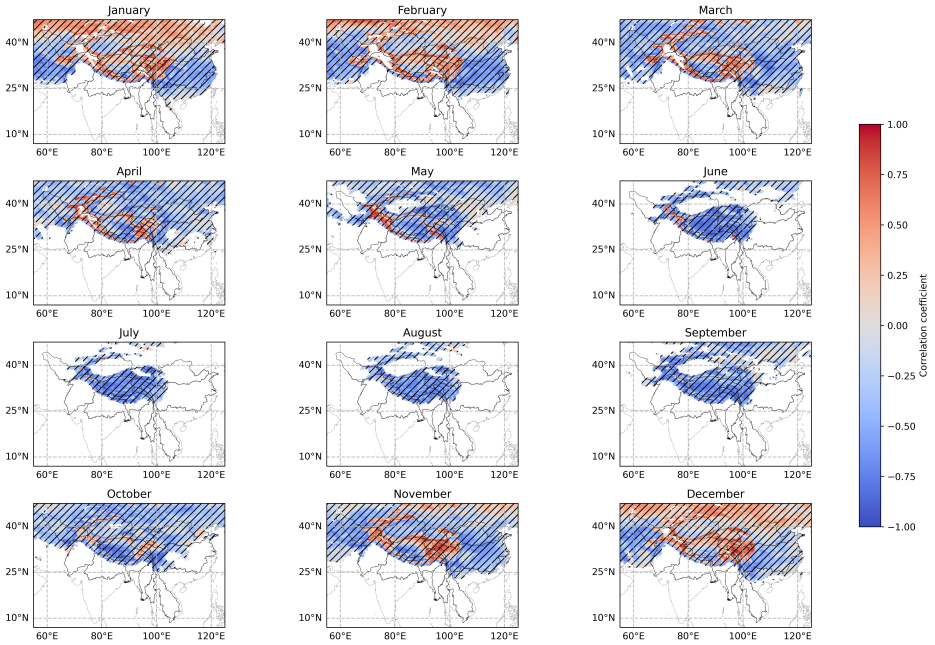

Figure 3.37: Correlation between temperature and snowmelt, with hatched area implying the 0.95 significance

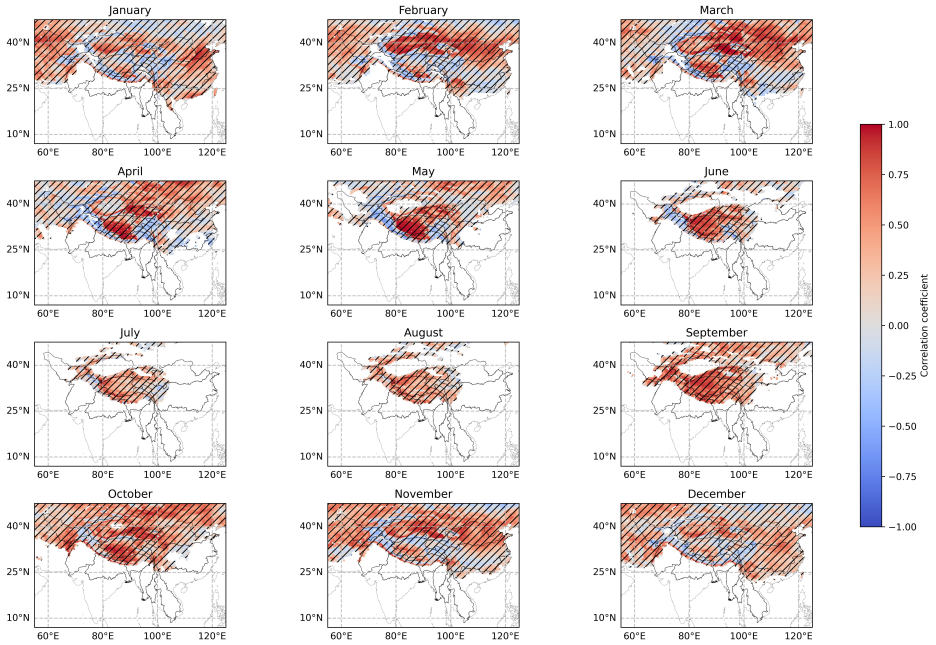

Figure 3.38: Correlation between total precipitation and snowmelt, with hatched area implying the 0.95 significance

In general, SWE is negatively correlated with temperature across the study area in all seasons as shown in Figure 3.39. This suggests that the influence of temperature on swe is quite homogeneous: higher temperature would result in less SWE. However, slightly positive correlation is also found in part of Pamir, Karakoram, and the eastern Himalayas in winter and spring seasons, from November to March. During these seasons, at the high alitutudes, higher temperature does not necessarily lead to less SWE, possibly as a result of compensation from increased precipitation.

As for precipitation, more spatiotemporal variations in correlation are found in Figure 3.40. From September to April, positive correlation dominates in the study area. Yet negative correlation appears intermittently in the Tien Shan, Eastern Tibetan Mountains and Tanggula Shan. From May to July, negative correlation presents in Tien Shan, Pamir, Karakoram, Tanggula, Hengduan Shan, and Eastern Himalayas. This indicates that in most regions, higher SWE coincides with more precipitation, but regional difference in temperature, geography, vegetation and etc. could also exert an influence.

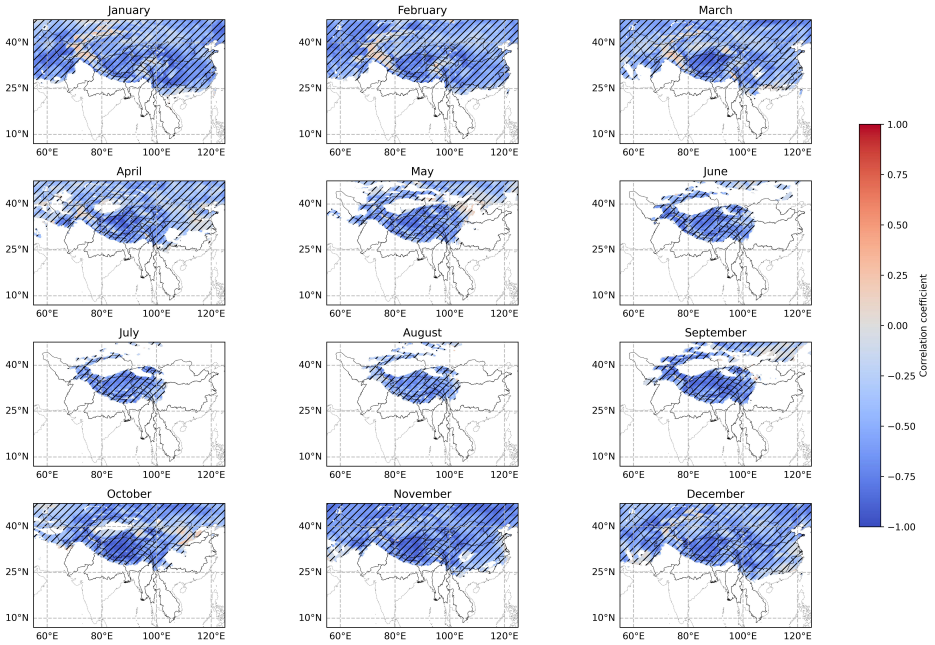

Figure 3.39: Correlation between monthly temperature and SWE from 1980 to 2020, with hatched area implying the 0.95 significance

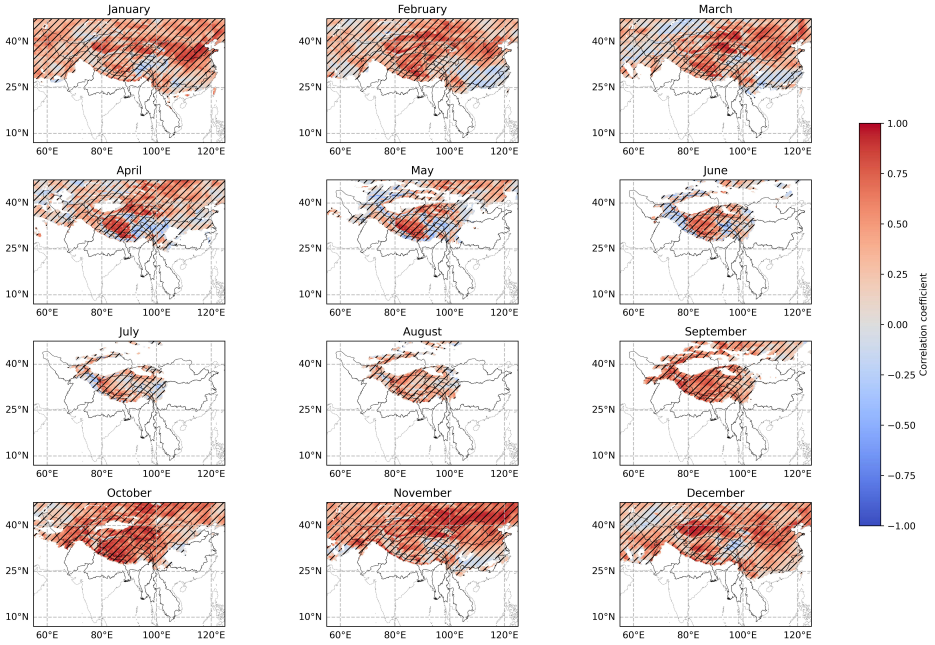

Figure 3.40: Correlation between total precipitation and SWE from 1980 to 2020, with hatched area implying the 0.95 significance

3.5.2. Composite analysis

Correlation analysis investigates the linear relationship between hydro-climatic factors with SWE and snowmelt: strongly correlated regions are identified and this could provide insights into the response mechanisms of snow to climate. Further, composite analysis is also conducted to elucidate the influence of extreme high (low) temperature and total precipitation on snowfall, snowmelt, and SWE.

Figure 3.41 and 3.42 show the impact of extreme low and high temperatures on snowfall. In general, their influence is heterogeneous, spatially and seasonally. Low temperature concurs with as high as 30 mm/month more snowfall in Tien Shan, Pamir, Karakoram, eastern Himalayas, Hengduan Shan, the central Yangtze basin, and Yellow River in winter. Yet less snowfall is also found, for instance, the Himalayas in March and April, and Tibetan in spring and autumn. In other regions, the influence of low temperature is less noticeable. On the other hand, with respect to high temperatures, most regions in the HMA are experiencing less snowfall. However, this is not applicable at Tibetan, where more snowfall coincides with high temperatures. In brief, extreme temperature could result in considerable difference snowfall amount in the HMA basins: with low temperature there is more snowfall, and with high temperature, snowfall is less.

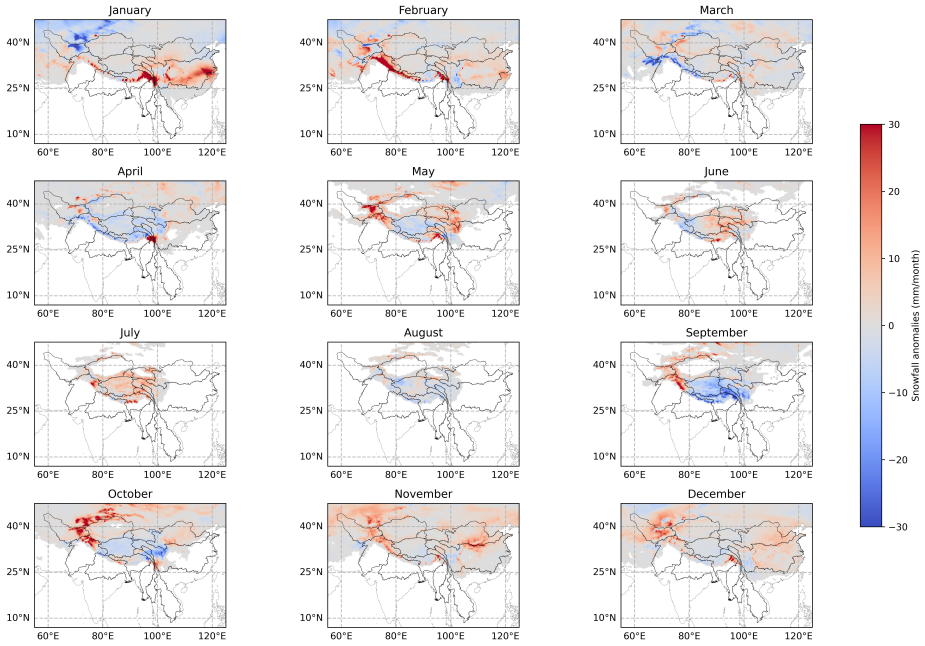

Figure 3.41: Snowfall anomalies in mm/month, constructed from composites of low temperatures (below-10% quantiles)

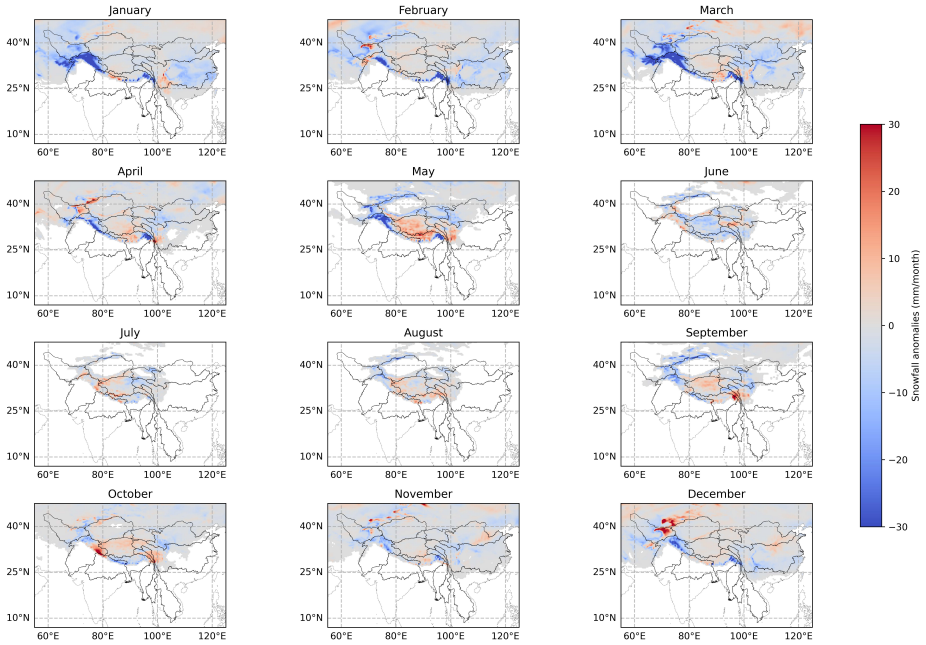

Figure 3.42: Snowfall anomalies in mm/month, constructed from composites of high temperatures (above-90% quantiles)

The impact of extreme precipitation on snowfall is different, and results are showing in Figure **??** and **??**. Low precipitations lead to less snowfall in winter from November to February, with the Pamir, Karakoram, Hindu Kush, and the Himalayas receiving the substantial less snowfall of about -30 mm/month. However, in May and June, low precipitation in Tien Shan, Kunlun Shan, and the central Himalayas corresponds with more snowfall. Comparatively, high precipitations are often associated with more snowfall in winter in the HMA basins, but the opposite in spring and summer in Tibetan and Kunlun Shan: less snowfall concurs with high precipitation. In summary, the influence of extreme precipitation varies largely, but extreme precipitation is highly negatively related with snowfall, particularly in winter.

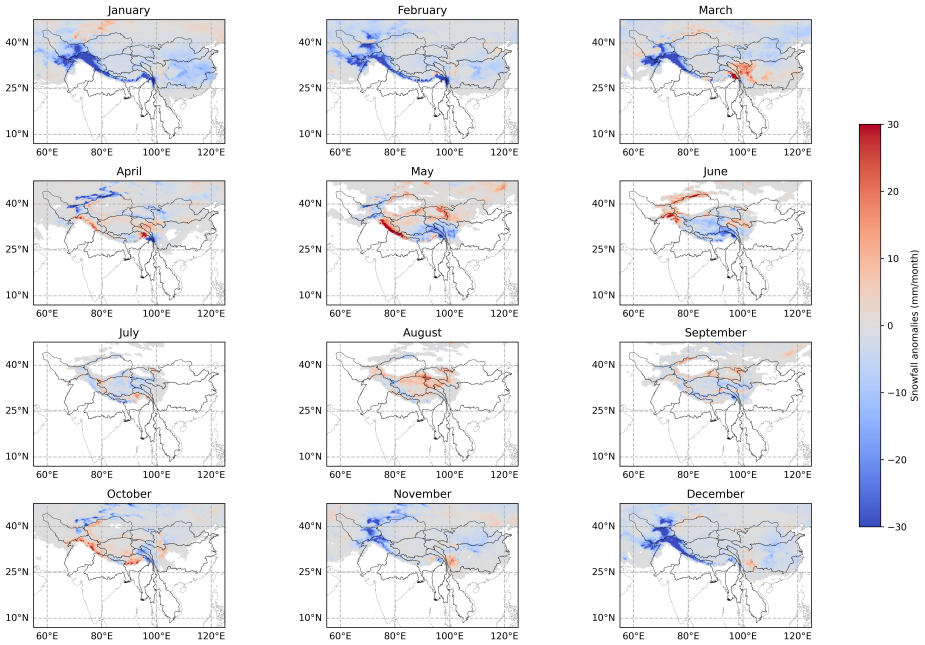

Figure 3.43: Snowfall anomalies in mm/month, constructed from composites of low total-precipitation (below-10% quantiles)

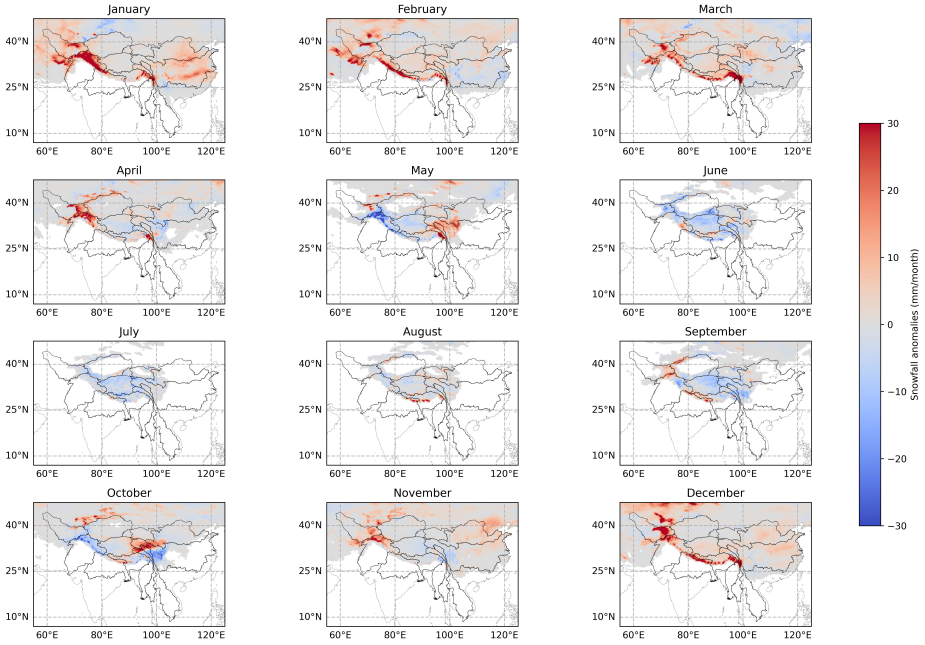

Figure 3.44: Snowfall anomalies in mm/month, constructed from composites of high total-precipitation (above-90% quantiles)

The influence of extreme temperature on snowmelt is more explicit, as depicted in Figure 3.45 and Figure 3.46. Similar to Figure 3.14, snowmelt is prominent in the spring and summer seasons and evolution of snowmelt from low elevation to high elevation is also observed. From February to May, extreme low and high temperatures play different roles in affecting snowmelt. From February to May, more snowmelt concurs with low temperature in relatively lower elevation regions, but less snowmelt in higher elevations. By contrast, when temperature is high, the opposite patterns are found: high temperature would lead to more snowmelt, but less SWE accumulation at low elevation so snomwlet is reduced. However, the impact of extreme temperature on snowmelt in June, July and August is more implicit, that in Pamir, Karakoram and Kunlun Shan, above-average snowmelt is found regardless of extremely low or high temperatures.

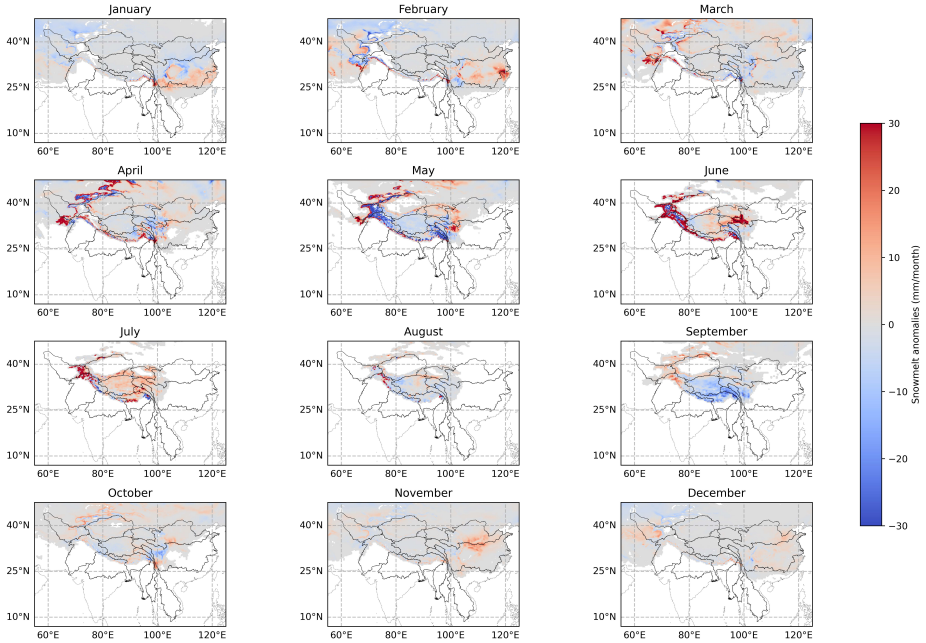

Figure 3.45: Snowmelt anomalies in mm/month, constructed from composites of low temperatures (below-10% quantiles)

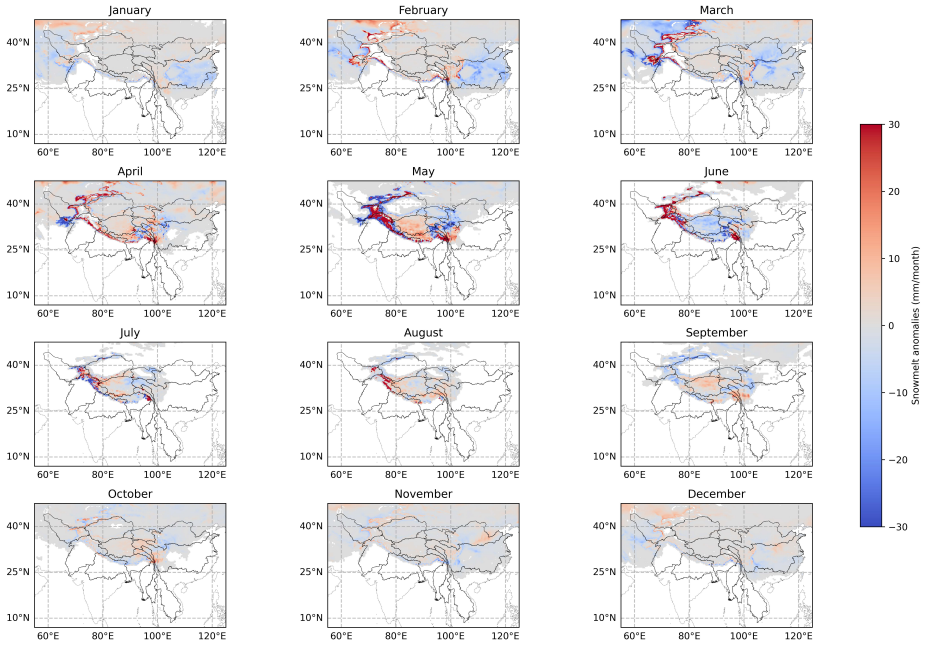

Figure 3.46: Snowmelt anomalies in mm/month, constructed from composites of high temperatures (above-90% quantiles)

Compared with extreme temperature, the influence of extreme precipitation on snowmelt is more spatially and seasonally heterogeneous. Under the condition of low precipitation, elevation is decisive for snowmelt: less snowmelt is identified in low altitudinal regions, whereas more snowmelt in higher alatitudes in Tien Shan, Pamir, Hindu Kush, and the Himalayas. From May to July, negative anomalies dominate in most high mountain regions, but an exception is found in Tien Shan in June that shows positive snowmelt anomalies. However, with respect to high precipitation, from February to March, more snowmelt is recognized in lower elevations, which is contrary to the low temperature case. In June and July, more snowmelt in Pamir, karakoram, and western Himalayas coincides with high temperature, but in Tibetan, central and eastern Himalayas, less snowmelt is resulted from high temperature.

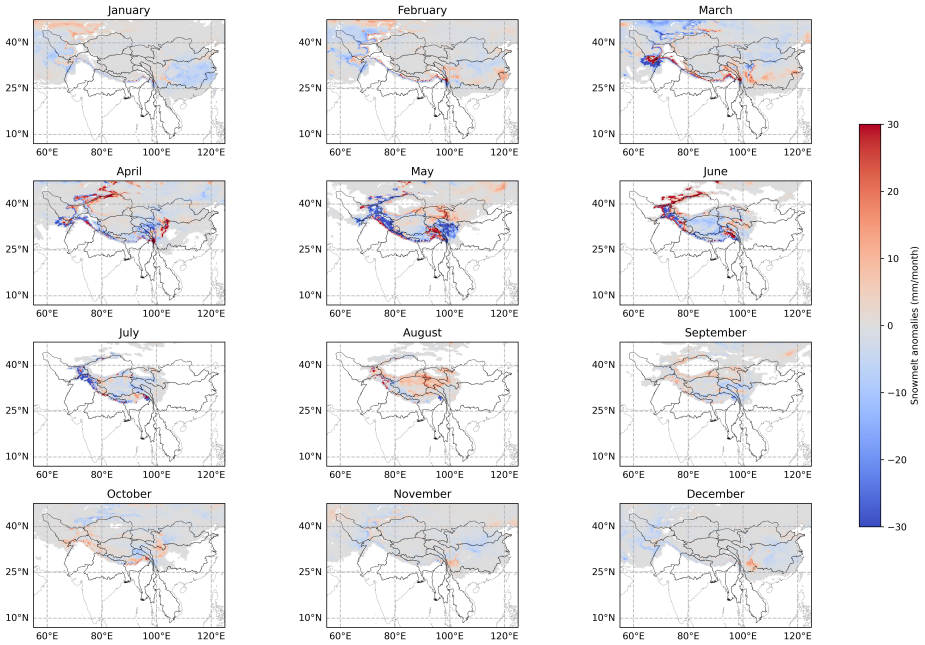

Figure 3.47: Snowmelt anomalies in mm/month, constructed from composites of low total-precipitation (below-10% quantiles)

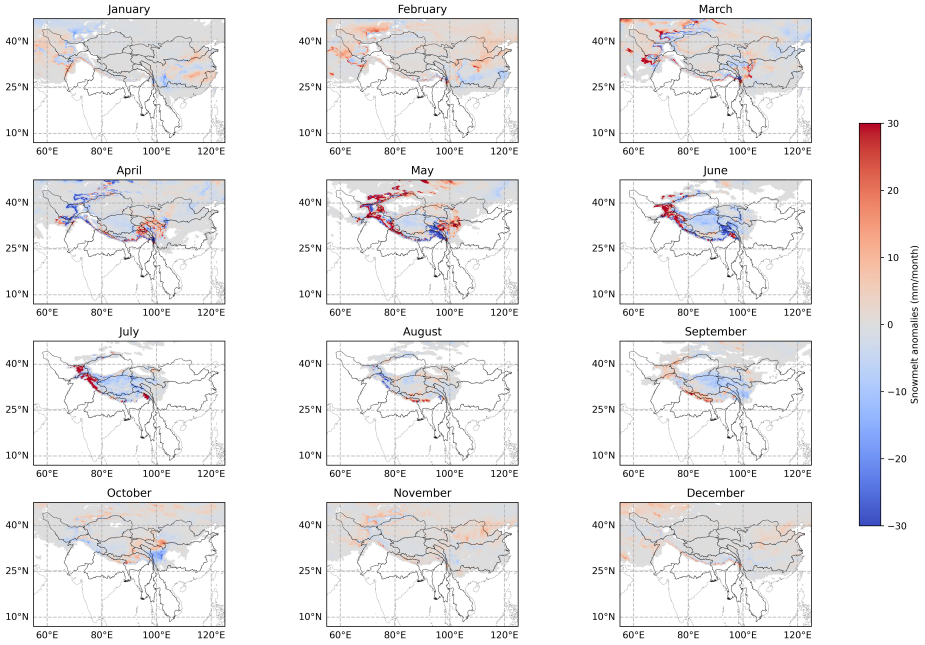

Figure 3.48: Snowmelt anomalies in mm/month, constructed from composites of high total-precipitation (above-90% quantiles)

Figure 3.49 gives information about the spatial and seasonal distribution of SWE anomalies under the low temperature conditions. Positive SWE anomalies signifies more SWE than 40-year average occurs with low temperatures concurrently, whereas negative SWE anomalies indicates less SWE than average presented with low temperatures. From July to September, no large-scale, noticeable SWE anomalies presented. Slightly positive SWE anomalies show in Pamir and Karakoram in July and August. However, from November to December, positive SWE anomalies coincides with low temperature in Tien Shan, Pamir, and Karakoram. Yet in December, negative SWE anomalies take place in Karakoram and the Himalayas. Subsequently, negative SWE anomalies in January predominates in Tien Shan, Pamir, Hindu Kush, and the Himalayas. Then, from February to June, positive anomalies gradually replace previous negativity from low-elevation to high-altitudes. In June, positive anomalies dominate given the extreme low temperature.

On the other hand, Figure 3.50 shows the SWE anomalies under the high temperature conditions. In general, high temperature leads to the opposite patterns of SWE anomalies distribution: high temperature mostly coincides with less SWE presence in Tien Shan, Pamir, Karakoram, Hindu Kush and the Himalayas. However, one pronounced singularity is that in June SWE also showes above-normal values under high temperature. This may suggest that temperature is not the decisive factor for SWE in June. In summary, extreme temperature is mostly negatively correlated with SWE, which aligns with findings in the correlation analysis. However, spatial and seasonal variations also exist.

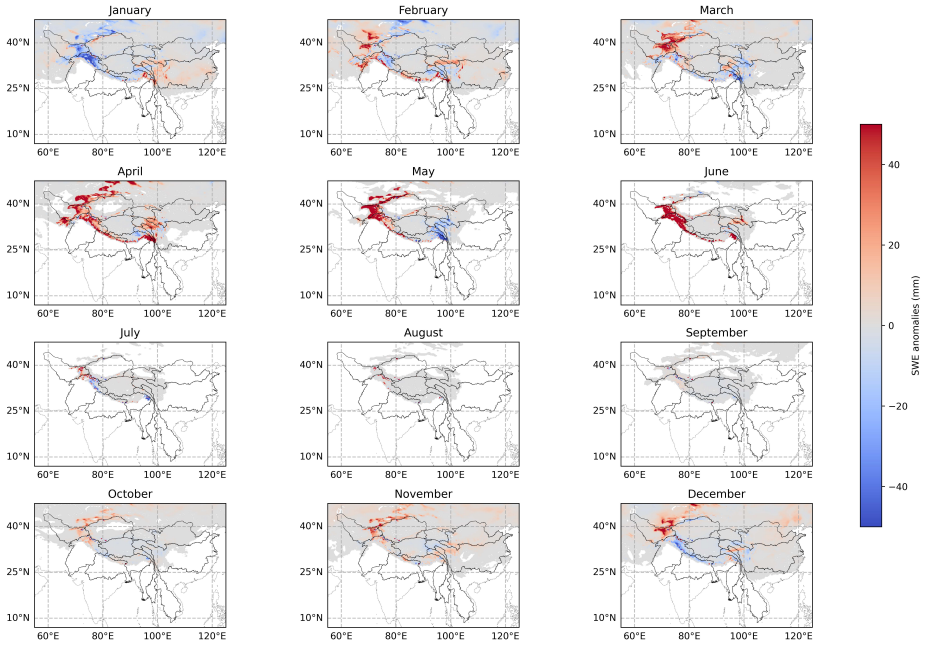

Figure 3.49: SWE anomalies in mm, constructed from composites of low temperatures (below-10% quantiles)

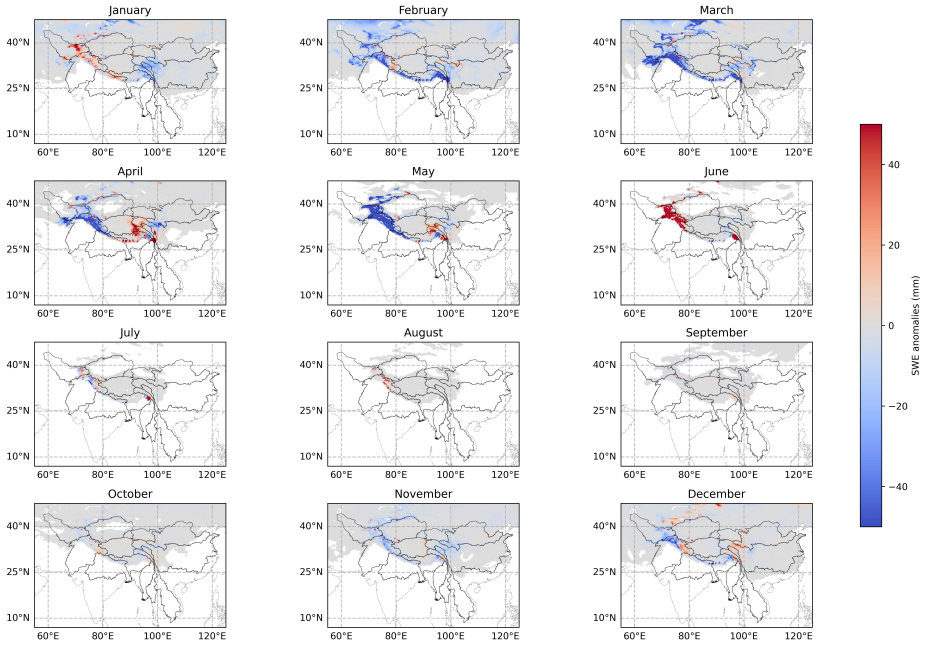

Figure 3.50: SWE anomalies in mm, constructed from composites of high temperatures (above-90% quantiles)

With respect to the relationship between extreme precipitation and SWE, results are shown in Figure 3.51 and Figure 3.52. With extreme low precipitation, the high mountain regions are mostly dominated by negative SWE anomalies from November to March. Yet positive anomalies emerge intermittently, for example, in Pamir and Tien Shan in December and March, and in the Himalayas in January. In contrast, from April to June, positivity prevails, indicating that low precipitation concurs with more SWE. When total precipitation is high, positive SWE anomalies present in most of the high elevation areas in the snow accumulation phase from November to March. However, in the snow depletion phase from April onwards, no consistent patterns are identified: in April and June negativity dominates, whereas in May and July positive SWE anomalies exhibit. In brief, SWE positively correlates with extreme precipitation during snow accumulation phase, yet negatively correlates with extreme precipitation during snow depletion phase in the high mountainous regions.

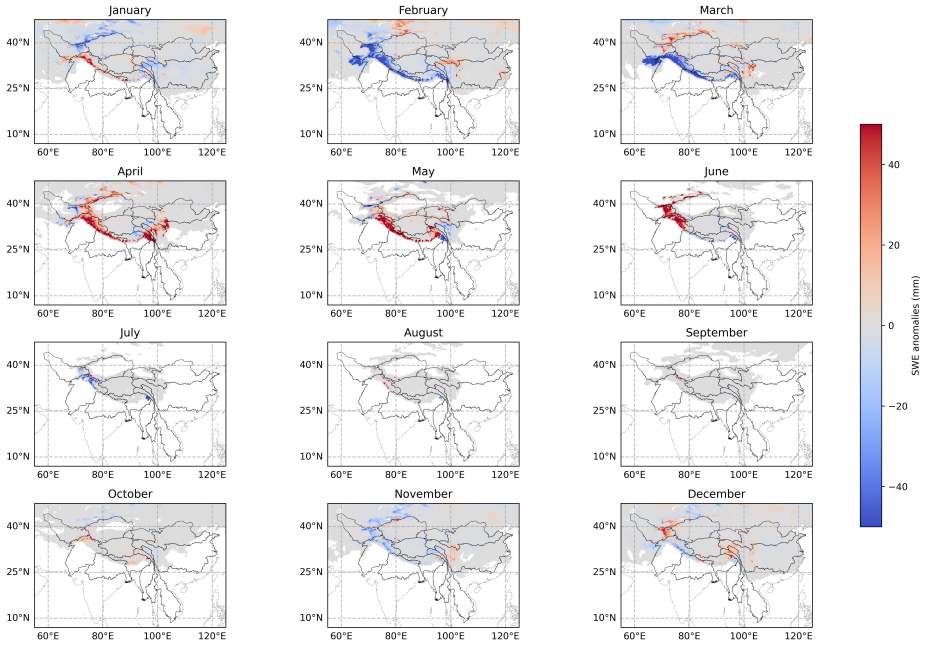

Figure 3.51: SWE anomalies in mm, constructed from composites of low total-precipitation (below-10% quantiles)

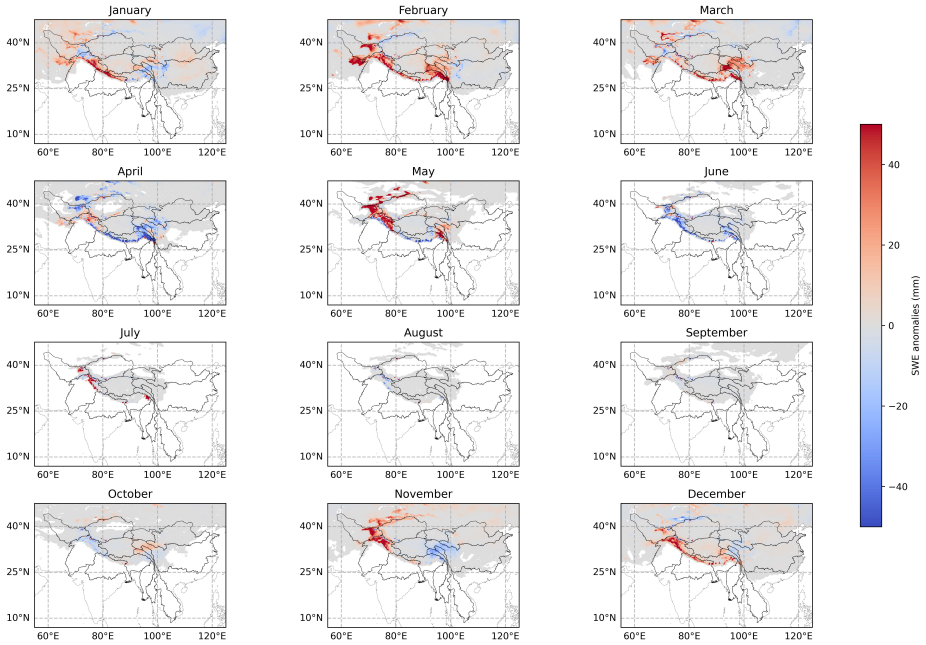

Figure 3.52: SWE anomalies in mm, constructed from composites of high total-precipitation (above-90% quantiles)

4

Dicussion

4.1. Spatiotemporal changes in snow regimes

In general, large-scale distribution and variations of snowpack are controlled by temperature, which are in turn related to elevation and latitude, as well as exposure to precipitation, radiation, and regional climate system. (Roth and Nolin 2017). Significant amount of snow water (> 1m) is stored in the high mountainous regions: Pamir, Karakoram, Hindu-Kush, the Himalayas, Tanggula Shan and Nyainqentanglha, etc., which aligned with Liu et al. 2021, Smith and Bookhagen 2018a. In general, decreasing trend (> 10 mm/year) of SWE dominated in the HMA, especially in Hindu Kush, Karakoram, Tibetan, and Hengduan Shan. This reduction in SWE coincides with rising temperatures in HMA that results in earlier snowmelt and shifting of precipitation from snowfall to rainfall in the HMA (Xu et al. 2016). However, strong increasing trends ($\tilde{5}$ mm/year) in SWE are identified in the northern-west regions in winter, i.e., Tien Shan and Pamir, which could be possibly attributed to the intensifying strength of the WWD and increasing precipitation that are capable to counteract the influence of increasing temperature (Cannon et al. 2014). Increasing SWE in Tarim, Eastern Asian, Kunlun Shan, and eastern Tibetan mountains in winter also concurs with analysis from Smith and Bookhagen 2018a.

SWE is non-linearly distributed across elevation as a result of topography and climatic setting in each catchment. Overall, SWE reduction is found across elevations in all basins, but at low-mid elevation where snowpack is shoallow, the decreasing trend is more pronounced and accentuated; snowpack in colder, high-elevation zones could be partially shielded from regional climate changes (Smith and Bookhagen 2018a). The reduction in SWE at low-mid elevation could be attributed to the decreasing of snowfall, which in turn leads to less snowmelt (Figure 3.22, Figure 3.12). This is substantiated by Figure 3.14 and Figure 3.22 that snowmelt at mid-altitudes in Pamir, the Himalayas, Tien Shan, Tanggula Shan and Nyainqentanglha is reduced. As seasonal snow at mid-elevation would be completely melted out and contributed most to regional snowmelt, its decrease in magnitude would lead to less snowmelt water.

On the other hand, as copious, permanent snowpack resided in the high elevation regions, though snowfall is also declining, snowmelt would not be limited by its magnitude. Hence more snowmelt is yielded as a result of changing climate (Figure 3.12, Figure 3.22, Figure 3.23). This is in line with hydrological simulations indicating that decline in snowpack due to warming would induce decrease in snowmelt, whereas snowpack and snowmelt could be boosted in high elevation regions with increased precipitation (Adam et al. 2009). Furthermore, with continued warming, snowpack and snowmelt in high elevation is also projected to decline as increase in precipitation could not further offset the effect from increasing temperature (Stewart 2009).

Average snow water storage is identified to have reduced in all catchments: though inter-annual increasing trend presented in some regions in certain months, these changes are outweighed by the net-loss of SWE. Specially, average SWE in Brahmaputra, Indus, Irrawaddy, Salween and Yellow River, are recognized to have shrunk significantly, with a rate of about -0.4 mm/year from 1980 to 2020 (Figure 3.31). As a result, total snowmelt is diminished in all basins except Tibetan (Figure 3.19): though rising snowmelt from high elevation is found, it could not compensate the drastic decline in snowmelt in low-mid elevations (Figure 3.23). This is supported by Khanal et al. 2021, stating that warming was broadly associated with earlier and faster snowmelt, yet due to precipitation shifting from snowfall to rainfall, eventually snowmelt would be reduced. As melt water is essential in household availability, hydropower generation and agricultural infrastructure (Smith and Bookhagen 2018a), the importance of understanding the interplay between snowmelt and re-

gional water budgets is accentuated and here highly recommended in future research, with special focus on Brahmaputra, Indus, Irrawaddy, Mekong, Salween, Yangtze and Yellow river where significant decline in annual total snowmelt distinguishes.

4.2. Impacts of hydroclimatic factors

Both temperature and precipitation had influence on snow regimes, but their effects showed considerable spatiotemporal difference and varies with geographic location, latitude, and elevation.

In general, temperature is negatively correlated with SWE across the study area, but in winter this correlation is reversed to be slight positive in Tien Shan, Pamir, and Karakoram (Figure 3.39). This coincides with results obtained by Stewart 2009 and Adam et al. 2009 that warmer temperature results in decline in snowpacks but at high elevation snowpack is sheltered from reduction as temperature is well below the freezing point in winter. Moreover, snowpack could have expanded from intensified precipitation (Moore et al. 2007). This is supported by positive correlation between precipitation and SWE in high mountains in winter season (Figure 3.40). However, in later spring and summer season, this positivity is replaced by negativity, indicating that even increase in precipitation could not overcome the effects of seasonal change in temperature. Also noteworthy is that in low-mid elevation regions, precipitation is positively correlated with SWE, which is counter-intuitive and further exploration and verification of this result should be conducted.

Temperature is mostly negatively correlated with snowfall in low-mid altitudes, but not in the high mountains. In warmer environment snowfall is less as precipitation is shifted from snow to rainfall (Räisänen 2016). With respect to the correlation between snowfall and precipitation, it is consistently positively correlated (3.36). In terms of temperature and snowmelt, negative correlation dominates in low-mid elevation regions, whereas positivity presentes in high mountains. This aligned with study from Adam et al. 2009. On the other hand, more precipitation concurs with less snowmelt in high elevations in cold seasons, and this negativity is replaced in warmer season. In contrast, increasing in precipitation results in more snowmelt in low-mid elevations regardless of seasonality (Figure 3.38).

The influence of extreme temperature and precipitation on snow is most prominent in high mountain regions. In general, relationship between extreme climates corresponded with results from correlation analysis, but spatial and seasonal variations exists. This analysis only provided primary insights into the effect of extreme climate on snow, and to elucidate the interplay in between, further research should be conducted.

4.3. Limitation and prospect

It is claimed that ERA5-Land is capable of accurately capturing the annual variability in regional analyses (Orsolini et al. 2019). However, ERA5-Land is substantiated to overestimate SWE, and the excessively high values are mostly concentrated in the mountainous regions where deep snowpacks resided, whereas estimates in the non-mountainous regions aligns better the reference data (Kouki et al. 2023). This discrepancy in SWE in high elevation areas arises from the scarcity of calibration data, terrain complexity, and poor measurements of snowfall and SWE in current stations, and undermines the parameterization and calibration of the climate model used in reanalysis (Smith and Bookhagen 2018a). For instance, according to Sorg et al. 2012, only three stations exist in Tien Shan at elevation above 3 km, and their measurements fails to correlate well with reanalysis data. This could have led to undistinguished changes in SWE and snowmelt, as shown in Figure 3.32 and Figure 3.21 and hence jeopardize the integrity of further trend analysis.

In this study, as only ERA5-Land is used, concerns of its accuracy and reliability arises. How well those spatio-temporal variations can be distinguished and how reliable those conclusions are, remained unknown. The complexity in terrain and uncertainty raised by coarse resolution in ERA5-Land could be reduced by incorporating and averaging multiple products to improve the efficiency (Mortimer et al. 2020). It is therefore suggested to include uncertainty analysis and employ more data as well as observations to enhance accuracy and trustability in future research.

5

Conclusion

This thesis concluded in this chapter by answering the research questions addressed in Chapter 1.

1. How are SWE, snowfall and snowmelt distributed spatially across the Himalayan basins?

   Intense snow water stores in the high mountainous regions: Tien Shan, Pamir, Karakoram, Hindu-Kush, the Himalayas, Kunlun Shan, Tanggula Shan and Nyainqentanglha. Persistent snowpack is identified in Pamir, Karakoram, and along the Himalayas, with SWE greater than 1 m. Shallow snowpack also presented in other regions, albeit to a lesser extent. Snowfall and snowmelt also accentuate in the hign mountains in winter and spring, respectively.

2. How are SWE, snowfall and snowmelt distributed across elevation?

   Abundant SWE (> 1 m) accumulates at high elevation, where persistent snow water resided. Seasonal snowpack presents in low-mid elevation and experiencing accumulation and melting cycles. Snowfall at mid-elevation is found to be the greatest share (max. 6% at 3.5 km) of basin total snowfall. Snowmelt from mid-elevation contributes most (max. 12% at 3.5 km) to the annual total snowmelt, whereas at high elevation its magnitude was reduced.

3. What are the temporal variability in snow regimes from 1980 to 2020?

   Snowfall is generally declining across all elevations (max. 1.5 mm/month/year), yet intermittent increasing trend also presents in winter (max. 0.5 mm/month/year). On the other hand, snowmelt from high elevation is identified to have increased over the study period for all basins (max. 1.5 mm/month/year), yet more intense decline (> 3 mm/month/year) prevails in low-mid elevation as less snowfall resides. These collectively result in changes in SWE: SWE at high elevation is largely unchanged relative to its copious amount. More pronounced decrease (> 5 mm/year) in SWE is found in low-mid elevations.

4. How do temperature and total precipitation contribute to changes in snow regimes?

   Both temperature and precipitation are vital to snow regimes. Overall, higher temperature lead to reduction in SWE, yet at high elevation snowpack shrinking is less noticeable (< 1%). Precipitation in high mountains could offset the warmer effect on SWE in winter. On the other hand, warmer temperature would induce more snowmelt in high mountains, but indirectly lead to less snowmelt in low-mid elevations as snowfall in these elevations are diminished. On the contrary, heavy precipitation concurred with more overall snowfall and more snowmelt in lowlands, yet less snowmelt in high elevation.

Appendices

A

Appendix A

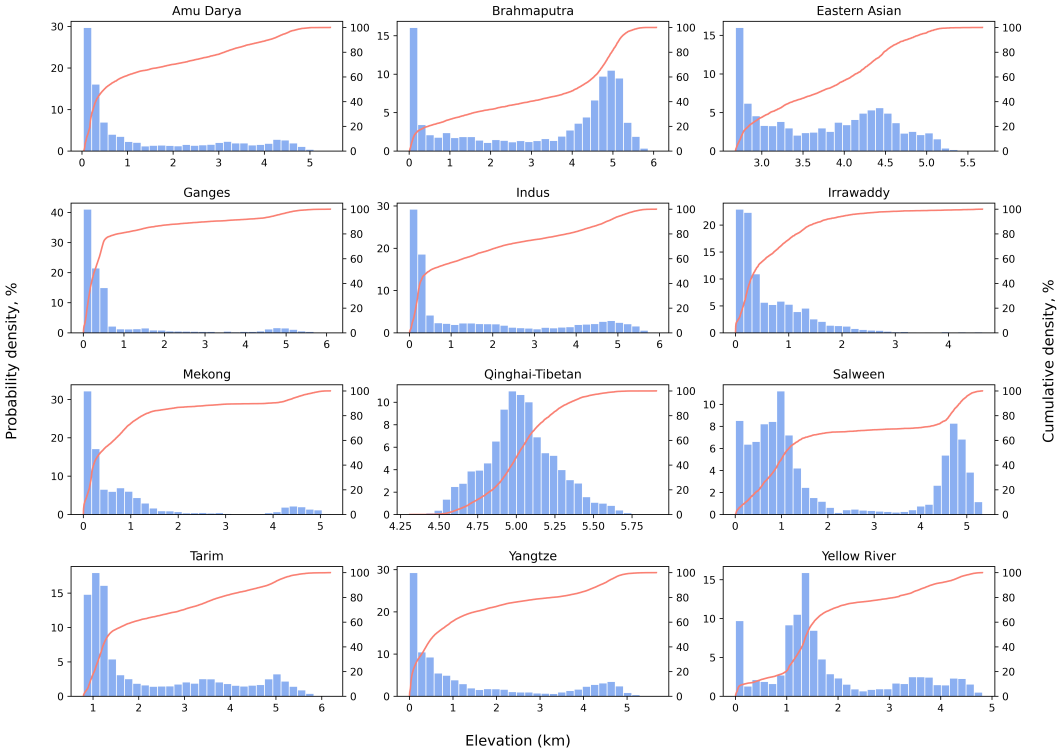

Figure A.1: Probability and cumulative distribution of elevation for each catchment in the study area

Bibliography

Jennifer C. Adam, Alan F. Hamlet, and Dennis P. Lettenmaier. Implications of global climate change for snowmelt hydrology in the twenty-first century. *Hydrological Processes*, 23(7):962–972, 2009. doi: https://doi.org/10.1002/hyp.7201. URL https://onlinelibrary.wiley.com/doi/abs/10.1002/hyp.7201.

Tracey Barnett, J. Adam, and Dennis Lettenmaier. Potential impacts of a warming climate on water availability in snow-dominated regions. *Nature*, 438:303–9, 12 2005. doi: 10.1038/nature04141.

Theodore B. Barnhart, Noah P. Molotch, Ben Livneh, Adrian A. Harpold, John F. Knowles, and Dominik Schneider. Snowmelt rate dictates streamflow. *Geophysical Research Letters*, 43(15):8006–8016, 2016. doi: https://doi.org/10.1002/2016GL069690. URL https://agupubs.onlinelibrary.wiley.com/doi/abs/10.1002/2016GL069690.

Ross D. Brown and Philip W. Mote. The response of northern hemisphere snow cover to a changing climate. *Journal of Climate*, 22(8):2124 – 2145, 2009. doi: 10.1175/2008JCLI2665.1. URL https://journals.ametsoc.org/view/journals/clim/22/8/2008jcli2665.1.xml.

Terry V. Callaghan, Margareta Johansson, Ross D. Brown, Pavel Ya. Groisman, Niklas Labba, Vladimir Radionov, Raymond S. Bradley, Sylvie Blangy, Olga N. Bulygina, Torben R. Christensen, Jonathan E. Colman, Richard L. H. Essery, Bruce C. Forbes, Mads C. Forchhammer, Vladimir N. Golubev, Richard E. Honrath, Glenn P. Juday, Anna V. Meshcherskaya, Gareth K. Phoenix, John Pomeroy, Arja Rautio, David A. Robinson, Niels M. Schmidt, Mark C. Serreze, Vladimir P. Shevchenko, Alexander I. Shiklomanov, Andrey B. Shmakin, Peter Sköld, Matthew Sturm, Ming ko Woo, and Eric F. Wood. Multiple Effects of Changes in Arctic Snow Cover. *AMBIO: A Journal of the Human Environment*, 40(sup1):32 – 45, 2011. doi: 10.1007/s13280-011-0213-x. URL https://doi.org/10.1007/s13280-011-0213-x.

Forest Cannon, Leila Carvalho, Charles Jones, and Bodo Bookhagen. Multi-annual variations in winter westerly disturbance activity affecting the himalaya. *Climate Dynamics*, 44:441–455, 07 2014. doi: 10.1007/s00382-014-2248-8.

Jeff Dozier, Edward H. Bair, and Robert E. Davis. Estimating the spatial distribution of snow water equivalent in the world's mountains. *WIREs Water*, 3(3):461–474, 2016. doi: https://doi.org/10.1002/wat2.1140. URL https://wires.onlinelibrary.wiley.com/doi/abs/10.1002/wat2.1140.

Keqin Duan, Tandong Yao, Ninglian Wang, Peihong Shi, and Yali Meng. Changes in equilibrium-line altitude and implications for glacier evolution in the asian high mountains in the 21st century. *Science China Earth Sciences*, 65(7):1308 – 1316, 2022. doi: 10.1007/s11430-021-9923-6. URL https://www.scopus.com/inward/record.uri?eid=2-s2.0-85131048547&doi=10.1007%2fs11430-021-9923-6&partnerID=40&md5=5d1db4ba06404a073169581f579096e6. Cited by: 11.

Ronald Gelaro, Will McCarty, Max Suárez, Ricardo Todling, Andrea Molod, Lawrence Takacs, Cynthia Randles, Anton Darmenov, Michael Bosilovich, Rolf Reichle, Krzysztof Wargan, Lawrence Coy, Richard Cullather, Clara Draper, Santha Akella, Virginie Buchard, Austin Conaty, Arlindo Da Silva, Wei Gu, and Bin Zhao. The modern-era retrospective analysis for research and applications, version 2 (merra-2). *Journal of Climate*, 30, 05 2017. doi: 10.1175/JCLI-D-16-0758.1.

Alexander R. Gottlieb and Justin S. Mankin. Evidence of human influence on northern hemisphere snow loss. *Nature*, 625(7994):293–300, Jan 2024. ISSN 1476-4687. doi: 10.1038/s41586-023-06794-y. URL https://doi.org/10.1038/s41586-023-06794-y.

Katherine E. Hale, Keith S. Jennings, Keith N. Musselman, Ben Livneh, and Noah P. Molotch. Recent decreases in snow water storage in western north america. *Communications Earth & Environment*, 4(1):170, May 2023. ISSN 2662-4435. doi: 10.1038/s43247-023-00751-3. URL https://doi.org/10.1038/s43247-023-00751-3.

Hans Hersbach, Bill Bell, Paul Berrisford, Shoji Hirahara, András Horányi, Joaquín Muñoz-Sabater, Julien Nicolas, Carole Peubey, Raluca Radu, Dinand Schepers, Adrian Simmons, Cornel Soci, Saleh Abdalla, Xavier Abellan, Gianpaolo Balsamo, Peter Bechtold, Gionata Biavati, Jean Bidlot, Massimo Bonavita, Giovanna De Chiara, Per Dahlgren, Dick Dee, Michail Diamantakis, Rossana Dragani, Johannes Flemming, Richard Forbes, Manuel Fuentes, Alan Geer, Leo Haimberger, Sean Healy, Robin J. Hogan, Elías Hólm, Marta Janisková, Sarah Keeley, Patrick Laloyaux, Philippe Lopez, Cristina Lupu, Gabor Radnoti, Patricia de Rosnay, Iryna Rozum, Freja Vamborg, Sebastien Villaume, and Jean-Noël Thépaut. The era5 global reanalysis. *Quarterly Journal of the Royal Meteorological Society*, 146(730):1999–2049, 2020. doi: https://doi.org/10.1002/qj.3803. URL https://rmets.onlinelibrary.wiley.com/doi/abs/10.1002/qj.3803.

M. Jenicek, J. Seibert, M. Zappa, M. Staudinger, and T. Jonas. Importance of maximum snow accumulation for summer low flows in humid catchments. *Hydrology and Earth System Sciences*, 20(2):859–874, 2016. doi: 10.5194/hess-20-859-2016. URL https://hess.copernicus.org/articles/20/859/2016/.

S. Khanal, A.F. Lutz, P. D. A. Kraaijenbrink, B. van den Hurk, T. Yao, and W. W. Immerzeel. Variable 21st century climate change response for rivers in high mountain asia at seasonal to decadal time scales. *Water Resources Research*, 57(5):e2020WR029266, 2021. doi: https://doi.org/10.1029/2020WR029266. URL https://agupubs.onlinelibrary.wiley.com/doi/abs/10.1029/2020WR029266. e2020WR029266 2020WR029266.

James D. Kirkham, Inka Koch, Tuomo M. Saloranta, Maxime Litt, Emmy E. Stigter, Knut Møen, Amrit Thapa, Kjetil Melvold, and Walter W. Immerzeel. Near real-time measurement of snow water equivalent in the nepal himalayas. *Frontiers in Earth Science*, 7, 2019. ISSN 2296-6463. doi: 10.3389/feart.2019.00177. URL https://www.frontiersin.org/articles/10.3389/feart.2019.00177.

K. Kouki, K. Luojus, and A. Riihelä. Evaluation of snow cover properties in era5 and era5-land with several satellite-based datasets in the northern hemisphere in spring 1982–2018. *The Cryosphere*, 17(12):5007–5026, 2023. doi: 10.5194/tc-17-5007-2023. URL https://tc.copernicus.org/articles/17/5007/2023/.

Philip D. A. Kraaijenbrink, Emmy E. Stigter, Tandong Yao, and Walter W. Immerzeel. Climate change decisive for asia's snow meltwater supply. *Nature Climate Change*, 11(7):591–597, Jul 2021. ISSN 1758-6798. doi: 10.1038/s41558-021-01074-x. URL https://doi.org/10.1038/s41558-021-01074-x.

Donghuan Li, Youcun Qi, and Deliang Chen. Changes in rain and snow over the tibetan plateau based on imerg and ground-based observation. *Journal of Hydrology*, 606:127400, 2022a. ISSN 0022-1694. doi: https://doi.org/10.1016/j.jhydrol.2021.127400. URL https://www.sciencedirect.com/science/article/pii/S0022169421014505.

Qian Li, Tao Yang, and Lanhai Li. Evaluation of snow depth and snow cover represented by multiple datasets over the tianshan mountains: Remote sensing, reanalysis, and simulation. *International Journal of Climatology*, 42(8):4223–4239, 2022b. doi: https://doi.org/10.1002/joc.7459. URL https://rmets.onlinelibrary.wiley.com/doi/abs/10.1002/joc.7459.

Hans Lievens, Matthias Demuzere, Hans-Peter Marshall, Rolf H. Reichle, Ludovic Brucker, Isis Brangers, Patricia de Rosnay, Marie Dumont, Manuela Girotto, Walter W. Immerzeel, Tobias Jonas, Edward J. Kim, Inka Koch, Christoph Marty, Tuomo Saloranta, Johannes Schöber, and Gabrielle J. M. De Lannoy. Snow depth variability in the northern hemisphere mountains observed from space. *Nature Communications*, 10(1):4629, Oct 2019. ISSN 2041-1723. doi: 10.1038/s41467-019-12566-y. URL https://doi.org/10.1038/s41467-019-12566-y.

Y. Liu, Y. Fang, and S. A. Margulis. Spatiotemporal distribution of seasonal snow water equivalent in high mountain asia from an 18-year landsat–modis era snow reanalysis dataset. *The Cryosphere*, 15(11):5261–5280, 2021. doi: 10.5194/tc-15-5261-2021. URL https://tc.copernicus.org/articles/15/5261/2021/.

Arthur Lutz, W.W. Immerzeel, Arun Shrestha, and M.F.P. Bierkens. Consistent increase in high asia's runoff due to increasing glacier melt and precipitation. *Nature Clim. Change*, 4:587–592, 06 2014. doi: 10.1038/nclimate2237.

Henry B. Mann. Nonparametric tests against trend. *Econometrica*, 13(3):245–259, 1945. ISSN 00129682, 14680262. URL http://www.jstor.org/stable/1907187.

Arathy Menon, Anders Levermann, and Jacob Schewe. Enhanced future variability during india's rainy season. *Geophysical Research Letters*, 40:3242–3247, 06 2013. doi: 10.1002/grl.50583.

Johnnie N. Moore, Joel T. Harper, and Mark C. Greenwood. Significance of trends toward earlier snowmelt runoff, columbia and missouri basin headwaters, western united states. *Geophysical Research Letters*, 34 (16), 2007. doi: https://doi.org/10.1029/2007GL031022. URL https://agupubs.onlinelibrary.wiley.com/doi/abs/10.1029/2007GL031022.

C. Mortimer, L. Mudryk, C. Derksen, K. Luojus, R. Brown, R. Kelly, and M. Tedesco. Evaluation of long-term northern hemisphere snow water equivalent products. *The Cryosphere*, 14(5):1579–1594, 2020. doi: 10.5194/tc-14-1579-2020. URL https://tc.copernicus.org/articles/14/1579/2020/.

J. Muñoz Sabater, E. Dutra, A. Agustí-Panareda, C. Albergel, G. Arduini, G. Balsamo, S. Boussetta, M. Choulga, S. Harrigan, H. Hersbach, B. Martens, D. G. Miralles, M. Piles, N. J. Rodríguez-Fernández, E. Zsoter, C. Buontempo, and J.-N. Thépaut. Era5-land: a state-of-the-art global reanalysis dataset for land applications. *Earth System Science Data*, 13(9):4349–4383, 2021a. doi: 10.5194/essd-13-4349-2021. URL https://essd.copernicus.org/articles/13/4349/2021/.

J. Muñoz Sabater, E. Dutra, A. Agustí-Panareda, C. Albergel, G. Arduini, G. Balsamo, S. Boussetta, M. Choulga, S. Harrigan, H. Hersbach, B. Martens, D. G. Miralles, M. Piles, N. J. Rodríguez-Fernández, E. Zsoter, C. Buontempo, and J.-N. Thépaut. Era5-land: a state-of-the-art global reanalysis dataset for land applications. *Earth System Science Data*, 13(9):4349–4383, 2021b. doi: 10.5194/essd-13-4349-2021. URL https://essd.copernicus.org/articles/13/4349/2021/.

L. Mudryk, M. Santolaria-Otín, G. Krinner, M. Ménégoz, C. Derksen, C. Brutel-Vuilmet, M. Brady, and R. Essery. Historical northern hemisphere snow cover trends and projected changes in the cmip6 multi-model ensemble. *The Cryosphere*, 14(7):2495–2514, 2020. doi: 10.5194/tc-14-2495-2020. URL https://tc.copernicus.org/articles/14/2495/2020/.

Keith N. Musselman, Nans Addor, Julie A. Vano, and Noah P. Molotch. Winter melt trends portend widespread declines in snow water resources. *Nature Climate Change*, 11(5):418–424, May 2021. ISSN 1758-6798. doi: 10.1038/s41558-021-01014-9. URL https://doi.org/10.1038/s41558-021-01014-9.

Y. Orsolini, M. Wegmann, E. Dutra, B. Liu, G. Balsamo, K. Yang, P. de Rosnay, C. Zhu, W. Wang, R. Senan, and G. Arduini. Evaluation of snow depth and snow cover over the tibetan plateau in global reanalyses using in situ and satellite remote sensing observations. *The Cryosphere*, 13(8):2221–2239, 2019. doi: 10.5194/tc-13-2221-2019. URL https://tc.copernicus.org/articles/13/2221/2019/.

Elisa Palazzi, J. Hardenberg, and Antonello Provenzale. Precipitation in the hindu-kush karakoram himalaya: Observations and future scenarios. *Journal of Geophysical Research*, 118:85–100, 01 2013. doi: 10.1029/2012JD018697.

Amita Prabhu, Sujata K. Mandke, and G. Pandithurai. Regional perspectives in eurasian snow - indian monsoon relationship: An observational study. *Polar Science*, 30:100718, 2021. ISSN 1873-9652. doi: https://doi.org/10.1016/j.polar.2021.100718. URL https://www.sciencedirect.com/science/article/pii/S1873965221001079. Special Issue on "Polar Studies - Window to the changing Earth".

Wei Qi, Lian Feng, Junguo Liu, and Hong Yang. Snow as an important natural reservoir for runoff and soil moisture in northeast china. *Journal of Geophysical Research: Atmospheres*, 125(22):e2020JD033086, 2020. doi: https://doi.org/10.1029/2020JD033086. URL https://agupubs.onlinelibrary.wiley.com/doi/abs/10.1029/2020JD033086. e2020JD033086 2020JD033086.

Yue Qin, John T. Abatzoglou, Stefan Siebert, Laurie S. Huning, Amir AghaKouchak, Justin S. Mankin, Chaopeng Hong, Dan Tong, Steven J. Davis, and Nathaniel D. Mueller. Agricultural risks from changing snowmelt. *Nature Climate Change*, 10(5):459–465, May 2020. ISSN 1758-6798. doi: 10.1038/s41558-020-0746-8. URL https://doi.org/10.1038/s41558-020-0746-8.

J. Räisänen. Changes in march mean snow water equivalent since the mid-20th century and the contributing factors in reanalyses and cmip6 climate models. *The Cryosphere*, 17(5):1913–1934, 2023. doi: 10.5194/tc-17-1913-2023. URL https://tc.copernicus.org/articles/17/1913/2023/.

Jouni Räisänen. Twenty-first century changes in snowfall climate in northern europe in ensembles regional climate models. *Climate dynamics*, 46:339–353, 2016.

M. Rodell, P. R. Houser, U. Jambor, J. Gottschalck, K. Mitchell, C.-J. Meng, K. Arsenault, B. Cosgrove, J. Radakovich, M. Bosilovich, J. K. Entin, J. P. Walker, D. Lohmann, and D. Toll. The global land data assimilation system. *Bulletin of the American Meteorological Society*, 85(3):381 – 394, 2004. doi: 10.1175/BAMS-85-3-381. URL https://journals.ametsoc.org/view/journals/bams/85/3/bams-85-3-381.xml.

T. R. Roth and A. W. Nolin. Forest impacts on snow accumulation and ablation across an elevation gradient in a temperate montane environment. *Hydrology and Earth System Sciences*, 21(11):5427–5442, 2017. doi: 10.5194/hess-21-5427-2017. URL https://hess.copernicus.org/articles/21/5427/2017/.

Jan Seibert, Michal Jenicek, Matthias Huss, Tracy Ewen, and Daniel Viviroli. Chapter 4 - snow and ice in the hydrosphere. In Wilfried Haeberli and Colin Whiteman, editors, *Snow and Ice-Related Hazards, Risks, and Disasters (Second Edition)*, Hazards and Disasters Series, pages 93–135. Elsevier, second edition edition, 2021. ISBN 978-0-12-817129-5. doi: https://doi.org/10.1016/B978-0-12-817129-5.00010-X. URL https://www.sciencedirect.com/science/article/pii/B978012817129500010X.

Pranab Kumar Sen. Estimates of the regression coefficient based on kendall's tau. *Journal of the American Statistical Association*, 63(324):1379–1389, 1968. doi: 10.1080/01621459.1968.10480934. URL https://www.tandfonline.com/doi/abs/10.1080/01621459.1968.10480934.

M. Serreze, John Walsh, F Stuart Chapin III, Tom Osterkamp, Mark Dyurgerov, Vladimir Romanovsky, Walter Oechel, James Morison, Tingjun Zhang, and Roger Barry. Observational evidence of recent change in the northern high-latitude environment. *Climatic Change*, 46:159–207, 07 2000. doi: 10.1023/A:1005504031923.

T. Smith, B. Bookhagen, and A. Rheinwalt. Spatiotemporal patterns of high mountain asia's snowmelt season identified with an automated snowmelt detection algorithm, 1987–2016. *The Cryosphere*, 11(5):2329–2343, 2017. doi: 10.5194/tc-11-2329-2017. URL https://tc.copernicus.org/articles/11/2329/2017/.

Taylor Smith and Bodo Bookhagen. Changes in seasonal snow water equivalent distribution in high mountain asia (1987 to 2009). *Science Advances*, 4(1):e1701550, 2018a. doi: 10.1126/sciadv.1701550. URL https://www.science.org/doi/abs/10.1126/sciadv.1701550.

Taylor Smith and Bodo Bookhagen. Changes in seasonal snow water equivalent distribution in high mountain asia (1987 to 2009). *Science Advances*, 4(1):e1701550, 2018b. doi: 10.1126/sciadv.1701550. URL https://www.science.org/doi/abs/10.1126/sciadv.1701550.

Annina Sorg, Tobias Bolch, Olga Solomina, and Martin Beniston. Climate change impacts on glaciers and runoff in tien shan (central asia). *Nature Climate Change*, 2, 07 2012. doi: 10.1038/NCLIMATE1592.

Iris Stewart. Changes in snowpack and snowmelt runoff for key mountain regions. *Hydrological Processes*, 23:78 – 94, 01 2009. doi: 10.1002/hyp.7128.

Matias Takala, Kari Luojus, Jouni Pulliainen, Chris Derksen, Juha Lemmetyinen, Juha-Petri Kärnä, Jarkko Koskinen, and Bojan Bojkov. Estimating northern hemisphere snow water equivalent for climate research through assimilation of space-borne radiometer data and ground-based measurements. *Remote Sensing of Environment*, 115(12):3517–3529, 2011. ISSN 0034-4257. doi: https://doi.org/10.1016/j.rse.2011.08.014. URL https://www.sciencedirect.com/science/article/pii/S0034425711003166.

Zhiguang Tang, Gang Deng, Guojie Hu, Hongbo Zhang, Haizhu Pan, and Guoqing Sang. Satellite observed spatiotemporal variability of snow cover and snow phenology over high mountain asia from 2002 to 2021. *Journal of Hydrology*, 613:128438, 2022. ISSN 0022-1694. doi: https://doi.org/10.1016/j.jhydrol.2022.128438. URL https://www.sciencedirect.com/science/article/pii/S0022169422010083.

Chad W. Thackeray and Christopher G. Fletcher. Snow albedo feedback: Current knowledge, importance, outstanding issues and future directions. *Progress in Physical Geography: Earth and Environment*, 40(3): 392–408, 2016. doi: 10.1177/0309133315620999. URL https://doi.org/10.1177/0309133315620999.

Hao Wang, Bin-Bin Wang, Peng Cui, Yao-Ming Ma, Yan Wang, Jian-Sheng Hao, Yu Wang, Ya-Mei Li, Li-Jun Sun, Jiao Wang, Guo-Tao Zhang, Wei-Mo Li, Yu Lei, Wen-Qing Zhao, Jin-Bo Tang, and Chao-Yue Li. Disaster effects of climate change in high mountain asia: State of art and scientific challenges. *Advances in Climate Change Research*, 2024. ISSN 1674-9278. doi: https://doi.org/10.1016/j.accre.2024.06.003. URL https://www.sciencedirect.com/science/article/pii/S1674927824000790.

Melissa L. Wrzesien, Tamlin M. Pavelsky, Michael T. Durand, Jeff Dozier, and Jessica D. Lundquist. Characterizing biases in mountain snow accumulation from global data sets. *Water Resources Research*, 55(11): 9873–9891, 2019. doi: https://doi.org/10.1029/2019WR025350. URL https://agupubs.onlinelibrary.wiley.com/doi/abs/10.1029/2019WR025350.

Wenfang Xu, Lijuan Ma, Minna Ma, Haicheng Zhang, and Wenping Yuan. Spatial-temporal variability of snow cover and depth in qinghai-tibetan plateau. *Journal of Climate*, 30, 12 2016. doi: 10.1175/JCLI-D-15-0732.1.

Tao Yang, Qian Li, Rafiq Hamdi, Xi Chen, Qiang Zou, Fengqi Cui, Philippe De Maeyer, and Lanhai Li. Trends and spatial variations of rain-on-snow events over the high mountain asia. *Journal of Hydrology*, 614:128593, 2022. ISSN 0022-1694. doi: https://doi.org/10.1016/j.jhydrol.2022.128593. URL https://www.sciencedirect.com/science/article/pii/S0022169422011635.

Tandong Yao, Tobias Bolch, Deliang Chen, Jing Gao, Walter Immerzeel, Shilong Piao, Fengge Su, Lonnie Thompson, Yoshihide Wada, Lei Wang, Tao Wang, Guangjian Wu, Baiqing Xu, Wei Yang, Guoqing Zhang, and Ping Zhao. The imbalance of the asian water tower. *Nature Reviews Earth & Environment*, 3(10):618–632, Oct 2022. ISSN 2662-138X. doi: 10.1038/s43017-022-00299-4. URL https://doi.org/10.1038/s43017-022-00299-4.

Ding Yihui and Johnny Chan. The east asian summer monsoon: An overview. *Meteorology and Atmospheric Physics*, 89:117–142, 01 2005. doi: 10.1007/s00703-005-0125-z.

Sheng Yue, Paul Pilon, Bob Phinney, and George Cavadias. The influence of autocorrelation on the ability to detect trend in hydrological series. *Hydrological Processes*, 16(9):1807–1829, 2002. doi: https://doi.org/10.1002/hyp.1095. URL https://onlinelibrary.wiley.com/doi/abs/10.1002/hyp.1095.

Xian Zhu, Shao-Yi Lee, Xiaohang Wen, Zhigang Wei, Zhenming Ji, Zhiyuan Zheng, and Wenjie Dong. Historical evolution and future trend of northern hemisphere snow cover in cmip5 and cmip6 models. *Environmental Research Letters*, 16(6):065013, jun 2021. doi: 10.1088/1748-9326/ac0662. URL https://dx.doi.org/10.1088/1748-9326/ac0662.